Gran Sasso Science Institute

PHD PROGRAMME IN MATHEMATICS IN NATURAL, SOCIAL AND LIFE SCIENCES

THE MATHEMATICAL MODELLING OF PLANT GROWTH AND APPLICATIONS TO ROBOTICS

PHD CANDIDATE
Tedone Fabio

ADVISORS
Prof. Pierangelo Marcati
Gran Sasso Science Institute
Dr. Barbara Mazzolai
Italian Institute of Technology

Gran Sasso Science Institute

PHD PROGRAMME IN MATHEMATICS IN NATURAL, SOCIAL AND LIFE SCIENCES

THE MATHEMATICAL MODELLING OF PLANT GROWTH AND APPLICATIONS TO ROBOTICS

PHD CANDIDATE
Fabio Tedone

ADVISORS
Prof. Pierangelo Marcati
Gran Sasso Science Institute
Prof. Barbara Mazzolai
Italian Institute of Technology

Thesis Jury Members

Prof. Roberto Natalini (Jury President, Direttore dell'Istituto per le Applicazioni del Calcolo del CNR)
Prof. Yasmine Meroz (Tel Aviv University)
Prof. Matteo Colangeli (DISIM- Università dell'Aquila)
Prof. Raffaele D'Ambrosio (DISIM- Università dell'Aquila)
Prof. Serena Cenatiempo (Gran Sasso Science Institute)

Thesis Referees

Prof. Roberto Natalini (Direttore dell'Istituto per le Applicazioni del Calcolo del CNR)
Prof. Yasmine Meroz (Tel Aviv University)

Originality and Copyright Declarations

I hereby confirm that I am the sole author of the written work here enclosed and that I have compiled it in my own words. Parts excepted are corrections of form and content by the supervisors.

Acknowledgements

Undertaking this PhD has been a truly life-changing experience for me and it would not have been possible to do without the support and guidance that I received from many people, who I wish to thank.

Firstly, I would like to express my sincere gratitude to my advisors Dr B. Mazzolai and Prof. P. Marcati. Their patience, motivation, and guidance helped me in all the time of research. Barbara, with her intuition, suggested to me valuable research questions at the crossroads of many disciplines. Piero, with his immense knowledge, encouraged me when problems seemed to be too much complicated to be solved.

I would also like to thank Dr E. Del Dottore, for her useful discussions and insights. Without her precious support, it would not be possible to conduct my research. Meetings with Emanuela at IIT provided many new directions to my research.

I am also deeply indebted with Dr M. Palladino, for his insightful comments and encouragements, but also for the hard questions which motivated me to grow up as a person and as a researcher. Michele, you have taught me something every meeting we had and it was a pleasure and an honour to collaborate with such a great researcher.

I wish to thank Alessandro, Antonio, Cristina, Francesco, Lorenzo, Luca, Roberta, Roberto, Thoa, Xuan and all the other friends at GSSI, from the students to the staff. Each one of them made this experience unique and awesome.

Special thanks to my Mom, Dad, Alessandra and Stefano for always believing in me and encouraging me to follow my dreams. And Enza, Biagio and Marilisa, for accepting me as a son.

Many other relatives and friends have encouraged me through this long path, even if I cannot mention all of them. Thank all of you.

Last but not least, I would like to thank my wife Katia: her patience during my sleepless nights of work and her unconditional love have inspired me when I thought I could not do it. Thank you for making me start this experience.

Abstract

In the thesis a novel modelling approach to study the plant growth is proposed. Motivated by the ability of plants to survive and develop in stressful environments, the analysis here proposed focuses on the *efficiency* of plant's growing strategies. Many mathematical models have been proposed in the literature to study plants. Here, most of them are critically reviewed. Among them it still misses a quantitative definition of what the plant is optimising during the growth. In the thesis the plant is thought as an active agent able to adapt its growing strategy to optimise something.

Both the metabolism and the movements of a plant can be assumed as functions to optimise. Firstly, a mechanistic model of the main signals driving the growth has been developed and a novel definition of the plant efficiency arises based on the metabolic needs of the plant. Then, the optimal control theory has been applied to investigate the efficiency of plant motions.

This thesis is the first application of optimal control theory to investigate plant motions while taking care of the quantitative and qualitative validation of the model with biological evidences and laboratory experiments. Such an approach is crucial to characterise the plant behaviour and to improve agricultural and ecological studies in that conditions in which laboratory experiments are difficult or expensive to perform.

Furthermore, engineers are developing a new technology of robots able to grow and move like plants. Optimal control theory is a suitable tool to translate the efficiency of plant behaviors in features to design plant-inspired robots. In this thesis, the focus is on a specific movement performed by roots during the soil penetration: the circumnutation. The results presented in the thesis help to better study the root-soil interactions (where data lacks due to the soil complexity) and to support the design of autonomous devices able to explore the soil in the most efficient manner.

In particular, the soil-root dynamics leads to a new class of optimal control problems describing phenomena in which a mechanical constrained is concerned. In this case, the investigation of the optimal trajectory does not follow in the standard manner. Then, the thesis concerns the characterisation of the optimal control for this new family of problems.

Contents

Introduction

Plants have a complex behaviour that offers many challenges to applied mathematicians interested in modelling and simulations. In particular, plants have developed, over generations, the ability to adapt their resource allocation, foraging strategies and growth according to the environmental conditions that change over space and time [1]. Such ability of processing and computing information as a response to the environmental stimuli is called *plant plasticity*, also referred to as *plant behaviour* [2, 3]. This notion of information processing in plants is crucial in biology, agriculture and ecology.

Indeed, to survive, plants must be able to optimise and exploit at the best all available resources, continuously adapting their growing strategies. To investigate the mechanisms of this adaptation, it is becoming increasingly important to understand the efficiency of plant plasticity. Here, by efficiency, it is meant the *ability to acquire resources and survive in both the presence of competition and stressful environments* [4].

Models and simulations are a useful tool in the study of plant plasticity since they can help to unravel growing mechanisms and to discern causes and effects [5]. Precise model descriptions can compress a lot of data and knowledge into a few equations. Despite approximations and simplifications, models are useful tools to synthesize data, to propose hypotheses and to make predictions. Model predictions help to set new experiments, to validate the hypothesis and to define concepts that cannot be measured in the laboratory. For example, their utility in investigating belowground interactions, where experiments are difficult to assess, and suggesting agricultural strategies to provide affordable food is well known [6, 7, 8, 9].

This thesis proposes a novel modelling approach to unveil the plant growing strategies, by introducing a performance criterion of the plant behaviour. In particular, the models here proposed estimate the efficiency of plant movements and justify the use of optimal control tools to investigate the mechanisms and signals driving the plant adaptability. In addition, the biological reliability of the models has been treated very carefully by validating the results with the experimental data in the literature.

This novel approach can be applied to investigate the behaviour of a whole plant, as well as a specific motion. For example, the root circumnutation is a widespread movement of roots that is still poorly understood [10]. The complexity of the soil and the difficulties of setting laboratory experiments

has limited the study of this peculiar movement [11]. More than biological implications, circumnutation is investigated by robotic engineers, since recent studies have proved that replacing this plant behaviour in autonomous robotic devices could reduce the mechanical work during the soil exploration [12].

Indeed, new connections between plants and robots are emerging. A novel technology of growing robots, capable of anchoring themselves, climbing, growing and moving like plants [13, 14, 15], has been inspired by the ability of plants to continuously grow to adapt their body and to survive also in the most limiting environments [16]. Furthermore, engineers are interested in the plant development mechanisms (rather than in the understanding of the plant chemical features) to design efficient plant-inspired devices.

This thesis provides useful mathematical tools to fit the needs of robotic engineers and to translate biological behaviours in robotic algorithms. This manuscript is structured as follows.

Chapter 1 is a critical review of the state-of-the-art. To grow up, the plant performs a complex series of biological and chemical processes that range from photosynthesis to resource consumption, from nutrient uptake to water transport, from internal signalling patterns to interactions with other plants and with the environment. Each of these processes is directly or indirectly involved in the growth of the plant. The variety of processes requires the application of several mathematical theories to describe each process in the most suitable manner. In the chapter, we will review some mathematical approaches proposed in the literature stressing the advantages and drawbacks of each modelling method.

In Chapter 2 of this thesis, the key processes involved in the plant growth are coupled to measure the *efficiency of a growing strategy*. In the literature, the efficiency of a growing strategy is defined only qualitative as the ability to survive (or, for plants, the biomass produced in a given environment). Quantitative formulations for such a concept have been proposed when the focus is on the efficiency of a specific process like the biomass produced concerning either the day-length (photosynthesis) or the soil content of nutrients (uptake). Here, we propose a mathematical expression to measure the plant efficiency when looking at all physiological processes and not only to a specific one. To this aim, the key signals driving the plant growth are coupled by a mechanistic model that is later validated by comparing many independent tests. The implications of the results in both agriculture and ecology are discussed.

In particular, the results of this Chapter represent a quantitative formulation of observations of Trewavas, 2009:

Plant behaviour is active, purposeful and intentional [. . .]. Plant behaviour involves the acquisition and processing of information. Informational terminology provides a suitable way of incorporating the concepts of learning, memory and intelligence into plant behaviour, capabilities that plants are rarely credited with. Finally, trade-offs, cost–benefit assessments and decision making are common plant behavioral attributes. It is suggested that intelligent assessments that involve the whole plant are essential to optimize these adap-

tive capabilities.

Motivated by such evidences, in Chapter 3 of this thesis, the previous modelling approach is specialised in the framework of optimal control theory to describe the dynamics of a parabolic root apex into an homogeneous soil. *Optimal control* deals with dynamical systems that influence themselves by adopting a strategy (or control) to optimise a given objective function over some time [17]. In this chapter, a generic device is moving into the soil under the action of a force (the control) that is relevant only at the tip and the frictional forces experienced during the motion are modelled. The objective is to minimise the dissipation of energy required by the control to oppose the friction on the tip. The model can help to estimate soil frictional forces and to address the setting of specific laboratory experiments. In particular, a direct method solves the optimal problem numerically. The results agree with the few experimental data available and strongly validate the hypothesis that the circumnutation emerges as a mechanical reaction to the soil friction. More than the biological implications, the results can be applied to robotics. The numerical simulations show how to design autonomous devices to reduce the friction during the soil penetration, further generalising the state-of-the-art [12].

In Chapter 4, the previous framework is further generalised to investigate the case of irregular shapes of the tip and heterogeneous soils. The aim is still to minimise the soil friction when a device penetrates the soil to reach a target under the action of a control. Due to the impulsive nature of frictional forces, the dynamics in this chapter is proposed as a differential inclusion with an averaged dynamic friction. The resulting dynamics is different from the classic literature [18, 19, 20]. Therefore, the chapter is devoted to study the well-posedness of the model and to characterise the optimal control that minimises the friction experienced.

Finally, chapter 5 is devoted to summarise the main results of the thesis and to discuss possible future research directions.

Chapter 1

MODELLING APPROACH FOR PLANT BEHAVIOUR AND GROWTH

In this chapter, we will review the main mathematical approaches proposed to investigate plant development and growth. Plants do not move like animals but, to acquire resources and survive and reproduce, they grow and adapt their morphology. The growth is performed adding new tissues and structures from the meristem. Meristem is the tissue in plants containing undifferentiated cells ant it is located in plant zones where the growth can take placed like the tip of organs (leaves and roots) or between mature tissues (fruits and seeds). Also, unlikely animals, plants do not have a central brain and each organ behaves like an independent entity, with different purposes. For example, leaves are devoted to the photosynthesis, fruits to the production of seeds, roots to uptake nutrients and anchorage. Therefore, a complex network of internal signals is required to drive the plant development while coordinating so many independent organs and, at the same time, exploiting the external resources. As a result, the growth of a plant is the consequence of a delicate balance between external stimuli (light, humidity, temperature, soil nutrients, herbivores, fungi and microbes, water, etc...), physiological processes (photosynthesis, uptake, circadian rhythms, transpiration, seed germination, defenses, etc...) and behaviors (starch accumulation, resource allocation, branching, primary and secondary growth, nutations, exploration, etc...). Besides, plants are used in many fields from agriculture to medicine up to manufacturing so that the study of the mechanisms underlying the plant growth is an active research field. Here we compare the mathematical approaches proposed to study the plant development at different space (from cellular level to whole organisms or entire species) and time scales (from instantaneous interactions in cells to daily movements of nutrients up to yearly and secular environmental changes).

1.1 FLUID DYNAMICS

To manage and sustain all the organs without a central brain, the plant has developed a complex and robust vascular system composed of xylem and phloem tubes. The former transport water from roots to leaves, where most of the water is lost by opening stomata to acquire CO_2 from the air (transpiration). Usually, the humidity in a leaf is around 100%, much higher than outside, so that many and many water molecules are lost for every CO_2 molecule gained. The water moves through the xylem according to the cohesion-adhesion-tension theory [21, 22]. Since molecules of water are polar, when they approach each other, the slightly negatively charged oxygen atom of one molecule forms a hydrogen bond with a slightly positively charged hydrogen atom in the other one (cohesion). The water goes up along the xylem (from roots to leaves) under the action of this attractive force. This force is made more effective by the natural adhesion of water molecules at the wall cells of the xylem and by the tension. Indeed, transpiration in leaves creates tension (differential pressure) in the leaves, that makes the water moving. In opposite to the xylem, phloem is composed of living cells and it carries sucrose from leaves (or sources) to non-photosynthetically organs (or sinks) like young leaves, roots and fruits. The main transport mechanism into the phloem, called the Munch mechanism [23, 24], is believed based on the passive osmotic pressure differences due to the sucrose gradient between sources and sinks. The diffusion of liquids from the xylem and the phloem to the organs occurs through ion-selective membranes at the cell walls.

Modelling the vascular system of a plant, the xylem is approximated to a one-dimensional porous medium, in which the water flow J obeys the *Darcy's Law*. Darcy's Law is an equation that describes the flow of a fluid in a porous medium and is derived as a simplification of the Navier-Stokes equation assuming the flow is incompressible and laminar in stationary conditions (therefore the medium is assumed to be saturated) [25]. Darcy's Law can be written as

$$J = -K\frac{\partial \Psi}{\partial x}$$

where K is the hydraulic conductivity of the stem, Ψ is the water potential and x the vertical position along the stem. Water potential quantifies the motion of water due to osmosis, gravity, hydrostatic pressure (Φ) or matrix effects such as capillary action (which is caused by surface tension). The storage of water within the plant is approximated by the xylem moisture content $\theta(t, x)$. Finally, a sink term $S(t, x)$ describes the water lost by evaporation and/or water uptaken by roots. To complete the description of the dynamics of $\theta(t, x)$, one could couple the previous Darcy's Law with a partial differential equation to describe the conservation of the quantity $A(t, x)\theta(t, x)$ along the stem (see figure 1.1(A)), being $A(t, x)$ the cross-sectional area of the tree. Examples of this approach can be found in [26, 27, 28, 29], where different formulations of both S and Ψ are proposed.

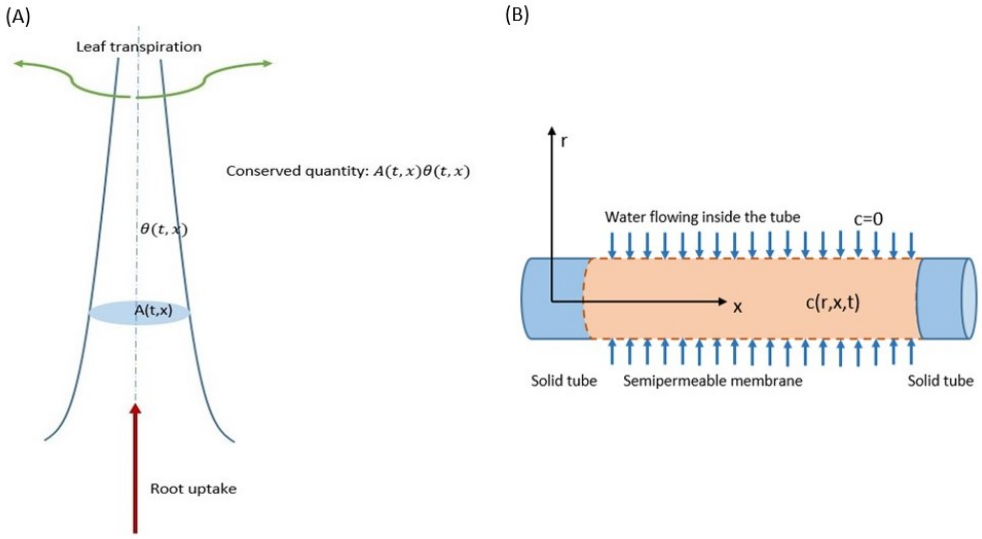

Figure 1.1: **(A) Schematic representation of a stem as a porous medium**. **(B) Framework for the Aldis flow**. A cylindrical tube has a semipermeable membrane of length L. Inside the tube the solute concentration is $c(r, x, t)$, while outside the tube there is only water ($c = 0$). The membrane is assumed to be impermeable to the solute so that the osmotic pressure makes the water flowing inside the tube (as indicated by arrows).

During this motion of the water into the xylem, the decrement of the water pressure in the direction of the flow increases the difference between the interior and exterior pressures of xylem tubes, creating a *transmural* pressure across the tube wall. When the transmural pressure exceeds a critical value, the tube collapses[30]. Therefore, the wall cells need to be strong enough to oppose transmural pressure. Furthermore, if the pressure decreases under the water vapour pressure, cavitation is expected [31]. Cavitation is the formation of bubbles (called *embolisms* in plants) that can block the flow of water. Besides the negative effects of cavitation, studies of tree water flows have discovered the role of cavitation in storing water [32, 33]. Recently, [34] has modified the formulation of conductivity K in the previous approach to take into account the effects of cavitation on the xylem water flow.

On the other hand, the flow into the phloem can be described by the *Aldis flow* [35], that models an aqueous sugar solution inside a cylindrical tube along the x axis with radius R_1. The liquid is characterised by pressure $p = p(r, x, t)$, velocity $v = v(r, x, t)$ and concentration $c = c(r, x, t)$, where $r \in [0, R_1]$. The sidewall of the cylinder is, for a length L, a permeable membrane with permeability L_p (see figure 1.1(B)). For plants, it is reasonable to assume low Reynolds numbers for the fluid into the phloem and $R_1 << L$ (lubrication assumption). Also, it is usually assumed that the water pressure around the tube is constant and, as boundary conditions, tangential no slip of the water, radial inflow of water and zero flux of the solute. Therefore, named $c =< c >_r$

and $u =< v_x >_r$ the radially averaged concentration and the axial flow speed, respectively, the radial-averaged equations describing the flow in the tube are similar to the following

$$\begin{cases} \frac{R_1}{2L_p}\frac{\partial^2 u}{\partial x^2} = RT\frac{\partial c}{\partial x} + \frac{8\eta}{R_1^2}u \\ \frac{\partial c}{\partial t} + \frac{\partial uc}{\partial x} = D\frac{\partial^2 c}{\partial x^2} + \Gamma \end{cases}.$$

In the previous equations, R is the gas constant, T the absolute temperature, η the viscosity, D the diffusivity of sucrose in water and Γ the loading term of sucrose into the stem. Examples of this approach can be found in [36, 37, 38]. More recently, to model interactions between the phloem and xylem tubes, authors [39] have proposed a discretised 1-D equation for the mass conservation to model the dynamics of the sucrose between 1 source and 1 sink.

1.2 DISCRETE APPROACH FOR WATER FLOWS IN PLANTS: ELECTRIC ANALOGY

The complexity of the partial differential equations (PDE) modelling the vascular system immediately increases when one tries to take into account the numerous branches of the system. Therefore, the description of a vascular system composed of several sources and sinks connected by xylem and phloem tubes is successfully modelled by approximating the plant to an electric circuit. An early example of this approach can be found in [40]. The xylem tube is discretised in smaller sections of resistance R and capacitance C. The capacitance represents the water storage into the xylem. Therefore, the conservation laws of the previous chapter are replaced by *Ohm's* and *Kirchhoff's laws*. In particular, the Ohm's Law is the analogue of the Darcy's Law for electrical networks and states that the current through a conductor between two points is directly proportional to the voltage across the two points. The constant of proportionality is the resistance of the circuit [41]. The Kirchhoff's laws are two equalities for the currents and the potential differences (or voltage) in the electrical circuit. The first Kirchhoff's law states that, for any node or junction, the sum of currents is zero. The second law states that the sum of voltages around any closed loop is zero [42].

The electric analogy is also used to model the phloem. Nevertheless, in this case, a solute (the sucrose) is dissolved into the water, whose potential is modified according to the *van't Hoff equation* [43]. Indeed, in the electric analogy, the water potential is replaced by the potential difference along the electric circuit. When a solute is dissolved into the water, the osmotic pressure, and therefore the potential, has to be modified according to the solute concentration. The van't Hoff equation describes this relationship. Some examples of this approach can be found in [44, 45].

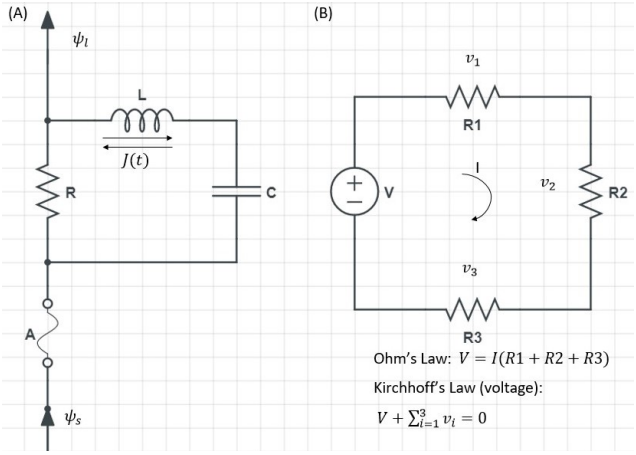

Figure 1.2: **Electric-based approach.** (A) Example of the Resistance-Inductance-Capacitance circuit. (B) Ohm's and Kirchhoff's laws for a simple electric circuit.

Modelling the vascular system by the electric analogy, authors in [46, 45, 47] have described a complex system with multiple sources and multiple sinks. In particular, it was possible to define a hierarchy between organs when allocating resources by looking at the size of the tubes in the vascular system. Finally, [48] has applied the same approach to a single-source, single-sink phloem tube with leakages, finding that the Darcy's Law assumed in the fluid dynamic approach does not hold anymore, unless to consider continuous reloading at the source. Finally, in [49] it has been proposed a resistance-inductance-capacitance circuit (figure 1.2) to model the water dynamics into the soil-plant-air system. Indeed, in a $3-$D architecture of the plant system, the water potential of leaves greatly vary with the height and the position of leaves along the stem [50, 51]. It produces instantaneous changes in the flow and introduces hysteresis effects in the dynamics. Thus, it is assumed an *inductance* effect, as instantaneous water flow rates at different parts of the plant may affect the average driving force of water flow in the plant. In addition, it is introduced a *contact potential* A which acts like a *fuse* in an electrical circuit and is susceptible to environmental stress due to more rapid decreases in root water potential than in soil water potential. The dynamics is described by

$$J(t) = \frac{\Psi_s - \Psi_l}{R} - \frac{L}{R}\frac{dJ(t)}{dt} - C\frac{d\Psi_l(t)}{dt} - \frac{A}{R},$$

where J is the water flow, Ψ_s and Ψ_l are the soil and leaf water potential respectively, R is the whole resistance offered from the xylem to the water flow, L is the inductance coefficient of the leaf biomass and C is the capacitance of the whole plant.

An early mathematical formalisation of this approach can be found in [52].

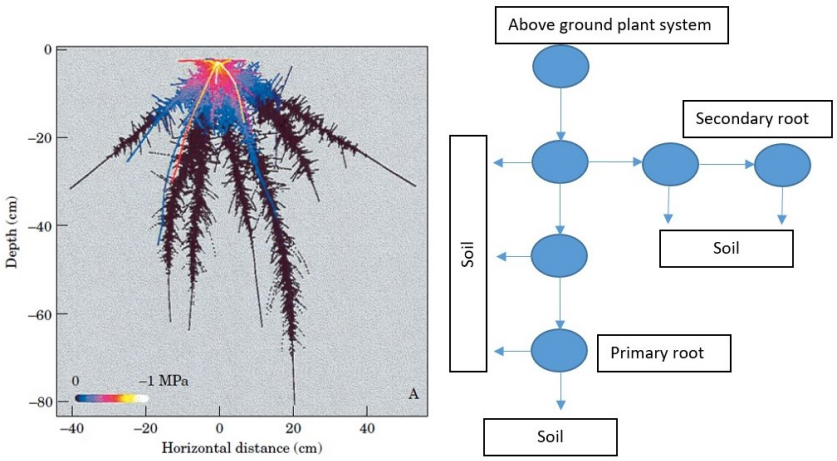

Figure 1.3: **Root system development as in [53].** Each node approximates a small part of the root and it is connected to the soil. The links of the graph follow the development (primary and secondary growth) of the root architecture.

The coupling of the electric representation with a 3-D *Richards' equation*

$$\frac{\partial \theta}{\partial t} = \nabla \cdot [K \nabla H_s] - S$$

for the water flow into the soil has provided sophisticated models of the root water uptake [53, 54, 55, 56, 57]. While the Darcy's Law describes the flow of a fluid in a saturated porous medium, the Richards' equation is a non-linear partial differential equation developed to describe unsaturated porous media. In the previous equation, θ is the volumetric water content, K is the unsaturated soil hydraulic conductivity, H_s is the total soil water potential and S is the sink term, representing the root water uptake. To take into account the growth, in [53], the root system is approximated by a graph. New connections are added to the graph to simulate the growth of roots (figure 1.3).

A possibility to approximate the sink term S in the Richards' equation consists of computing the root water uptake as proportional to the transpiration rate (depending on environmental conditions and spatial density of roots). This aim is reached introducing macroscopic parameters (like the root length density or the stress function due to the soil water potential or the compensatory function, i.e. the ability of plants to release water during the night) to summarise the development of roots [58, 59]. More recently, in [60], it was presented a novel approach that simplifies the detailed electric representation of root architecture [55, 56] and averages the local terms to extrapolate macroscopic information. As a consequence, the approach in [60], compared to the detailed representation of the root system, requires fewer parameters to estimate the soil water potential and the root-soil interactions.

1.3 DISCRETE APPROACH FOR PLANT DEVELOPMENT: FUNCTIONAL STRUCTURAL PROBLEMS

The electric analogy presented in the previous section is an example of the discrete modelling approach, is used, generally, to describe the plant growth and development [47]. In the discrete approach, the organs of a plant (leaves, roots and stem) are discretised in basic elements. The physiological processes underlying the growth are used to define algorithmic rules to add or delete new elements, defining, in the end, the architecture of the system. Some older examples of this approach with application in the root modelling can be found in [61, 62, 63, 64, 65]. More recently, in [66], authors have proposed a $3-$D description of root branching and growth combining the plant development with the nitrogen uptake and the carbon allocation.

The desire of providing computational tools to represent $3-$D plant structures while looking at the metabolic and physiological processes not only in roots but also in leaves and fruits and seeds production, has resulted in the development of discrete models, also called *Functional Structural Plant Models* (FSPM) [67]. As an example, in [68] it is modelled the carbohydrate cycling in a tree, estimating both the allocation among sinks and the annual storage. Applications of these models range from estimating limiting factors on the photosynthesis in canopies [69] and investigating the crown shapes in pines [70] to computing tree anchorage strength by measuring the mechanical strength of each root [71]. In addition, the FSPM approach has been used to describe the morphological growth of tissues and cellular growth, like in [72], where the development of vascular tubes in growing plant stems is analysed, or like in [73], focused on the bark formation during the growth.

To assist in the development of the discrete models, several formal languages have been provided. Most of them arise from the *L-system formalism* [74]. An L-system is a recursive language to produce fractal-like forms and is composed by a tuple

$$L = (A, a_0, R),$$

where A (the alphabet) is a set of symbols that can be rearranged to compose strings, a_0 (the axiom) is an initial string to start the L-system and R is the set of rules to create strings. If there is only one rule for each symbol, the L-system is deterministic. The L-system is said stochastic if, at each iteration and for each symbol, one can choose with a certain probability a rule from a set of possible rules. Associating a geometric scheme to each string, it is possible to generate a tree similar to the reality as reported in figure 1.4.

Figure 1.4: **Example of trees simulated by an L-system in 3-D.** The figure is available for free at https : //upload.wikimedia.org/wikipedia/commons/a/af/Fractal_weeds.jpg

1.4 CONTINUOUS APPROACH

As opposed to the discrete approach, in the continuous approach, the plant is described looking at the changes in size and form over time. The kinetic description of the plant is an example [75, 76, 77]. In this approach, $L(t)$ is the size of the object and its evolution in time follows the empirical law

$$\frac{dL(t)}{dt} = F(L).$$

F could be proportional to L (autocatalytic growth) or constant (linear growth) or quadratic ($F(L) = a + L(L_0 - L)$ where a, L_0 are parameters) to take into account a saturating effect. Recently, authors in [78], have proposed a $3-$D description of the kinematics of a plant organ during the growth. Previous models have focused on the kinematics of the apical tip, disregarding the three-dimensional geometry. Instead, in this work, authors propose a growth-driven model in the three dimensional geometrical framework to relate the orientation of the curvature with the differential growth of the plant organ.

Besides the kinetic models, in the continuous approach one can find the so called *dynamic models* [79]. This approach is based on two main concepts. First, the distribution of leaves, as well as the root system architecture, can be prescribed in a representative volume. This volume will depend on the environment (for example the soil structure for roots) and the genotype of the plant studied (for example the above-ground crown shape). Secondly, variations in space and time of the volume are assumed to be smooth. This approach has been used to describe the meristem dynamics. Named ρ the meristem density in a root or a stem, the conservation law follows

$$\frac{\partial \rho}{\partial t} + \nabla \cdot (\rho u) = b - d,$$

where u represents the direction of growth, b the creation of new meristem zones by branching and d the death of tissues. The branching and the death rates could be modified to take into account the availability of the nutrients. To do this, the *convection-diffusion* equation

$$\frac{\partial c}{\partial t} = \nabla \cdot (D \nabla c) - \nabla \cdot (vc)$$

describes the dynamics of the nutrient concentration c into the plant with diffusivity D and the velocity v. Applications of this approach to model the root development can be found in [80, 81, 82]. A more mathematically treatment of the same topic is presented in [83, 84]. The growth and development of aboveground biomass is, instead, described in [85].

Besides the applications for the roots and leaves development, the continuous approach has been applied to investigate both the cellular development of hormones and the interactions among different plants. Indeed, in [86], it is proposed a *reaction-diffusion equation*, coupled with an ordinary differential equation (ODE), to investigate the spatial and temporal dynamics of molecules of two hormones involved in the plant growth, the brassinosteroid and the gibberellin. On the other hand, to investigate the effects of herbivores outbreaks on plant development, in [87], it has been proposed the following 1-D model

$$\begin{cases} \frac{\partial I(x,t)}{\partial t} = R_I(I(x,t), H(x,t-\tau)) \\ \frac{\partial H(x,t)}{\partial t} = R_H(I(x,t), H(x,t)) + \frac{\partial^2}{\partial x^2}(D(I(x,t))H(x,t)) \end{cases}.$$

The first equation models the dynamics of defences I in plants as proportional to the herbivore density H after a delay τ. The second equation assumes that herbivores move away from areas according to the *Fokker Plank equation* (a partial differential equation that describes the time evolution of the probability density function of the velocity of a particle, or a herbivore in the previous system, under the influence of drag forces, or the plants' defences, and random forces, as in Brownian motion [88]).

R_H follows the logistic growth, reduced by a factor depending on the plant defences. D is the diffusivity rate, that increases linearly with the infected plants. Finally, in [89], to describe the diffusion of a plant population, the diffusion equation is replaced by an integrodifferential equation where the migration process is modelled by a *dispersal kernel*. In biology, dispersal refers to both movements of animals and plants from their born site to another one (by locomotion for animals or by seeds diffusion for plants). The average diffusion of elements in a population is modelled through functions called dispersal kernels, which give the probability distribution of the distance travelled by an individual [90]. Another example of the continuous approach is proposed in [91], to predict tropic responses of a growing plant shoot to time-varying stimuli. In here, an integrodifferential equation models the orientation of a tip. The main novelty of the paper consists of the introduction of a temporally

non-local function to simulate the experimental evidence that the plant does not react instantaneously to either the presence or absence of a stimulus but, therefore, retains a memory of its history.

1.5 OPTIMALITY

The optimal approach is a consequence of the evolution of organisms, more commonly known as the natural selection of Darwin [92]. This approach assumes that plants (or in general individuals) have differences among the same species, partially as a result of heritable features. At least part of the inherited phenotype affects the fitness of the individual [93], i.e. its ability to survive and reproduce in a competitive environment. If the heritable structures increase the fitness of single individuals, then the number of bearers of that feature should increase in frequency and the species will evolve toward a greater average in the relative fitness [94]. The optimal approach was initially applied to plants in the 1970s [95, 96, 97] and can be formulated in terms of a plant trait x that can vary in a domain X, an environmental stimulus y, a plant process modelled by the function $f = f(x, y)$ and a fitness function $F = F(f, x, y)$, which is related to the capacity of reproduction of individuals. The goal is to find the optimal trait x^* such that

$$f(x^*, y) = \max_{x \in X} F(f, x, y).$$

Typical applications include problems of resource allocation among organs [98, 99], the balance between photosynthesis and transpiration [100, 101, 102] and the timing of seed production [103].

An optimal control based approach is proposed in [104] to investigate the optimal flowering time for plants. The life-cycle of a plant is composed of four stages: the germination from seeds, the vegetative phase devoted to the growth, the reproductive phase in which the plant produces fruits and seeds and the senescence. The passage from one stage to another one depends heavily on the climate so that one can assume the whole life-cycle has to be performed in a limited temporal season. In the following let $[t_0, T]$ the season in which the vegetative and the reproductive phases can happen. Authors in [104] assume that, at the time $t \in [t_0, T]$, the plant is composed of a vegetative biomass $V(t)$ devoted to increase the productivity of the plant by growing ($F(V)$ is the biomass production rate) and a reproductive biomass $R(t)$, i.e. the fruit production. Both $V(t)$ and $R(t)$ evolve in time depending on an internal control signal $u(t)$ devoted to the biomass partitioning, as follows

$$\begin{aligned} \frac{dV}{dt} &= uF(V) \quad t \in [t_0, T], \\ \frac{dR}{dt} &= (1-u)F(V)s(t), \end{aligned}$$

where $s(t)$ is a survival function that decays exponentially. Since the reproduction is the only way in which organisms can ensure the species continue to live, authors in [104] couple the previous dynamics with the gain function

$$W = \int_{t_0}^{T} (1 - u(t))s(t)F(V(t))dt$$

and find that the optimal control $u^*(t)$ that maximise the gain function W is a bang-bang control with only one switching time

$$u^*(t) = \begin{cases} 1 & t \in [t_0, t_f] \\ 0 & t \in (t_f, T] \end{cases},$$

where t_f is the *flowering time* at which the plant stops the vegetative phase to start the reproductive stage. The result in [104] is a generalisation, to the nonlinear growth case, of results in [105, 106, 107].

Moreover, if the survival of a species depends on the frequency of individuals with a given feature or trait, then the optimisation problem can be formulated as an evolutionary game theory, i.e. the application of game theory to evolving populations in biology. A system of differential equations, called *replicator equations*, describe the evolution of individuals by ruling the born and death of new individuals and the inhered features (without mutation). The replicator equations are run repetitively with no terminal condition and the stability properties are studied. For example, in [108], the leaf development in forest herbs is investigated in the presence of competitors. More recently, the evolutionary game approach has been used to compare nitrogen fixation strategies in tropical forests [109].

For the sake of completeness, the approach presented in [110] is worthy to note. In their paper, authors propose a model for the growth of a vine stem as a curve in the 3-D space. The gravity (or more generally an external stimulus) affects the curvature of the curve, as well as the presence of obstacles and the tendency of vine stems to curl around objects. An exponential term simulates the stiffness of older parts of the stem. Finally, the optimal angular velocity that minimises the curvature while avoiding obstacles or clinging obstacles is provided. Unlikely the previous optimal models, this is the first application of optimality to describe the growth of an individual plant, more than the evolution of a population. The advantage of such an approach is the analysis of developmental mechanisms and a detailed validation could make the model a useful tool for biological investigations.

1.6 MECHANISTIC MODELS

Mechanistic approach aims to provide models able to investigate the mechanisms underlying the growth (the main drawback of continuous, optimal and fluid dynamical approach) without increasing the computational costs (as in

the discrete and electrical circuit approaches). Mechanistic models are based on detailed physiological evidence unveiled by laboratory experiments. As an example, in [111], a dynamical model of the total biomass of a young plant is coupled with a detailed formulation of the photosynthetic rate. The aim is to investigate how different chemical forms of nitrogen N uptaken affect the growth of the plant. The dynamics is described by the following two equations for the total biomass (shoots and roots) B and the nitrogen N, respectively

$$\frac{dB}{dt} = [Af_sB - \frac{dN}{dt}r_A - r_mN]\frac{y}{f_C},$$
$$\frac{dN}{dt} = u(1 - f_s)\frac{dB}{dt},$$

where A is the shoot photosynthetic rate, f_s is the fraction shoot biomass, r_A is the cost of assimilating N into biomass, r_m is the maintenance respiration of living tissues, f_C is the biomass carbon concentration and u is the N uptake per root biomass. In particular, the photosynthetic rate depends on the day-length and the nitrogen concentration, according to the biological evidence of saturating effects of light intensity on the photosynthesis production. Similarly, in [112], is modelled the nitrogen cycle in the leaves, i.e. the main chemical reactions involving the nitrogen. A different modelling approach is proposed in [113]. Indeed, an experiment is addressed to collect data about the development of root branches in a plant, to estimate an empirical distribution of probability for the emergence of lateral roots. Such a distribution has been used as a physiological rule to design a mechanistic model of auxin dynamics in roots. Another example of a mechanistic model to describe the dynamics of hormones can be found in [114]. In this paper, the cross-talk of auxin and cytokinin (two key hormonal signals in the development of primary root and emergence of lateral roots) is investigated. The dynamics proposed describes the signalling pathways at a cellular level and how interactions of the two hormones affect the root development. Other physiological processes investigated by mechanistic models are about the sucrose and starch dynamics and the circadian clock. As an example, one could refer to [115, 116, 117, 118]. Finally, mechanistic models have been successfully used to describe how interactions among different physiological processes affect the growth and the allocation of resources among organs [119, 120, 121]. As an example, in [121], the plant is assumed composed of two organs: the leaves and the roots. The leaves are devoted to the sucrose and starch production as a result of the photosynthesis. The roots are devoted to the phosphorus uptake. The number of phloem and xylem tubes to transport phosphorus and sucrose among organs is estimated. The growth is simulated modelling the dynamics of the volume of leaves and roots, while all the biological processes are computed as proportional to three *saturating functions*: the Monod function $M(x)$, the increasing Sigmoid $S^+(x)$ and the decreasing Sigmoid $S^-(x)$. For example, the volumes of leaves (V^{sh}) and roots (V^r) evolve according to the following:

$$\dot{V}^s = g^s M(V^s) S^+(C^s_{\text{su}}) S^+(C^s_{\text{ph}}),$$
$$\dot{V}^r = g^r M(V^r) S^+(C^r_{\text{su}}) S^+(C^p_{\text{ph}}),$$

where C^s_{su}, C^r_{su} are the leaf and root sucrose content respectively and, similarly, C^s_{ph}, C^r_{ph} the leaf and root phosphorus content. The model presented in the paper describes the effects of light and phosphorus on the differential growth of leaves and roots and helps to understand the resource partitioning in plants as an emergent property of many physiological and local processes in leaves and roots.

1.7 DISCUSSION

In the previous sections, the main modelling approaches proposed in the literature are reviewed. Let us note that the mathematical tools used and the processes studied are very close among different approaches. For example, the electrical analogy is often coupled with the fluid dynamic approach [122]. Or, the mechanistic approach has been coupled with the electric analogy [45] to investigate mechanisms of water flows. Nevertheless, the categories presented in the previous sections are motivated by the desire of pointing out the main plant's behaviors and processes and what are the most suitable tools to investigate them (as summarised in table 1.1).

The fluid dynamic approach is a powerful tool to model the vascular system of the plant and to model both water and sucrose flow in xylem and phloem. In ecological studies, this approach has been successfully used to estimate the impact of water uptake by roots on the soil moisture [123, 29, 27]. In addition, authors in [122] have applied this approach to investigate the adaptation of the water uptake in limiting light conditions (a.g. in presence of taller trees). Finally, in [28], the optimal sizes of leaves and vascular tubes has been estimated by modelling the water flows. On the other hand, the electrical analogy is another modelling approach to estimate the vascular system. The main difference among them is that the electric-based approach can describe, in detail, the branching and therefore, can provide accurate descriptions of the plant architecture. Moreover, the electric-based approach relies on measurable parameters with a clear physical meaning (like the resistance and the conductivity of a tube).

Anyway, neither the fluid dynamic nor the electric-based approach can investigate the plant growth since they neglect the growth-induced signals and the internal mechanisms of the plant behavior [124]. Indeed, the mechanistic approach is better suited to study and approximate the principles driving the growth. Mechanist models provide causality among processes and are used as predictive tools in agricultural and ecological studies [125]. Even if mechanistic models have been used both at the cellular and the whole organism levels, the

integration from different time and space scales is not straightforward [125]. Therefore, to simulate the development of the plant looking at the changing morphology and geometry, both the functional structural models and the continuous approach can be used. The former provides an accurate description of branching and growing organs and, due to the high computational costs, it is limited to the analysis of the above-ground or the below-ground plant architecture [67]. The latter, however, starts from oversimplified assumptions [126] but allows to simulate the morphological development of organs and tissues. Moreover, the continuous approach makes easy the coupling of morphological development with environmental changes and internal physiological processes [127].

In general, the mechanistic and the functional-structural model are used to investigate the development from the cellular level to the whole organism and are coupled for more detailed approximations [99]. On the other hand, the continuous approach relies on partial differential equations and stochastic approximations and is suited to investigate the development of entire populations [89].

Finally, quite different from the previous categories is the optimal approach. Instead of investigating the growing mechanisms or simulating the tissues, vascular systems or morphological changes, the optimal models are used to investigate new processes [94]. While the other categories are focused on supporting the biologists in those cases in which the set of experiments is expensive or difficult to be carried out, the optimal approach aims to propose a new hypothesis that can be later verified with specific experiments. When carrying out an optimal analysis, the main difficulty is the setting of the optimal problem. Indeed, specific optimal behaviors are the result of many external variables and internal processes interacting with each other. Isolating the link between an optimal result and a plant process is not an easy task [94].

This thesis aims to investigate the efficiency of the growing strategies of a plant. Therefore, the novel modelling approach can be seen as a coupling of the mechanistic and the optimal approach. Indeed, the former describes the growth in a biologically reliable manner. Then, the latter method is applied to analyse what the growing strategy is optimising. As we will see in the following chapters, this approach allows to both predict biological behaviors and provide new testable hypothesis (Chapter 2). On the other hand, the approach here proposed is suited to translate biological behaviors in robotic solutions (Chapter 3).

Table 1.1: **Summary of modelling approaches in plant studies.** By cellular we mean cells, molecules and chemical interactions among them. By tissues we mean internal structures like vascular tubes. By organs we mean the single root apex or leaf as well as the whole below-and above-ground structure. By population we mean a group of plants.

CATEGORY	METHOD	SCALE	PRO	CONS
Fluid dynamic	PDE (like Darcy's Law, Aldis flow, Richards' equation)	Tissues [28], Organs [29]	Detailed description of vascular tubes [39], predictions of water cycles in soil-plant-air system [122]	Neglects mechanisms of growth [5], Cannot describe the vascular system in its branches [124]
Electric analogy	ODE, Ohm's Law, Kirchhoff's Laws	Tissues [45], Organs [60]	Detailed development of plant architecture [52], Measurable parameters with physical meaning [124], Description of branches and resource allocation among them [47]	High computational costs [67], Expensive estimation due to an high number of parameters [60]
Functional structural models	ODE, L-system	Tissues [73], Organs [128]	Detailed simulations of branching [129] and root exudates [130], estimation of the plant growth as depending on detailed root-soil interactions [66]	High computational costs [67], Expensive estimation due to an high number of parameters [60]

Continuous approach	PDE (like conservation laws, reaction-convection-diffusion equations), dispersal kernels, ODE	Cellular [86], Organs [85], populations [89]	Morphogenesis of tissues and organs [127], reduced computational costs [131]	Oversimplified [126], many non-realistic parameters [132] to be estimated with dedicated procedures [131]
Optimality	ODE, PDE, Optimization techniques, Optimal control theory, Replicator equations	Organs [102], populations [104]	Leads to novel testable hypothesis [94]	Does not investigate internal mechanisms and it is difficult to isolate processes to optimise [94]
Mechanistic models	ODE, Saturating functions	Cellular [114], Organs [121]	Provides causality among behaviors and it is used as a powerful predictive tool [125]	Difficult to integrate different space and time scales [125]

Chapter 2

PLANT EFFICIENCY: A COMPREHENSIVE AND QUANTITATIVE DEFINITION THROUGH A PHYSIOLOGICAL PLASTIC APPROACH

2.1 BACKGROUND

While animals and other mobile organisms are capable of locomotion to escape from dangers or reach targets, the sessile life of plants has forced them to develop internal mechanisms inducing physiological and morphological adaptations [133]. For example, plants can easily adapt their sucrose allocation among organs, their foraging strategies and their growth according to extrinsic environmental conditions that often change over time and space [1]. This adaptation is called plant plasticity and often referred to as plant behavior [2, 3].

Evolution has indeed equipped plants with the ability to cope with a multitude of different internal and external signals [134]. Due to the complexity of such signal networks, plant stimulus-response pathways remain largely unknown. This lack of knowledge also limits our understanding of the fundamentals of plant plasticity. Nevertheless, mathematical models have helped in the analysis of selected signalling pathways and internal dynamics to unveil the processes driving plant behavior, as reviewed in Chapter 1. The interest in understanding plant behavior is recently increasing across multiple disciplines; starting from agronomy, to better control crops and improve productivity [9], to engineering and robotics. The latter is now promoting a new generation of robots capable of apical growth that parallels that seen in plants [135, 136].

A better understanding and definition of plant growth performance and plant plasticity (how efficiently plants grow and adapt) can help to define new design and control strategies for plant-inspired robots [16, 15, 13].

Plant efficiency has been defined as
"the ability to acquire resources and survive in either the presence of competition or stressful environments" (Younginger et al., 2017)
To date, the efficiency has been evaluated as the ratio between an output parameter (the biomass or the crop yield), expressing the result of the growth, and an input (a resource like water, nitrogen or phosphorus) that has been consumed for the growth [8].

However, growth efficiency cannot be evaluated considering a single parameter at a time, but looking at the plant as a whole and its interactions with the environment. In this chapter, we propose a novel and measurable definition for plant efficiency, which considers the needs (light and nutrients) of each organ in the plant, the biomass allocation and the costs involved in its growth. To describe the relationship between these elements we also provide a comprehensive mathematical model setting together key physiological dynamics in plants. The model has been validated with extensive and independent data collected from the literature.

The chapter is structured as follows. Section 2.2 describes the main assumptions motivating the model. Section 2.4 discusses the cases of excess and deficiency of nutrients. Section 2.5 is devoted to the parameter estimation and sets out the tests carried out to validate the model. Section 2.6 compares simulations with data collected for each test. Section 2.7 propose a new formulation to estimate the efficiency of a growing strategy. Section 2.8 carries out the Floquet analysis for the model. Section 2.9 investigates the implications of the results for biology and describes potential future steps for model improvement and generalization.

2.2 THE MODEL

2.2.1 The Plant Growth

The life cycles of most plants are divided into four main stages: germination of the seeds, a vegetative phase, flowering and maturation of fruits and senescence. Among these stages, the vegetative phase is the main focus of our analysis, since it is the period were plant development is arguably the most active, with the plant being busy in attributing resources (energy and biomass) to vegetative growth and carrying out fundamental activities, such as photosynthesis and accumulation of resources needed for the next flowering and reproductive phase [2].

For simplicity, we modeled the plant as being composed of two apparatuses and four resources. Specifically, one apparatus corresponds to the aboveground leaf biomass, used for photosynthesis, and the second represents the

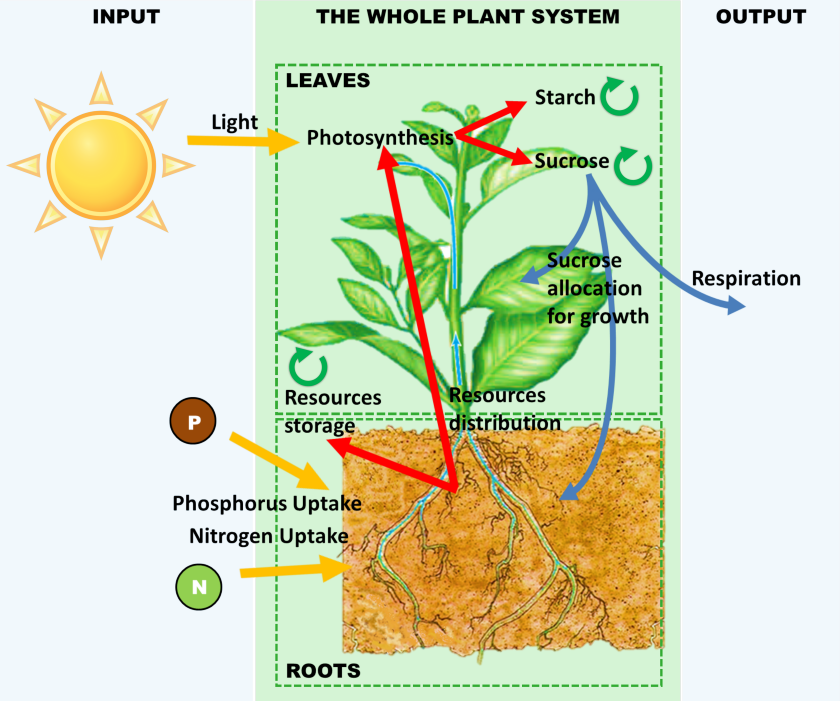

Figure 2.1: **Representation of the main plant processes and resources analyzed in the model.** The plant is decomposed into its two main apparatus characterizing the above- and below-ground: leaves and roots. The whole plant system accounts for many different functions: photosynthesis, starch production and degradation, sucrose production and consumption, root and shoot growth and maintenance, store maintenance, nutrients uptake and distribution. These functions take as inputs light, phosphorus and nitrogen, and provide feedback signals such as starch, sucrose and the stored nitrogen and phosphorus. The outputs of the system are oxygen (through respiration), morphological responses, and physiological plasticity.

below-ground biomass, mainly devoted to the nutrient uptake. From the nutrients, new resources can be generated, namely starch and sucrose. All together (starch, sucrose, nitrogen and phosphorus) constitute a set of resources that the plant can store or distribute among different organs for their consumption in order to maintain organs and stores [137], to grow and to perform chemical processes. A schematic representation of such system is presented in figure 2.1, while in figure 2.2, section 2.3, it is reported a logic scheme of the model and the related sections.

The model is composed of 11 non-linear equations, reported in details in the following sections. All the parameters are then summarised in Appendix A. We point out that that, to estimate model parameters, only data in [138] are used, while all the tests in Section 2.6 are performed from independent datasets. Recall that the biomass is assumed to be measured in grams of fresh weight (gFW). Finally, in some equations, we have introduced a small

correction factor ($\varepsilon = 1e^{-20}$) which prevents discontinuities in the model when some variables go to 0. It is only a numerical adjustment and does not affect the results of simulations.

2.2.2 Photosynthesis

The photosynthesis ($[\frac{\mu molC_6}{gFW \cdot h}]$) process is approximated as a time-dependent function describing the content of sugar produced by each gram of photosynthetically active leaf biomass:

$$p_h = \begin{cases} LCp_h^{\max} \min(n_t, p_t) & b_l \geq b_l^{\min} \\ 0 & b_l < b_l^{\min} \end{cases} \tag{2.2.1}$$

where:

- L $[-]$ is a binary function to distinguish day ($L = 1$) from night ($L = 0$). L can be easily modified in a continuous time-dependent function assuming values in the range $[0; 1]$, so to consider temperature and light intensity effects.

- C $[-]$ is a positive function in the range $[0, 1]$. It represents a limitation to the photosynthetic rate depending on the plant status. In fact, different saturating processes can affect the stomatal conductance, reducing the photosynthesis production (in [139] are reviewed many modelling approaches). Authors in [140] suggest a saturating process to avoid the production of starch and sucrose in excess. In accordance with [141, 121], C depends on the maximum starch that the plant can consume in nightly hours:

  $$C = \lambda_c + (1 - \lambda_c)(\frac{a_{\max} - a}{a_{\max}}), \tag{2.2.2}$$

  where:

  $$a_{\max} = \tau_{as}^{\max}(24 - f). \tag{2.2.3}$$

  The parameter λ_c is the strength of the feedback due to the starch stored, a is the starch content, $a_{\max}$ is the maximum starch that can be consumed at the maximum rate $\tau_{as}^{\max}$ (defined later) during the night and f is the photo-period.

- $p_h^{\max}$ $[\frac{\mu molC_6}{gFW \cdot h}]$ is the maximum rate of photosynthesis. In [116], it is fixed to $12.7\frac{\mu molC_6}{gFW \cdot h}$.

- n_t and p_t represent the nitrogen and phosphorus saturating thresholds, respectively. Both these nutrients play a role in the photosynthesis process (see [142] for an explanation of the role of nitrogen, and [143] for the phosphorus influence on photosynthesis). In fact, according to the law

of the minimum [144], the most limiting nutrient will affect the photosynthesis. By evidence in [111], the rate of carbon production obtained from nitrogen content is estimated as:

$$15.44\frac{gC}{gN \cdot h} = 2.21\frac{\mu molC_6}{\mu molN \cdot h}. \tag{2.2.4}$$

Hence, the minimum nitrogen content required to sustain the maximum rate of photosynthesis is:

$$n_{ph} = \frac{12.7}{2.21} = 5.75\frac{\mu molN}{gFW}. \tag{2.2.5}$$

The saturating function n_t can be computed as:

$$n_t = \frac{2n}{n + n_{ph}} - 1. \tag{2.2.6}$$

Not having found similar information for phosphorus, saturating function of this nutrient is estimated by assuming the consumption of phosphorus as one-tenth of the nitrogen's one, according to the estimated optimal ratio $\mathcal{O} = 10$ among these two nutrients (as reviewed in [15]). Therefore:

$$p_{ph} = \frac{n_{ph}}{\mathcal{O}}, \tag{2.2.7}$$

$$p_t = \frac{2p}{p + p_{ph}} - 1, \tag{2.2.8}$$

where n $[\frac{\mu molN}{gFW}]$ and p $[\frac{\mu molP}{gFW}]$ are, respectively, the nitrogen and phosphorus content in the plant.

- b_l $[gFW]$ is the leaf biomass (the root biomass and the total biomass will be b_r and B $[gFW]$, respectively);
- $b_l^{\min}$ $[gFW]$ is the minimum amount of leaf biomass to start the production of photosynthesis. In the whole chapter it is assumed $b_l^{\min} = b_l$ so that no limitation to the photosynthesis production is experienced by the plant. The choice is due to the fact that none of the experimental data has this situation.

In particular, if $n < n_{ph}$ or $p < p_{ph}$, then it is assumed $n_t = 0$ or $p_t = 0$, respectively, just because there are not enough resources to start the chemical processes.

2.2.3 Starch and Sucrose

The photosynthesis product can be used to synthesise starch and sucrose. The former is stored to sustain nocturnal respiration, the latter is immediately available for non-photosynthetically active tissues [145]. The amount of photosynthesis devoted to the starch production depends on both the sucrose consumption [146] and the nightly starvation [121, 147]. Independently from the night length, the starch is degraded into sucrose in a nearly linear manner (at a rate τ_{as}), such that almost all of the starch is used by dawn [145]. In addition, the circadian clock monitors the starch degradation [118]. The starch and sucrose dynamics follows:

$$\frac{da}{dt} = \gamma p_h - \tau_{as}, \tag{2.2.9}$$

$$\frac{ds}{dt} = (1-\gamma)p_h + \tau_{as} - r_m^u - r_m^t - r_m s - \eta r_g. \tag{2.2.10}$$

From now on,

$$C_s = r_m^u + r_m^t + r_m s + \eta r_g.$$

A very similar dynamic can be found in [118, 148]. Nevertheless, some important differences deserve to be outlined:

- The photosynthesis p_h in the current model is not a constant, but it is a time-dependent function depending on nutrient availability, light and sugar-signalling (as described in Section 2.2.2);
- The starch partition coefficient γ is not a constant, neither it is not estimated to assume sucrose homoeostasis (as was in [149]). It provides instead plant adaptation as a function of time (see Section 2.2.5);
- The starch degradation rate τ_{as} is simpler with respect to the dynamics proposed in [118, 148], and does not depend on subjective dusk, as in [150]. However, despite the simplification adopted here, its dynamics remains correct (see the appendix B for the demonstration);
- Similar to the work in [121], both uptake (r_m^u) and transport (r_m^t) processes are sucrose consuming, as opposed to the usual maintenance respiration (r_m);
- The rate of sucrose sent into the phloem intended for growth (ηr_g) is affected by nocturnal efficiency [147].

2.2.4 Starch Degradation

It is well established that maintenance and growth respiration occur during the day and extend overnight. The sucrose to sustain nightly metabolism is

provided by the degradation ($[\frac{\mu molC_6}{gFW \cdot h}]$) of starch stored in the morning [145], and here is defined as:

$$\tau_{as} = (1 - L) \min \left(\tau_{as}^{\max}, \left(\frac{t}{24} + (1 - \frac{t}{24})(1 - \frac{s}{s + s^{\max}}) \right) \frac{a_{|dusk} - a_{\min}}{24 - f} \right), \tag{2.2.11}$$

where:

- $\tau_{as}^{\max} = 6 \ \frac{\mu molC_6}{gFW \cdot h}$ is the maximum degradation rate estimated by the results shown in [116];
- $s^{\max} = 2 \ \frac{\mu molC_6}{gFW}$ is the maximum sucrose content in leaves, estimated by experimental values in [138]. The use of a maximum threshold is justified by the observation of negative feedback on starch degradation due to high sucrose levels [146]. On the other hand, a minimum threshold should also be expected to trigger sugar production or starch degradation in the case of starvation. According to the result in [116], $s^{\min}$ is estimated as $1.3 \frac{\mu molC_6}{gFW}$;
- $a_{|dusk} \ [\frac{\mu molC_6}{gFW}]$ is the starch content at the beginning of the night. If $a_{|dusk} < a_{\min}$, then $\tau_{as} = 0$;
- $a_{\min} = 0.15 \ \frac{\mu molC_6}{gFW}$ is the minimum amount of starch that a plant has to ensure. It is estimated by values in [118].

Hence, during the night ($L = 0$), the starch is degraded with a rate that depends both on the time t with respect to the next expected dawn (circadian clock), the sucrose signalling and the constant rate necessary to consume almost all of the starch by dawn. This strategy holds unless the required rate is greater than the maximum one. The starch dynamic here proposed has differences with respect to the one in [118], where: I) the function proposed is independent from the starch content parameter and has a peak at dawn; II) starch degradation is assumed also to exist during the light period; and III) the non-linear discontinuous function proposed takes into account the surface of the starch granule. In appendix B we compare the two approaches.

2.2.5 Starch and Sucrose Partitioning

In [146], rising levels of sucrose are explained regarding the stimulation of starch synthesis, while daily sucrose starvation decreases starch accumulation. On the other hand, nightly sucrose starvation promotes starch production [121]. Thus, the dynamics of starch-sucrose partitioning can be defined as:

$$\frac{d\gamma}{dt} = L(-\gamma \lambda_{sdr} \frac{s^{\min}}{s^{\min} + s} + (1 - \gamma) \lambda_{sdi} \frac{s}{s + s^{\max}}) + \tag{2.2.12}$$

$$+ (1 - L)(1 - \gamma) \lambda_{sni} \frac{s^{\min}}{s^{\min} + s}, \tag{2.2.13}$$

where $\lambda_{sdr}, \ \lambda_{sdi}, \ \lambda_{sni} \ [\frac{1}{h}]$ are frequency parameters to be estimated.

2.2.6 Nitrogen and Phosphorus

Photosynthesis [112], sucrose assimilation in tissues [111], respiration [121] and storage structures production [137] are metabolic activities consuming nutrients.
The nutrients reach the root surface by water flow in soil. Nevertheless, the plant can reduce or increase the uptake, according to its metabolic needs [151]. This ability is called affinity to the nutrient. The model is focused only on nitrogen (N) and phosphorus (P), since they are fundamental nutrients for growth in plants: nitrogen is an essential constituent of protein and chlorophyll, that promotes root growth, and encourages the uptake and utilisation of other nutrients [152], while phosphorus is essential for cell division, root lengthening and supports the energy carriers within the plant [153]. Moreover, in [133], it is reported that root proliferation and nutrient uptake are energy demanding operations and finding a balance between costs and gains of these two processes could explain the plastic response taken by the plant. The dynamics of nitrogen n $[\frac{\mu molN}{gFW}]$ and phosphorus p $[\frac{\mu molP}{gFW}]$ content in the plant is:

$$\frac{dn}{dt} = u_n^{\text{real}} - (r_m(s+a) + \eta r_g)c_{sn}\frac{b_l}{B+\varepsilon} - \frac{p_h}{p_h^{\max}}n_{ph}\lambda_f, \tag{2.2.14}$$

$$\frac{dp}{dt} = u_p^{\text{real}} - (r_m(s+a) + \eta r_g)c_{sp}\frac{b_l}{B+\varepsilon} - \frac{p_h}{p_h^{\max}}p_{ph}\lambda_f. \tag{2.2.15}$$

λ_f is a conversion parameter to be estimated and B the total biomass. u_n^{real} $[\frac{\mu molN}{gFW\cdot h}]$ and u_p^{real} $[\frac{\mu molP}{gFW\cdot h}]$ are the nitrogen and phosphorus uptake rates, respectively (see section 2.2.7 for details).
In [111], the cost of assimilating n into the biomass is estimated as $r_A = 4.06\frac{gC}{gN} = 0.58\frac{\mu molC_6}{\mu molN}$. Hence the n cost of assimilating C_6 can be estimated as proportional to:

$$c_{sn} = \lambda_{csn} 1.724 \frac{\mu molN}{\mu molC_6}, \tag{2.2.16}$$

being λ_{csn} a parameter to be estimated. Instead, the p cost of assimilating C_6 can be approximated using the optimal ratio value as $c_{sp} = \frac{c_{sn}}{\mathcal{O}}$ (as done in the equation (2.2.7)). In particular, metabolism, transport and growth will be reduced if the nutrient content is not sufficient to sustain the costs (c_{sn} and c_{sp}). Then:

$$\chi_{np} = \min(1, \frac{n}{s^{\max}c_{sn}})\min(1, \frac{p}{s^{\max}c_{sp}}), \tag{2.2.17}$$

$$r_m = \bar{r}_m\chi_{np}, \tag{2.2.18}$$

$$r_g = r_g\chi_{np}. \tag{2.2.19}$$

The values for $\bar{r}_m, r_g$ are reported in section 2.2.8.

The second terms of Eq (2.2.14) and (2.2.15) are the n and p costs because of the use of sucrose for maintenance and growth. Additionally, the starch

requires a maintenance respiration (and then a cost in nutrients) due to the production of storage structures [137]. Finally, the last terms of Eq (2.2.14) and (2.2.15) express the nutrient costs due to photosynthesis. Knowing the nutrient cost for the maximum rate, n_{ph} (Eq (2.2.5)) and p_{ph} (Eq (2.2.7)), the actual consumption will be proportional to the intensity of photosynthesis. Finally, the last terms of Eq (2.2.14) and (2.2.15) express the nutrient costs due to photosynthesis. Knowing the nutrient cost for the maximum rate, n_{ph} (Eq (2.2.5)) and p_{ph} (Eq (2.2.7)), the actual consumption will be proportional to the intensity of photosynthesis.

2.2.7 Nutrient Uptake

It is well established that nutrients uptake follows Michaelis-Menten kinetics [154, 155], and that plants are able to modify Michaelis-Menten parameters to be more or less affine with a specific nutrient [156, 157, 158]. Even though this adaptive behaviour has been measured by changing the nutrient content in soil [159], there are studies relating the evolution of kinetic parameters to the plant internal status (e.g., evaluating the kinetic parameters given different nutrient pre-treatments of the plants [157, 158]). In this thesis, a new modified Michaelis-Menten kinetics is proposed, in which the usual dynamics is limited or enhanced by an internal feedback control for the uptake. For nitrogen (and similarly for phosphorus), the uptake will be:

$$u_n^{\text{pot}} = u_n a_n \frac{b_r}{B + \varepsilon}, \tag{2.2.20}$$

where b_r is the root biomass. The internal feedback a_n is the strength of the uptake (as explained later). If the hourly potential uptake u_n^{pot} needs excessive sugar consumption with respect to the available one, the forage is decreased. Thus:

$$u_n^{\text{real}} = u_n^{\text{pot}} \frac{s}{s + n_c u_n^{\text{pot}} \cdot 1h + \varepsilon}, \tag{2.2.21}$$

where n_c is the sucrose consumed for the uptake (as explained later). Finally, u_n $[\frac{\mu molN}{gFW \cdot h}]$ is the nutrient uptake rate. It is well established that the uptake follows the Michaelis-Menten kinetics [154, 155]:

$$u_n = I_n^{\max} \frac{n_s}{n_s + k_n}. \tag{2.2.22}$$

$I_n^{\max}$ $[\frac{\mu molN}{gFW \cdot h}]$ is the nutrient maximum uptake, k_n $[\frac{\mu molN}{cm^3}]$ is the Michaelis-Menten constant and n_s $[\frac{\mu molN}{cm^3}]$ is a time-dependent function describing the nutrient content in the soil zone. Similar equations are defined for the phos-

phorus. The maximum values are extrapolated by values in [160, 156]:

$$
\begin{aligned}
I_n^{\max} &= 6.44 \frac{\mu molN}{gFW \cdot h}, \\
k_n &= 0.125 \frac{\mu molN}{cm^3}, \\
I_p^{\max} &= 0.4 \frac{\mu molP}{gFW \cdot h}, \\
k_p &= 0.006736 \frac{\mu molP}{cm^3}.
\end{aligned}
$$

The nutrient affinity is reduced or increased by the plant through the internal controls $a_n,\ a_p \in [0,1]$ $[-]$. Their dynamics are described as:

$$
\begin{aligned}
\frac{da_n}{dt} = (1-a_n)((1 - \frac{u_n^{\text{real}}}{u_n^{\text{real}} + C_n + \varepsilon})\frac{n^{\max}}{n^{\max} + n} + \frac{p_h}{p_h^{\max}} - a_n \lambda_k \frac{n - \mathcal{O}p}{n + \mathcal{O}p + \varepsilon}) - \\
- a_n(\frac{n}{n + n^{\min}} + \frac{n_c u_n^{\text{real}}}{n_c u_n^{\text{real}} + p_h(1-\gamma) + \tau_{as} + \varepsilon}),
\end{aligned}
\tag{2.2.23}
$$

$$
\begin{aligned}
\frac{da_p}{dt} = (1-a_p)((1 - \frac{u_p^{\text{real}}}{u_p^{\text{real}} + C_p + \varepsilon})\frac{p^{\max}}{p^{\max} + p} + \frac{p_h}{p_h^{\max}} + a_p \lambda_k \frac{n - \mathcal{O}p}{n + \mathcal{O}p + \varepsilon}) - \\
- a_p(\frac{p}{p + p^{\min}} + \frac{p_c u_p^{\text{real}}}{p_c u_p^{\text{real}} + p_h(1-\gamma) + \tau_{as} + \varepsilon}),
\end{aligned}
\tag{2.2.24}
$$

again the frequency parameter fixed to $\frac{1}{h}$ is omitted in the previous equations. λ_k is a parameter to be estimated, whereas C_n and C_p represent the nitrogen and phosphorus costs due to the actual strategy

$$
\begin{aligned}
C_n &= (r_m(s+a) + \eta r_g) c_{sn} \frac{b_l}{B + \varepsilon} + \frac{p_h}{p_h^{\max}} n_{ph}, \\
C_p &= (r_m(s+a) + \eta r_g) c_{sp} \frac{b_l}{B + \varepsilon} + \frac{p_h}{p_h^{\max}} p_{ph}.
\end{aligned}
$$

$n^{\max}$ and $p^{\max}$ describe the memory of a plant. In fact, according to the discussion in [112], plants manage their foraging strategies in order to avoid both scarcity and excess of nutrients in stores. In particular, the optimal nutrient status is defined by how many days the plant can survive, maintaining the same rate of growth, if a specific nutrient is no longer available. Since in [112] it was estimated, for herbaceous plants (such as *Arabidopsis*), a memory of 4 days, we fixed $D = 4$ $[-]$. Hence, the minimum amount of nitrogen content ($[\frac{\mu molN}{gFW}]$) required to sustain photosynthesis and respiration for one day at the maximum sugar content is:

$$
n^{\min} = ((r_m(s^{\max} + a_{\max}) + \eta s^{\max})(1 + 0.035) c_{sn} 24 + n_{ph} \lambda_f f). \tag{2.2.25}
$$

Then, $n^{\max} = Dn^{\min}$ and $p^{\max} = \frac{n^{\max}}{\mathcal{O}}$. The term:

$$(1 - \frac{u_n^{real}}{u_n^{real} + C_n + \varepsilon})\frac{n^{\max}}{n^{\max} + n} \tag{2.2.26}$$

describes the active incentive for the uptake rate according to the internal status and the cost-gain balance as reported in [133]. On the other hand, the last terms in Eq (2.2.23) and (2.2.24) represent the active limitation to the uptake due to the same concepts. Moreover, as emphasised by authors in [161], further to the active control of nutrient affinity, the uptake rate is passively increased by photosynthesis and leaves transpiration. The term:

$$\frac{p_h}{p_h^{\max}} \tag{2.2.27}$$

is used to describe this behaviour. However, since the content of nutrients in the soil is relevant in plant process dynamics [159], we additionally modelled the effects on the behaviour of the plant by considering limiting conditions of the deficiency of nutrients or the excess in soil (see section 2.4).

2.2.8 Costs

All the sucrose s produced by photosynthesis and starch degradation is used for maintenance and growth respiration costs.
As in [148], we assumed the respiration to be proportional to the sucrose content. The former has a frequency of $\bar{r}_m = 0.79\frac{1}{h}$. The frequency of loading sucrose into the phloem dedicated to grow has a frequency of $\eta = 1.98\frac{1}{h}$. However, the nightly starvation reduces the growth rate [147]. To consider this negative feedback, we reduced r_g under the parameter γ, which describes in the model the nightly efficiency of starch. Hence:

$$r_g = \min(s, s^{\max})(\lambda_g + (1 - \lambda_g)(1 - L + L(1 - \gamma))). \tag{2.2.28}$$

where λ_g is a parameter to be estimated. The minimum takes into account the physical limit of the phloem capacity in loading sucrose. The more γ increases, the more r_g decreases. Apart from maintenance and growth respiration, sucrose is consumed for the transport of carbon along the plant and for the uptake of nutrients. Authors in [121] estimate the costs of uptake phosphorus as:

$$p_c = 0.053\frac{\mu gSugar}{\mu gP} = 0.308\frac{\mu molC_6}{\mu molP},$$

with a sugar transport cost of $\bar{r}^t = 0.035$ $[-]$ (carbon consumed for each gram of carbon allocated in the phloem). The cost of nitrogen uptake (n_c) is assumed, in our model, to be the same as phosphorus (p_c), since the uptake mechanism is similar among all chemical elements. Hence:

$$n_c = 0.053\frac{\mu gSugar}{\mu gN} = 0.68\frac{\mu molC_6}{\mu molN}.$$

Named u_p^{real} $[\frac{\mu molP}{gFW \cdot h}]$ and u_n^{real} $[\frac{\mu molN}{gFW \cdot h}]$ the phosphorus and nitrogen rates of uptake, respectively, the whole uptake (r_m^u) and transport (r_m^t) costs are:

$$r_m^u = n_c u_n^{\text{real}} + p_c u_p^{\text{real}}, \tag{2.2.29}$$

$$r_m^t = \bar{r}^t (r_m s + \eta r_g). \tag{2.2.30}$$

2.2.9 Resource Allocation

Once the sucrose is loaded into the phloem, it can be devoted to the growth of tissues being allocated among organs. In particular, testing the Münch hypothesis, in [99] it is described the sucrose loading into the phloem and the resulting osmotic pressure that drives water and sucrose from source tissues (e.g., leaves) to sinks [24], where by sinks we intend all non-photosynthetically active tissues, such as roots, shaded and/or young leaves, and other storage organs [162]. The priority of each sink is defined by the osmotic pressure between the source and the sink. This description is hard to apply when the focus is on the nutrients from the soil. For example, according to results in [163], root priority increases when nutrients decrease and vice versa. In addition, authors in [164] stress that sink priority is affected by the most limiting resource and authors in [165, 166] highlight how plants are able to adapt their allocation strategies according to internal and external stimuli. The most general definition of sink priority is reported in [167]:

$$\textit{Sink Priority} = \textit{ Sink Size } \times \textit{ Sink Activity}$$

By *Sink Activity*, it is meant the efficiency of an organ, even if a mathematical formulation for it is missing and a new one is proposed later in section 2.7.

Instead of the usual definition of *Sink Priority*, in the model it is introduced a feedback signal f_r to model the priority of an organ as depending on the resources internally available, organ size and the active controls the organ is performing. In greater detail, f_r is the portion of sucrose in the phloem allocated to the roots, while $1 - f_r$ is the portion of sucrose allocated to the leaf biomass:

$$\frac{df_r}{dt} = (1 - f_r)(a_n f_n + (1 - f_n)a_p) - f_r\left(\frac{n f_n}{n + n^{\min}} + \frac{p(1 - f_n)}{p + p^{\min}} + \frac{s^{\min}}{s + s^{\min}}\right), \tag{2.2.31}$$

where $f_n = \frac{\mathcal{O}}{\mathcal{O} + \frac{n}{p+\varepsilon}}$ is a stoichiometric signal with respect to the optimal nutrient ratio $\mathcal{O} = 10$ $[\frac{\mu molN}{\mu molP}]$ estimated as done in [15]. The frequency parameter fixed to $\frac{1}{h}$ is omitted in the previous equation.
The functions a_n and a_p are the uptake signals. They describe the strength with which the plant is absorbing nutrients from the soil.
As result, the function f_r balances the nutrients demand with respect to the most limiting resource and describes the sucrose allocation between leaves and roots.

2.2.10 Growth

The growth dynamics of leaves and roots can be described with:

$$\frac{db_l}{dt} = \lambda_{sb}(1 - f_r)\eta r_g b_l - \mu_l b_l - \delta_l b_l^2, \tag{2.2.32}$$

$$\frac{db_r}{dt} = \lambda_{sb} f_r \eta r_g b_l - \mu_r b_r - \delta_r b_r^2. \tag{2.2.33}$$

λ_{sb} is a conversion parameter from sucrose to biomass. The growth, according to the specific tissue priority (f_r), will be proportional to the whole sucrose exported by photosynthetically active leaf biomass. μ_l and μ_r $[\frac{1}{h}]$ are the death rate of tissues. δ_l and δ_r $[\frac{1}{hgFW}]$ are the competitive rate due to the overproduction of leaves and roots respectively. In particular, in the literature it was not possible to find values for these parameters. For the simulations these parameters have been fixed to the small value $5e^{-6}$, assuming that, during the vegetative phase, they are negligible with respect to the growth rate, since also the experimental data do not describe this limitation.

2.3 OVERVIEW

In figure 2.2 it is reported a logic representation of the model, the main equations (according to the notation in previous sections) and, for each process, the reference section.

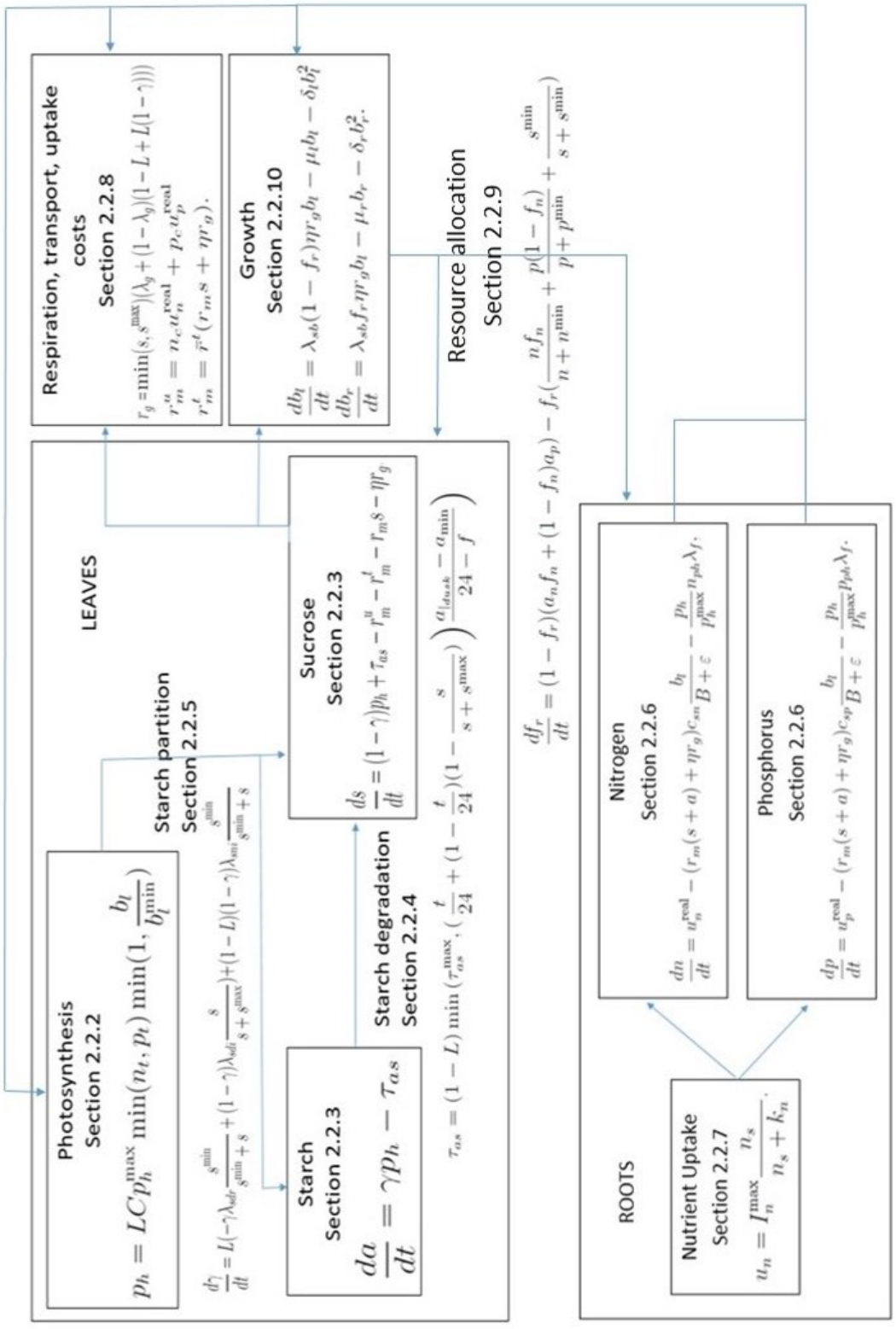

Figure 2.2: **Scheme of the model with references to each section.**

2.4 ENVIRONMENTAL CONTRIBUTIONS

The model cannot be realistic enough until the effects of toxicity or deficiency levels of nutrients in soil are not investigated. For instance, authors in [168] show that, in nutrient-poor soils, the secondary metabolism and the plant defence overcome the growth stimulus. For this reason, it is important to quantify nutrient excess or deficiency with respect to an optimal threshold. For N-free medium the value of $\bar{n}_s = 12\frac{\mu molN}{cm^3}$ is used in [169], and this value is adopted as the optimal threshold in our model for nitrogen. In [159], treatments were defined in low P content up to $0.1\frac{\mu molP}{cm^3}$, while treatments in high P content start from $0.2\frac{\mu molP}{cm^3}$. Hence, we fixed the optimal value for phosphorus to $\bar{p}_s = 0.15\frac{\mu molP}{cm^3}$. Therefore, named n_s and p_s the nitrogen and phosphorus soil contents, the excess or deficiency will be measured with respect to the distance from the defined optimal thresholds:

$$\tilde{n} = \frac{n_s}{12}, \tag{2.4.1}$$

$$\tilde{p} = \frac{p_s}{0.15}. \tag{2.4.2}$$

The increased defence-signal can be simulated by limiting the conversion parameter λ_{sb} (and therefore increasing the difficulties to grow up). The increased need for forage will lead to greater nutrient stocks. We can simulate it increasing $n^{\min}$ and $p^{\min}$. Both N and P are primary elements required for plant growth and a negative feedback should be present to consider their combined effect.
The function R^- (defined in Eq (2.4.3)) is used to reduce λ_{sb} and it is symmetric with respect to $\tilde{n}$ and $\tilde{p}$; its maximum is found in $(\tilde{n}, \tilde{p}) = (1, 1)$. Moreover, it is null if both nitrogen and phosphorus are missing in soil ($(\tilde{n}, \tilde{p}) = (0, 0)$), while all negative values are also reduced to 0.

$$g(\tilde{n}, \tilde{p}) = -\frac{1}{2}(\tilde{n}^2 + \tilde{p}^2) + (\tilde{n} + \tilde{p}), \tag{2.4.3}$$

$$R^-(\tilde{n}, \tilde{p}) = \max(g(\tilde{n}, \tilde{p}), 0). \tag{2.4.4}$$

Hence, in the model, one should replace λ_{sb} with

$$\bar{\lambda}_{sb} = \begin{cases} \lambda_{sb} R^-(\tilde{n}, \tilde{p}) & \min(\tilde{n}, \tilde{p}) < 1 \text{ (limiting soil)} \\ \lambda_{sb} & \min(\tilde{n}, \tilde{p}) \geq 1 \end{cases} \tag{2.4.5}$$

The function R^+ is instead used to increase nutrient demand and regulate deficiency conditions in soil, and it is again symmetric and positive. It has a point of minimum in $R^+(1, 1) = 1$, and an arbitrary value was fixed for $R^+(0, 0) = 139$. Hence:

$$R^+(\tilde{n}, \tilde{p}) = 69(\tilde{n}^2 + \tilde{p}^2) - 138(\tilde{n} + \tilde{p}) + 139 \tag{2.4.6}$$

and, in the model, one should replace $n^{\min}$ and $p^{\min}$ with the following

$$\bar{n}^{\min} = n^{\min} R^{+}(\tilde{n}, \tilde{p}), \tag{2.4.7}$$

$$\bar{p}^{\min} = p^{\min} R^{+}(\tilde{n}, \tilde{p}), \tag{2.4.8}$$

where $R^{+}(\tilde{n}, \tilde{p})$ is truncated to 1 if $\min(\tilde{n}, \tilde{p}) \geq 1$ (non-limiting soil).

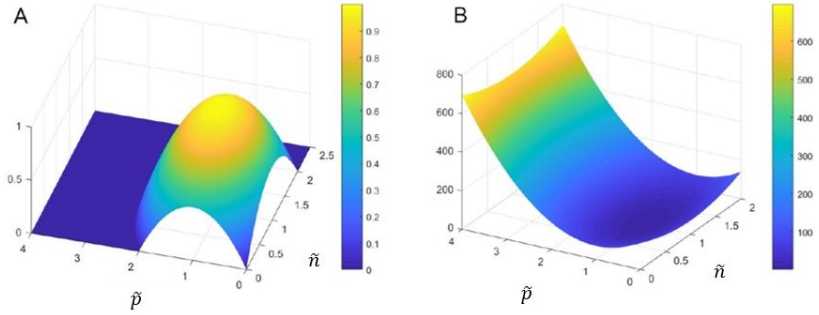

Figure 2.3: **Reduction functions.**(A) Dynamics of $R^{-}(\tilde{n}, \tilde{p})$. (B) Dynamics of $R^{+}(\tilde{n}, \tilde{p})$.

Toxicity levels of nutrients will induce negative feedback in the plant internal processes. For instance, an excess of some forms of nitrogen can change the soil pH, making phosphorus more available [170]. Other forms of nitrogen can modify the C:N soil stoichiometry and stimulate a greater demand of other micro-nutrients (with possible negative effects) [170]. Moreover, the high nitrogen content in plants can increase the secondary metabolism instead of growth [168]. Other examples relate to the phosphorus. According to evidence in [170], a high phosphorus content in soil can promote a luxury uptake of P. The plant absorbs more P than it needs, modifying the P:Fe and P:Zn stoichiometric ratios in the plant. The consequences are the same as a deficiency in Fe and Zn.
As case study, we wanted to include in our model the plant behaviour in case of luxury levels of P. To this aim, we should insert new equations for Fe and Zn dynamics and, consequently, more parameters to estimate the optimal stoichiometric ratio. However, these data are not easily available in the literature. Hence, we introduced a function in the model that simulates Fe deficiency when P content overcomes an optimal threshold. Iron is fundamental in many metabolic pathways and photosynthetic organs. In fact, in [171] it is shown that Fe deficiency affects the development of chlorophyll, limiting the rate of photosynthesis. In the paper, the authors conduct some experiments pointing out the strength of this inhibition. It can induce up to a 50% decrement in chlorophyll accumulation. Moreover, in [171], it is argued that it is not possible to induce a greater decrement. Hence, if $p_s \geq 1$, the maximum photosynthesis is reduced depending on the amount of phosphorus

excess, according to the following:

$$p_h^{\max} = \frac{12.7}{2}(1 + e^{1-p_s}). \tag{2.4.9}$$

If there is no excess, the photosynthesis does not experience any limitation ($p_h^{\max} = 12.7$). The more excess, the more reduction will occur until reaching 50%.

2.5 ACCURACY OF PARAMETER ESTIMATION AND VALIDATION

In this section, it is detailed the numerical simulation of the model and it is described the experimental set-up used to estimate the model parameters not collected by the literature. Furthermore, the tests used to validate the model are presented. It is worthy to note that to validate the model are used independent papers collected by the literature and different with respect to the paper used to estimate the model parameters.

2.5.1 Numerical Simulations

The differential equations are integrated using the numerical solver $ODE45$ of Matlab. The initial conditions, unless otherwise specified, are specified as follows. The starch and sucrose initial contents are equal to the minimum thresholds. The initial nitrogen and phosphorus contents are arbitrarily fixed to satisfy the stoichiometric ratio and above the minimum storage thresholds. The leaf and root initial biomass or their ratio are estimated from experimental results. All control signals (starch partition, uptake strength and root priority) can vary between 0 and 1 and the initial value for all of them is 0.5 to start from an equilibrium.

2.5.2 Parameter Estimation

The model accounts for a total of 33 parameters. Values for most of them are obtained by the literature, 6 are fixed arbitrarily small to not affect the dynamics because their effect is not described in the experimental data used for the validation. Only 10 parameters are estimated by fitting the biological results reported in [138]. In that work, the authors grew Arabidopsis under 5 different photoperiods ($4h$, $6h$, $8h$, $12h$, $18h$ of light) for 29 days, assuming non-limiting medium growth. From their results we obtained five fixed values and 3 parameters dependent on the photoperiod, being the plant development affected by the thermal time [172]. To verify the correctness of the fitting, we compared the dynamics of sucrose and starch content during the day and the above-ground rate of growth after 29 days. For the estimation of the parameters, only data from [138] have been used, while all the tests in section 2.4 of the main article are performed from independent datasets.

2.5.3 Accuracy of the fitting

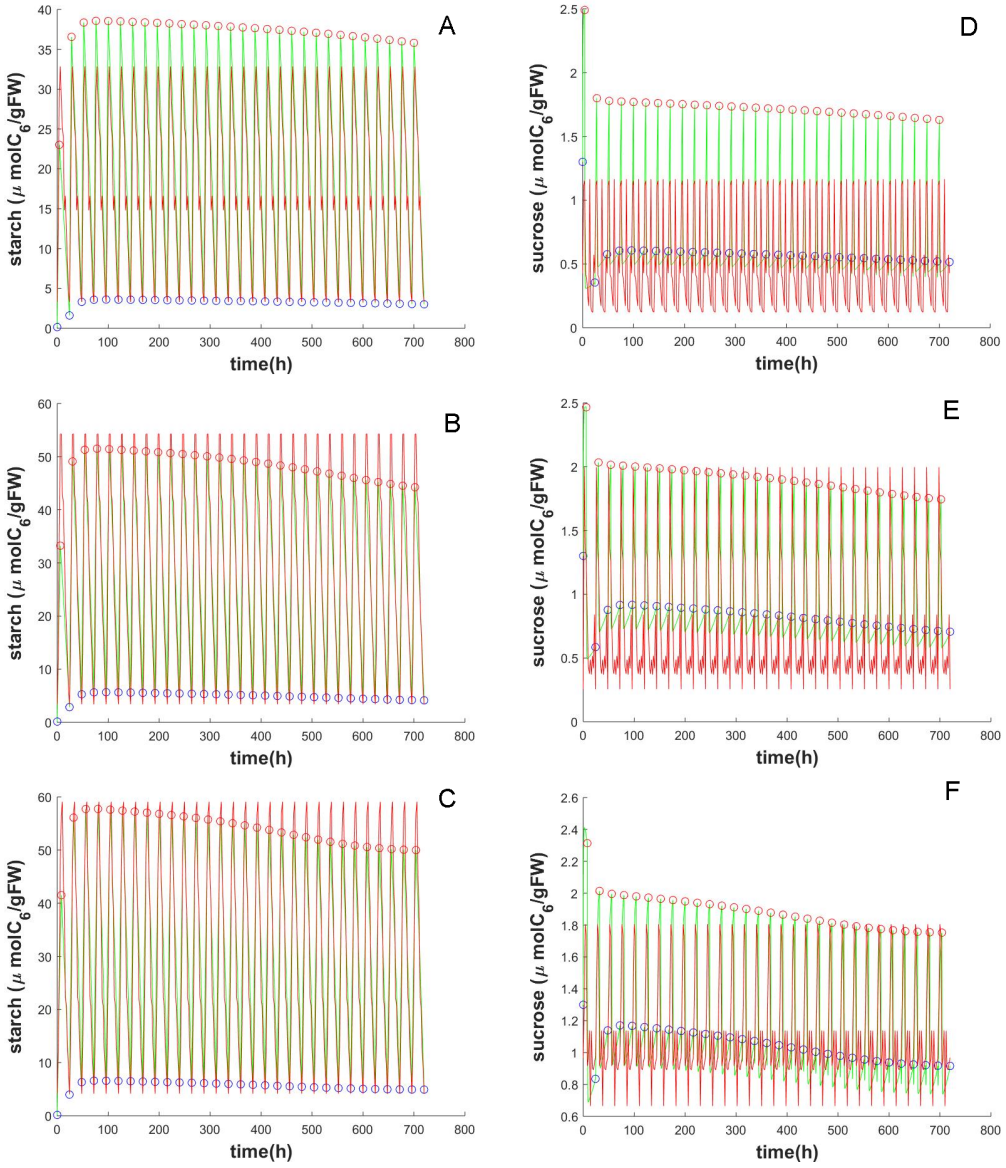

Figure 2.4: **Sucrose and starch evolution in plant growing with short photo-periods**. In red, data from [138]. In green, values from simulations. Blue and red dots indicate the dawn and the dusk, respectively. Starch (from A to C) and sucrose (from D to F) dynamics for $4h$ day length (in A and D), $6h$ day length (in B and E), $8h$ day length (in C and F).

To validate the correctness of the model the values of averaged starch and sucrose content from [138] are collected. The starch dynamics simulated by the model follows the starch content values of [138] for most of the time (figures 2.4A-C and figure 2.4A-B). The behaviour of the sucrose from numerical simulations can be considered in agreement on average with the biological

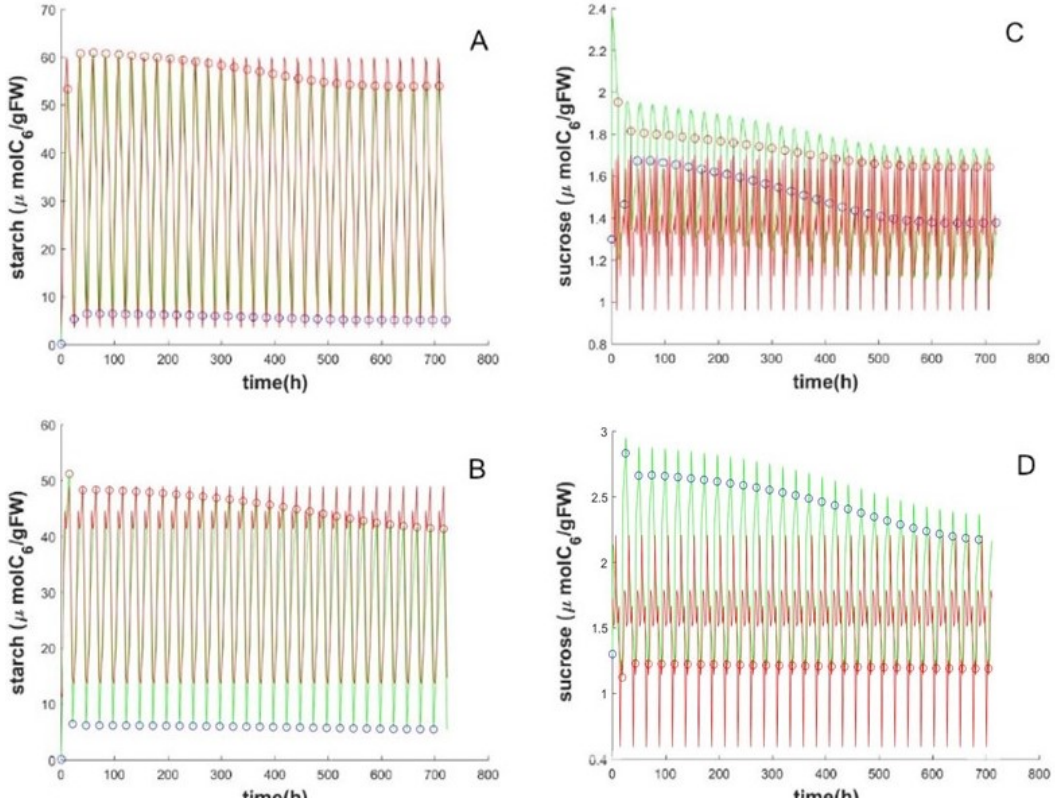

Figure 2.5: **Sucrose and starch evolution in plant growing with long photo-period**. In red, data from [138]. In green, values from simulations. Blue and red dots indicate the dawn and the dusk, respectively. Starch (in A and B) and sucrose (in C and D) dynamics for $12h$ day length (in A and C), $8h$ day length (in B and D).

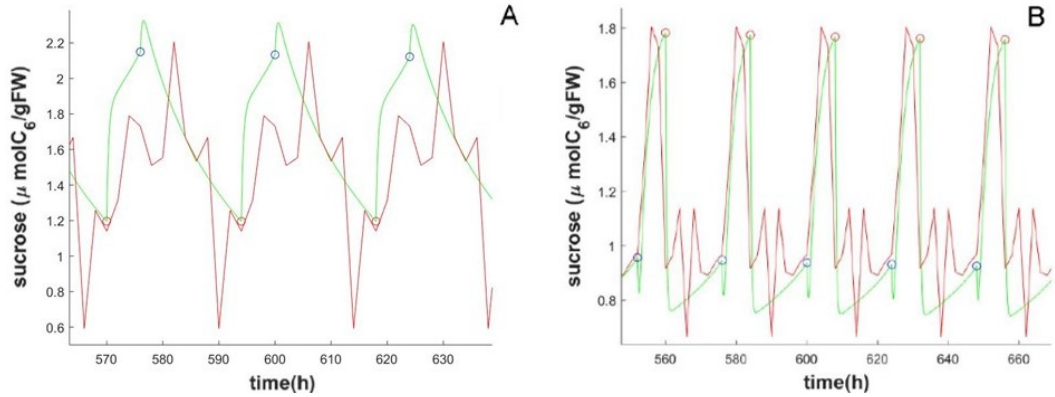

Figure 2.6: **Behaviour inaccuracies**. In red, data from [138]. In green, values from simulations. Blue and red dots indicate the dawn and the dusk, respectively.(A) Detail of sucrose content for $18h$ day length. (B) Detail of sucrose content for $8h$ day length.

data, even though less match is found between the peaks at dawn and dusk. The oscillations in sucrose content are smoothed in the model. For instance, from the $4h$ photoperiod (figure 2.4D), one can observe a single higher peak in sucrose dynamics during night obtained from the model instead of two as for the biological data. A smoother behaviour is more evident in $18h$ of light (figure 2.5D); a closer view on the oscillations for this photoperiod is reported in figure 2.6A. Another defect concerns the delay in the numerical results with respect to the experimental data. For instance, in the highest peak in the $18h$ photoperiods, the delay is approximately of $6h$ (figure 2.6A), while in the $8h$ photoperiods (figure 2.6B), there is a delay of $4h$.

Such a delay can be due to the starch degradation equation, whose formulation requires further investigations. In fact, both the delay and the smoother dynamic effects could imply an on/off mechanism with respect to some thresholds, that should first be investigated from biological experimentation. Finally, from data in [138], it has been possible to compare the Relative Growth Rate (RGR) of the above-ground leaf biomass computed as in [173]:

$$RGR(t) = \frac{ln(gFW(t)) - ln(gFW(t_0))}{t - t_0}, \tag{2.5.1}$$

where t_0 is the initial starting time. In [138], the RGR of a fresh biomass of leaves is measured at the end of the night after 29 days. The results of the comparison are summarised in Table 2.1, with a total absolute error of 3.6283 10^{-4}.

Table 2.1: The mean values of RGR.

Source	$4h$	$6h$	$8h$	$12h$	$18h$
[138]	0.068	0.1135	0.1708	0.26	0.3065
model	0.0683	0.1135	0.1708	0.2599	0.3063

2.5.4 Validation

The model has been qualitatively and quantitatively validated through multiple investigations whose numerical results were compared with biological results obtained from independent laboratories; taking care of using disjoint data sets for defining and validating the model. Five different investigations have been carried out. Specifically, 1) how the model simulates the adaptation of sucrose production to changes in day lengths, 2) the starch partition dynamics, 3) the research of an optimal stoichiometric ratio, 4) the uptake feedback in different soils assuming fixed Michaelis-Menten parameters, and 5) the biomass and root priority dynamics in limiting or toxic soils.

Effects of Abrupt Day-length Change

This test aims to verify the dynamics of the sucrose when the day-length changes, while the soil remains non-limiting. Results of [148] are used for validation. In [148], the sucrose content in the sink is measured when the day length changes from $8h$ to $16h$ and vice versa. The model is simulated for 1 day in $8h$ of light. From the 2^{nd} day, the light is $16h$ long. The opposite is simulated too and the sucrose dynamics is compared with the behaviour observed in [148]. Since the model does not distinguish between sucrose in sinks or sources, the results of this test are qualitative.

Study on the Starch Partition Dynamics

This test aims to investigate the value of the starch partition coefficient, expressed by γ, in non-limiting soils and different photoperiods. It is well known that the length of the day affects γ [148, 118]: if the day-length is longer, then the starch decreases. This relation makes also the coefficient γ lower. For example, with a photoperiod of $12h$ of light, in [174] it was obtained approximately 50% of starch accumulation. Recently, authors in [175] have verified changes in starch accumulation depending on the photoperiod length and light intensity: the higher the light intensity, the less the starch that is stored.

To compare these data, the model is simulated for 10 days of growth, in order to avoid dependence on the initial data. The average is compared with the range of values extrapolated from the previous papers [148, 174, 175].

Search for the Optimal Stoichiometric Ratio

This test aims to study the velocity of the plant in restoring the optimal stoichiometric ratio. A plant keeps the ratio between nutrients almost constant and adapts its growth strategy to recover fast the optimal ratio as soon as it is not satisfied [15]. It is fixed a day of $12h$ of light, no-limiting soil conditions and the same initial value as in section 2.5.1, except for the initial nitrogen and phosphorus values, which are in here chosen to study three different conditions: the case in which their ratio is very low (N:P= 0.5), very high (N:P= 30) or equal to the optimal one (N:P= 10) [15]. The model was run to simulate 15 days for the first case and 30 days for the others. A longer period for the optimal and high nutrients ratio has been selected since they require more time to reach periodic stationary dynamics.

In addition, in [176], it is pointed out that the optimal stoichiometric ratio is species-specific and affected by limiting nutrients, suggesting that different nutrient content into the soil affects the optimal value of N:P ratio that the plant tries to preserve. Therefore, it has been simulated a plant that is growing in $12h$ of light for 30 days, starting from settings as described in section 2.5.1 but varying the nutrient soil contents.

Study on the Uptake Dynamics

This test aims to check the uptake dynamics in poor and rich soils. In [156], it is studied the dependence of the Michaelis-Menten parameters (the maximal uptake rate $I_p^{\max}$ and the concentration with half of the maximal rate of absorption k_p) on soil phosphorus content. Different ecotypes of *Arabidopsis* are grown, for 7 days with $16h$ of light, in soils with low and high phosphorus contents. In the 8^{th} day, $I_p^{\max}$ and k_p are measured for each ecotype. Their averages ($\bar{I}_p^{\max}$ and $\bar{k}_p$) are used to estimate the hourly uptake U_1 of phosphorus, as follows:

$$U_1 = \bar{I}_p^{\max} \frac{p_s}{p_s + \bar{k}_p}.$$

To perform this test, it is fixed $I_p^{\max}$ and k_p as explained in Section 2.2.7. The soil phosphorus content is varied according to the values in [156], while the nitrogen into the soil is non-limiting. Simulations are run in $16h$ of light for 7 days. After 7 days of growth, the mean uptake in one hour U_2 is measured.

Study on Plant Growth in Extreme Soil Conditions

This test aims to analyse the dependence of the growth on limiting or toxic soils. In [177], two experiments on *Arabidopsis* are reported. Plants grow in $16h$ of light for 19 days under two different P treatments. The first treatment consists of a limited P medium ($p_s^L = 0.006 \frac{\mu molP}{cm^3}$), and the second consists of a saturated P medium ($p_s^H = 1 \frac{\mu molP}{cm^3}$). The authors measured the total dry biomass (DW) and the root:shoot ratio every 4 days. Using data from the 7^{th} day as the initial condition for the model, the dry biomass and root fraction at the 11^{th}, 15^{th} and 19^{th} days has been compared. Since the model is characterised on fresh biomass (FW), from [138] it has been estimated the relation $DW = 0.08FW$.

2.6 RESULTS OF VALIDATION

2.6.1 Effects of Abrupt Day-length Change

The dynamics of sucrose content in the sink, when there is a change in day-length, has been evaluated. According to results obtained from biological experimentation (figure 2.7A-B), the results from the model here proposed (figure 2.7C-D) show an intermediate adaptive behavior to the change in photoperiod.

2.6.2 Study on the Starch Partition Dynamics

Table 2.2 compares the values of the starch partition coefficient γ collected from the literature with the average values arising from the model. The range

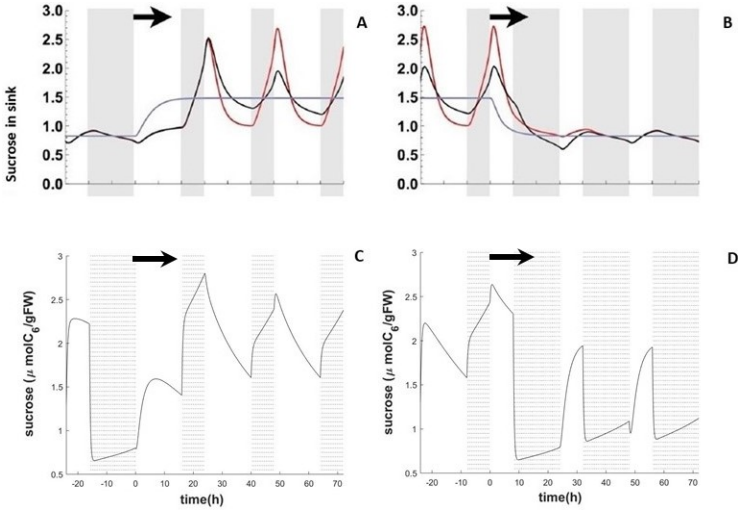

Figure 2.7: **Sucrose adaptation to photoperiod change**. (A)-(B) Dynamic of sucrose content in sinks in *Arabidopsis* from [148] when passing from $8h$ to $16h$ of light (A) and vice-versa (B). The black line refers to wild-type plants. The red and blue lines refer to different genetic types of *Arabidopsis* (that we are not considering here) and the dark period is shown in grey. (C)-(D) Dynamic of sucrose from the model when passing from $8h$ to $16h$ of light (C) and vice-versa (D). The black arrows indicate the change in the photoperiod.

.

Table 2.2: Values of γ at different photoperiods

	$6h$	$8h$	$9h$	$10h$	$11h$	$12h$
[148, 174, 175]	$[0.5; 0.69]$	0.68	0.64	0.6	0.6	$[0.36, 0.6]$
model	0.6877	0.6525	0.6285	0.6082	0.5887	0.5709

of values estimated from the literature can be very large (case of $6h$ and $12h$), but the introduction of a dependence on light intensity in the model can help to restrict this range.

2.6.3 Search for the Optimal Stoichiometric Ratio

Figure 2.8 shows how fast the plant, starting from non-optimal nutrient ratios, adapts its growing strategy in such a way as to recover and to keep almost constant the best stoichiometric ratio. This ability is called *stoichiometric homeostasis*, as well summarised by Peng et al. in their paper [178]:
Stoichiometric homeostasis is the ability of plants remaining their element composition relatively stable regardless of changes in nutrient availability, via various physiological mechanisms.

Figure 2.9 shows that the optimal stoichiometric ratio is affected by soil

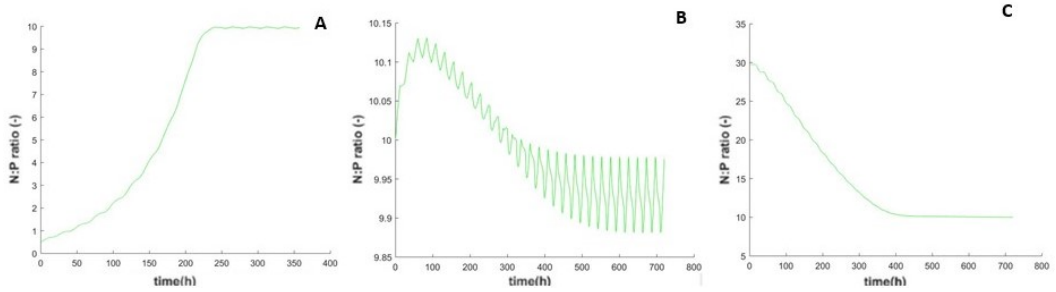

Figure 2.8: **Evolution of N:P from different initial conditions**. (A) very low initial condition (N:P= 0.5); (B) Optimal initial condition for the N:P ratio; (C) High initial condition (N:P= 30).

nutrient contents: in very limited soils, the ratio is higher. Let us note that it is possible to get wider ranges of $N : P$ ratio if the initial conditions for the plant are in agreement with the soil conditions (for example assuming lower initial resources into the plant when the soil is limiting or higher initial conditions for richer soils).

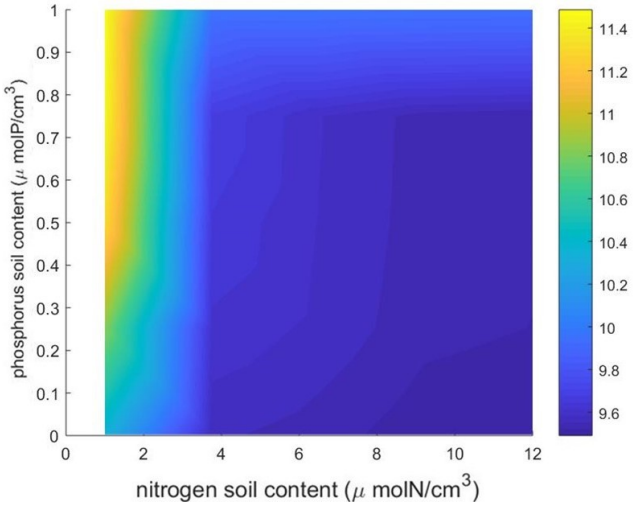

Figure 2.9: **Dependence of N:P on the soil conditions**. The colour bar expresses the N:P ratio. The condition with nitrogen equal to 12 and a phosphorous of about 0.2 correspond to a stoichiometric ratio of about 10 (the optimal value).

2.6.4 Study on the Uptake Dynamics

Table 2.3 compares the hourly uptake (U_1 from [156] and U_2 from the model) of phosphorus in rich and poor soils. Let us remark that the model can well simulate the hourly uptake measured in [156], even if the Michaelis-Menten

Table 2.3: Hourly uptake of P in poor and rich soils.

Source	$p_s = 0.0025 \frac{\mu molP}{cm^3}$	$p_s = 0.5 \frac{\mu molP}{cm^3}$
U_1	0.108	0.142
U_2	0.1075	0.185
Relative error (%)	0.46	30.3

parameters are fixed and the internal feedback drives the uptake. Let us note that the errors are affected by the fact that we could only guess the initial condition for the biomass and the nutrient content in the plant. For example, as showed in the code, by slightly modifying the initial biomass it is possible to get, for the case of the rich soil, $U_2 = 0.147$, reducing the error to 3.52%.

2.6.5 Study on Plant Growth in Extreme Soil Conditions

Table 2.4 compares data from [177] with the results from the model. On

Table 2.4: Total biomass and root:shoot biomass ratio.

Source	Parameter	Treatment	11^{th} day	15^{th} day	19^{th} day
[177]	Root fraction (%)	p_s^H	22.2	23.1	24.7
Model	Root fraction (%)	p_s^H	23	24.46	25.24
	Error		**0.8**	**1.36**	**0.54**
[177]	Root fraction (%)	p_s^L	49.4	50	54.6
Model	Root fraction (%)	p_s^L	45.36	51.53	54.9
	Error		**4.04**	**1.53**	**0.3**
[177]	total biomass (gDW)	p_s^H	0.01675	0.0398	0.057
Model	total biomass (gDW)	p_s^H	0.016	0.0392	0.0938
	Error		**0.00075**	**0.0006**	**0.0368**
[177]	total biomass (gDW)	p_s^L	0.00287	0.00425	0.004875
Model	total biomass (gDW)	p_s^L	0.0024	0.004	0.0064
	Error		**0.00047**	**0.00025**	**0.0015**

the whole, our model can predict the total biomass and the root:shoot ratio with very small errors with respect to the biological data. Such divergences, especially concerning the total biomass in the rich soil, could be induced by the approximation adopted for converting FW to DW. In fact, the water content could vary along the plant lifespan, affecting the relationship between dry and fresh weight. The evolution in time of the biomass and the root:shoot biomass ratio obtained from our numerical simulations are also reported in figure 2.10.

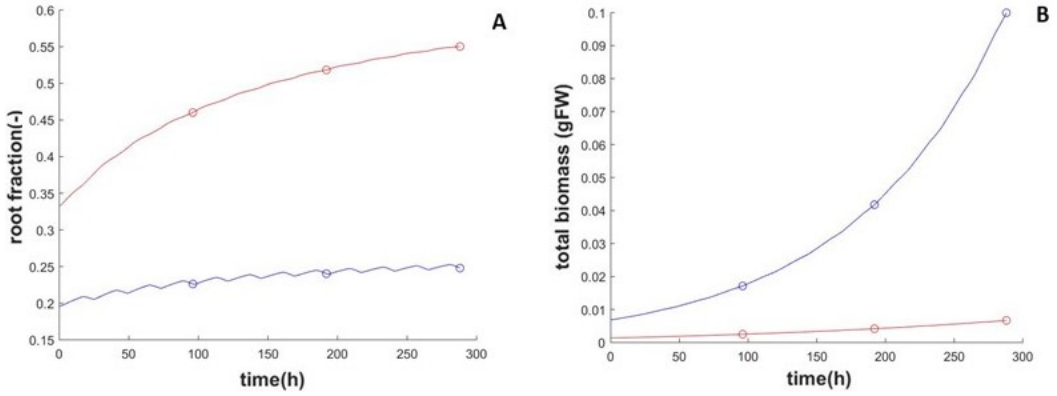

Figure 2.10: **Evolution in time of the biomass and the root:shoot biomass ratio**. In blue, simulations for the saturated P soil, while in red, simulations for the limiting P soil. Dots indicate days used for the validation. (A) Root percentage. (B) Biomass dynamics.

2.7 PLANT EFFICIENCY

By efficiency, or performance, we mean *the ability to acquire resources and survive in the presence of competition or stressful environments* [4], and in first approximation, it can be defined as:

$$\text{efficiency} = \frac{\text{output}}{\text{input}}$$

The output could be represented by the yield in crops or the total biomass in herbaceous plants [179, 8, 4]. While, the input is the resource of interest: nitrogen [180], phosphorus [181] or water [182]. Sometimes, looking at the photosynthetic products as output and the light as input, the efficiency of the photosynthesis is investigated. Nevertheless, these approaches do not provide a complete representation of plant efficiency; in fact, as pointed out in [8], the environment, the other internal plant processes, the storage structure and the other nutrients interact and affect the whole efficiency. In this chapter, a novel definition of efficiency $\mathcal{E}$ is proposed. It measures, at the end of a period, the gain in biomass and the level of resources stored with respect the nutrient soil conditions.

$$\mathcal{E} = e^{\text{RGR}} \left[\left(1 - \left(\frac{n - n^*}{n + n^*} \right)^2 \right) + \left(1 - \left(\frac{p - p^*}{p + p^*} \right)^2 \right) + \left(1 - \left(\frac{s - s^{\min}}{s + s^{\min}} \right)^2 \right) \right], \tag{2.7.1}$$

being

$$n^* = \frac{n^{\min} - 2u_n}{2},$$
$$p^* = \frac{p^{\min} - 2u_p}{2}.$$

RGR is the relative growth rate (as defined in Eq 2.5.1), n, p are the nitrogen and phosphorus contents, $n^{\min}$, $p^{\min}$, and $s^{\min}$ are the minimum nitrogen, phosphorus and sucrose thresholds, as explained in the previous sections, and u_n, u_p are the maximum uptake rates, multiplied for a conversion factor.
The exponential in Eq 2.7.1 measures the gain in the biomass and the time spent to reach it. Indeed, by the definition of the relative growth rate RGR, it results

$$e^{\mathrm{RGR}} = \left(\frac{gFW(t)}{gFW(t_0)}\right)^{\frac{1}{t-t_0}}.$$

The remaining terms measure both the sucrose, nitrogen and phosphorus stored. A plant will be efficient if it is able to grow fully exploiting resources into the soil and, at the same time, storing all nutrients needed to sustain the metabolism, still avoiding to waste them for over-filled stocks.

Coefficients in equation (2.7.1) can be changed to set a different weight for each term and, consequently, to modify the priority of each resource during the growth. Since both the deficiency and the excess of a nutrient into the soil have negative effects on the usual formulation of nutrient use efficiency [183], it is firstly verified if the behaviour of $\mathcal{E}$ agrees with the expected parabolic-like shape (figure 2.11A). Figure 2.11B plots the dynamics of $\mathcal{E}$ when the soil

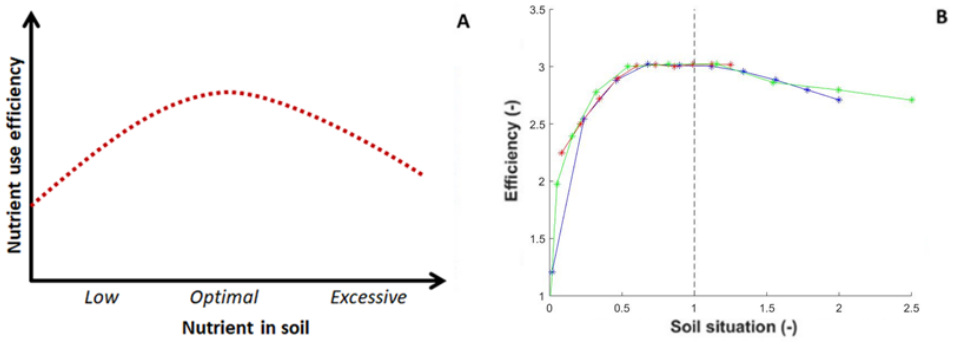

Figure 2.11: **Nutrient use efficiency in different soils**. (A) Conceptual behaviour of the nutrient use efficiency in plants at different levels of nutrient content in soil (figure adapted from [183]). (B) Values of $\mathcal{E}$ at different nutrient soil contents ($12h$ of light for 30 days). On the x axis, the product $\frac{\text{nitrogen soil content}}{\text{optimal nitrogen soil content}} \frac{\text{phosphorus soil content}}{\text{optimal phosphorus soil content}}$ with respect to the optimal one (black dashed line). In red, blue and green the cases in which respectively only nitrogen content, phosphorus content and both of them are changing into the soil.

passes from low to high nutrient contents. Let us recall that, as reported in the section 2.4, the toxic effect of nitrogen excess on the uptake is not modelled (due to insufficient data from the literature), while it is considered the phosphorus toxic case. This explains why efficiency is not affected at high levels of nitrogen contents (red line in figure 2.11B).

In figure 2.12, the level of soil nutrients is optimal and the dynamics of $\mathcal{E}$ is investigated when the starch accumulation (green line), the sucrose allocation (blue line) or the nitrogen affinity (magenta line) are kept constants or forced to change periodically but without satisfying the model (dotted red lines). The soil conditions are optimal, the day is $12h$ long and the simulations are run for 10 days. From now on, the label $\bar{\mathcal{E}}$ represents the efficiency measured once initial conditions are fixed. The label $\mathcal{E}$ represents the efficiency obtained when the previous internal signals are modified as described above. $\bar{\mathcal{E}}$ is the

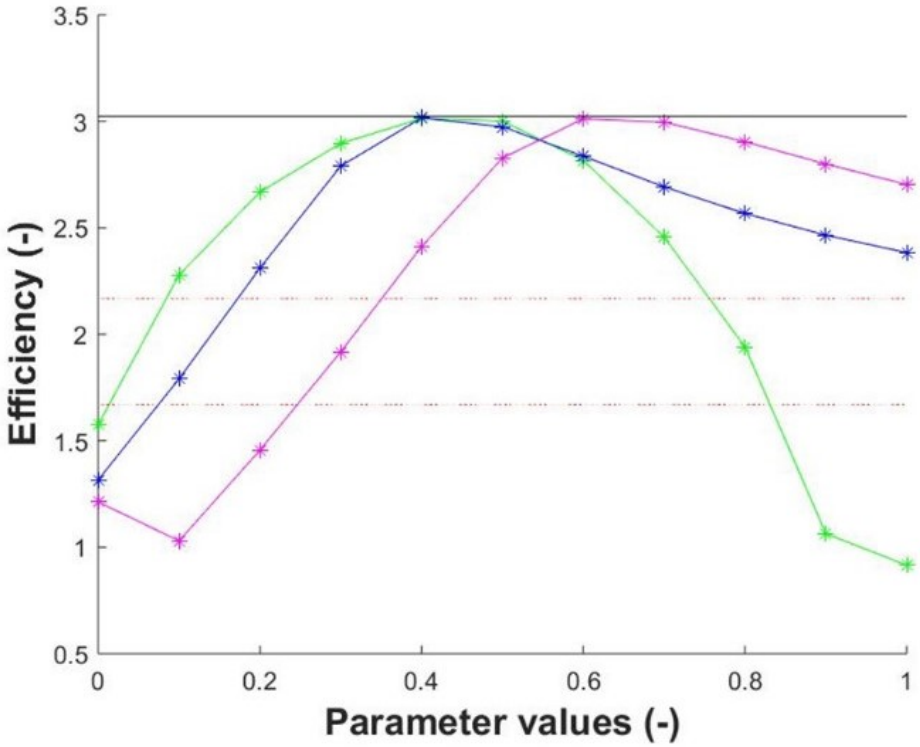

Figure 2.12: **Efficiency of the plant in optimal soil conditions**. In black, the efficiency $\bar{\mathcal{E}}$. In green, blue and magenta, the dynamics of $\mathcal{E}$ when the starch accumulation, the sucrose allocated to roots and the nitrogen affinity signals are kept constant. In dotted red lines, two examples of $\mathcal{E}$ when the previous signals are periodic but do not satisfy the model.

greatest value reached in that soil conditions. As expected, it means that the dynamics described by the model converged into the best growth strategy having maximal efficiency. The key signals described by the model aim to maximise the biomass, to minimise the stores of different nutrients, and to satisfy the metabolic needs, all at the same time. It is worth noting that $\mathcal{E}$ is computed using values of quantities easily measurable at the end of an entire growth period, disregarding, for instance, the daily costs of nutrients consumption, the costs of starvation or of sucrose overproduction, even though they are important indicators of the plant's ability to grow up (as reviewed in [184]). The choice of disregarding these costs in the definition of $\mathcal{E}$ is

dictated by the desire to propose a parameter that is simple to be measured and validated, but still able to consider all plant key signals (final biomass, final nitrogen content, final phosphorous content, and sucrose level).

To further investigate the role of instantaneous costs, the total cost due to the resources consumption and the starvation during the growth is defined as:

$$\mathcal{C} = \int_0^{t_f} \frac{C_s}{s^{\min}} + \frac{C_n}{n^{\min}} + \frac{C_p}{p^{\min}} + \rho_s dt,$$
$$\rho_s = \begin{cases} 1 & s < s^{\min} \\ 0 & s \geq s^{\min} \end{cases}.$$

t_f is the final time of simulations ($t_f = 960h$, corresponding to 40 days). C_s, C_n and C_p are the sucrose, nitrogen and phosphorus costs as described in the previous sections. ρ_s is a function that counts how long the sucrose remains under the starvation threshold during the growth. Let $\bar{\mathcal{C}}$, $\mathcal{C}$ be the total costs computed while measuring $\bar{\mathcal{E}}$ and $\mathcal{E}$, respectively. The comparison between $\bar{\mathcal{E}}$ and $\mathcal{E}$ (computed forcing γ, f_r or a_n to be constant. The constant values are reported in the appendix C) is repeated varying the soil conditions from limiting to toxic soils. The results are reported in tables from C.2 to C.4 in the appendix C. The main observation is that, for some values, $\bar{\mathcal{E}} < \mathcal{E}$. It means that it could be possible to obtain greater biomass or further reduce the resources stored, still sustaining the metabolism. Nevertheless, when $\bar{\mathcal{E}} < \mathcal{E}$, then $\bar{\mathcal{C}} < \mathcal{C}$. Therefore, it is possible to obtain greater efficiencies, but the consumption of resources during the growth is greater. Only in one case it is verified $\bar{\mathcal{E}} < \mathcal{E}$ and $\bar{\mathcal{C}} < \mathcal{C}$, but it could be due to the arbitrarily choice of coefficients in the formulation of equation (2.7.1). It means that the value $\bar{\mathcal{E}}$ can be thought as a maximal boundary in the growing strategy: it is not possible to obtain higher efficiency without further increasing the instantaneous cost of resources consumption (with disadvantages as reviewed in [184]).

This result validates the idea that plants adapt their growing strategies aiming to reach this efficient threshold. Even if it is a reasonable conclusion, $\mathcal{E}$, as the first definition of efficiency able to take into account all the key processes during the growth, represents the first strong validation of this hypothesis.

2.7.1 Root and Leaf Competition

We investigated the dynamics and relationships between biomass production and plant efficiency. As commonly accepted, a plant behaving optimally should produce biomass, in roots or shoots, until there is a net benefit. When the above-ground biomass increases, external and upper leaves shade internal and lower leaves, reducing the light intercepted and negatively affecting the photosynthesis. It is what we refer to as *leaf competition*. On the other hand, if too many roots are produced in an environment with limited nutrients, the new roots will steal the nutrients from the others and the uptake is negatively

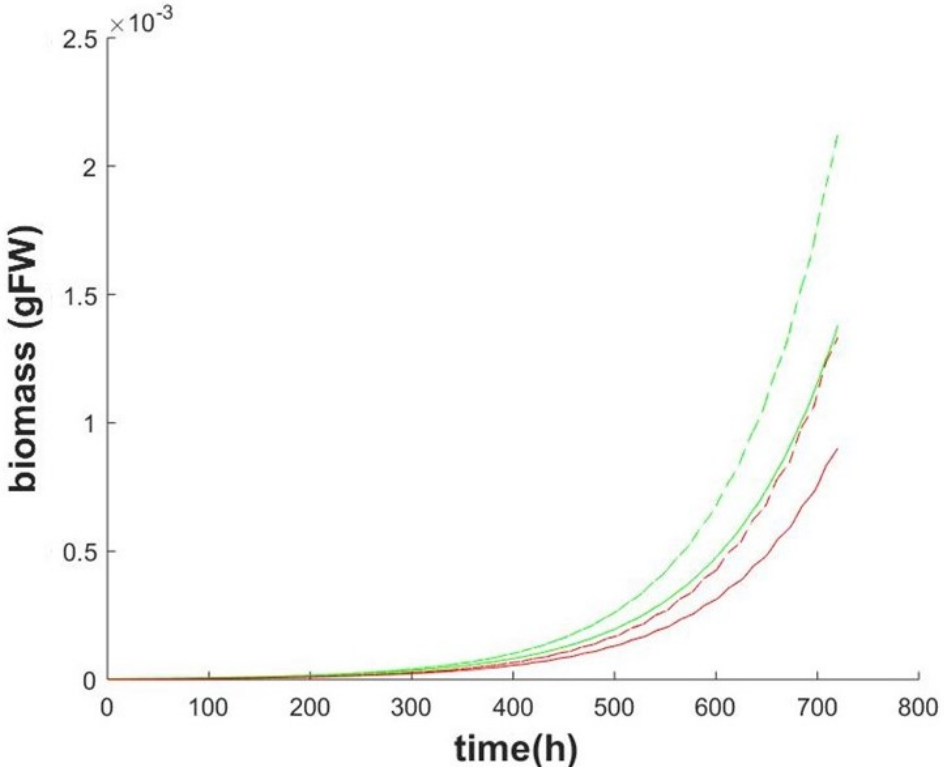

Figure 2.13: **Leaf and root biomass**. Solid lines are the leaf (in green) and the root (in red) biomass produced in optimal soil conditions at $12h$ of light. Dotted lines are the leaf (in green) and the root (in red) biomass produced in the same conditions but keeping constant at $\gamma = 0.4$ the starch accumulation.

affected. It is what we call *root competition*. In nature, the plant prevents the biomass overproduction by self-limiting growth [185].
Such behavior is also observable from the model simulations. Figure 2.13 shows a comparison between the condition in which the root and leaf biomasses are computed naturally by the model (solid lines) and the condition in which the model is computed forcing the starch accumulation to be constant at 0.4 (dotted lines). In both conditions, 30 days are simulated and the nutrient content into the soil and the photoperiod were non-limiting (nitrogen at $12\frac{\mu molN}{cm^3}$, phosphorus at $0.15\frac{\mu molP}{cm^3}$, and $12h$ light). When the model is solved with the first condition, the total biomass reached is $0.0023gFW$, with an efficiency of $\bar{\mathcal{E}} = 3.0065$. Solving the model with the second condition (where the starch accumulation is constant), higher total biomass can be reached ($0.0035gFW$) but the efficiency of the plant is lower $\mathcal{E} = 2.9686$. It means that the internal network of signals of the model is autonomously able to limit the growth to avoid overproduction and the increased resource consumption (plant physiological plasticity).

2.8 STABILITY ANALYSIS

In this section, we will investigate the mathematical properties of the ODE system presented in this chapter. The existence and the uniqueness of Charatheodory solutions will be addressed. Secondly, the main results of the Floquet theory are recalled and applied to study the stability properties of periodic orbits.

Existence and Uniqueness of Solutions

The model described in the previous sections can be summarised as the following periodic nonlinear non-autonomous non-smooth time-switched system:

$$\dot{x}(t) = f(t, x(t)) = \begin{cases} f_1(t, x) & t \in [t_0, \Delta) \\ f_2(t - \Delta, x) & t \in [\Delta, T) \end{cases}, \tag{2.8.1}$$

$$x(t_0) = x_0, \tag{2.8.2}$$

where Δ is the switching time, T is the period and $K \in \mathbb{Z}$. f is a switched vector field from $\mathbb{R} \times \mathbb{R}^{10}_+ \to \mathbb{R}^{10}_+$. According to the notations in previous sections,

$$x = [x_1, \ldots, x_{10}] = [a, s, \gamma, n, p, a_n, a_p, f_r, b_l, b_r].$$

It is easy to verify that $f(t, x)$ is bounded, continuous with respect to x for any $t \in [t_0, T]$, measurable with respect to t for any x fixed and Lipschitz with respect to x. Therefore, by applying the classic theory [186, 187], the following result holds.

Proposition 2.8.1. *Let* $\tilde{R} = \{(t, x) \in [t_0, +\infty) \times \mathbb{R}^{10}_+ : t_0 \leq t \leq t_0 + a_1, ||x - x_0|| \leq a_2,\ a_1, a_2 \in \mathbb{R}_+\}$. *Then, for the Cauchy problem* (2.8.1) *with initial conditions* (2.8.2)*, there exists a unique Caratheodory solution* $x(t)$ *for all* $t > t_0$.

Periodic orbit

Being the system nonautonomous, it is interesting to study the existence of periodic solutions, namely trajectories $x(t)$ such that $x(t) = x(t+T^*)$ for some $T^* \in \mathbb{R}$. Let us label Ψ the image, or orbit, of the periodic trajectory. The system switches at time Δ from f_1 to f_2 and at time T to come back at f_1. Thus, it is reasonable to investigate periodic solutions such that $T^* = T$. Let

$$x_0 = [a_0, s_0, \gamma_0, n_0, p_0, a_{n,0}, a_{p,0}, f_{r,0}, b_{l,0}, b_{r,0}]$$

be a given initial condition. Firstly, there exist infinite periodic orbits

$$x^p(t) = [a^p, s^p, \gamma^p, n^p, p^p, a^p_n, a^p_p, f^p_r, b^p_l, b^p_r]$$

such that $\frac{dx_i^p(t)}{dt} = 0$ for all $i \neq 3$ and

$$x_3^p(t) = \gamma^p(t) = \gamma^p(t+T) = x_3^p(t+T).$$

In particular, $n^p = n_0$, $p^p = p_0$, $b_l^p = 0$, $b_r^p = 0$, $s^p = 0$, $a^p = a^*$ where $a^* = a_{\min}$ if $a_0 > a_{\min}$ (otherwise $a^* = a_0$, being $a_{\min}$ as defined in Section 2.2.4). $a_n^p = a_n^*$, $a_p^p = a_p^*$ and $f_r^p = f_r^*$ are constants whose values depend on n_0 and p_0. Finally, γ^p can be computed analytically as dependent on parameters λ_{sdr} and λ_{sni} (see Appendix A for their meaning):

$$\gamma^p(t) = \begin{cases} \gamma_0 e^{-\lambda_{sdr}(t)} & t \in [t_0, \Delta) \\ 1 + (\gamma_0 e^{-\lambda_{sdr}\Delta} - 1)e^{-\lambda_{sni}(t-\Delta)} & t \in [\Delta, T) \end{cases}, \tag{2.8.3}$$

$$\gamma(0) = \gamma_0 = \frac{e^{-\lambda_{sni}(T-\Delta)} - 1}{e^{-\Delta\lambda_{sdr} - \lambda_{sni}(T-\Delta)} - 1}. \tag{2.8.4}$$

More than the infinite periodic orbits like

$$x^p(t) = [a^*, 0, \gamma^p(t), n_0, p_0, a_n^*, a_p^*, f_r^* 0, 0],$$

only one non-trivial periodic orbit $y^p(t)$ has been found, given an initial condition x_0 and simulating the model for $n = 800$ days. For example, let us assume non-limiting soil conditions and a day of $12h$ of light. Fix $[t_0, T] = [0, 24]$. Then $\Delta = 12$. Assume

$$x_0 = [0.15,\ 1.3,\ 0.5,\ 300,\ 30,\ 0.5,\ 0.5,\ 0.5,\ 3e^{-6},\ 1e^{-6}].$$

Running simulations for $n = 800$ days, it results an error in the detection of the periodic orbit of $|y^p(t_0) - y^p(T)| = 1.4476e - 14$, where the starting point of the periodic orbit is

$$y^p(0) = [6.1745,\ 1.5801,\ 0.6174,\ 82.2705,\ 8.1157,\ 0.2365,\ 0.4549,\ 0.2726,\ 0.1185,\ 0.0787].$$

Monodromy matrix and Floquet theory

Once a periodic trajectory is detected, its stability can be studied. Here, the orbital stability is defined as follows

Definition 2.8.2. A periodic solution $x(t)$ with orbit Ψ is orbitally stable if, given $\varepsilon > 0$ there exists $\delta > 0$ such that $\inf_{z\in\Psi} ||f(t,x) - z|| < \varepsilon$ for all $t > 0$ and all x such that $\inf_{z\in\Psi} ||x - z|| < \delta$. It is orbitally asymptotically stable if it is orbitally stable and (by choosing δ smaller enough) $\inf_{z\in\Psi} ||f(t,x) - z|| \to 0$ as $t \to +\infty$.

As usual, a periodic solution is (orbitally) unstable if it fails to be stable by this definition. The following definition will be useful too ($\mathbb{B}$ represents the unit ball in $\mathbb{R}_+^{10}$).

Definition 2.8.3. A set $\mathcal{S} \subseteq \mathbb{R}^{10}_{+}$ is called *locally stable* if and only if there exists $\varepsilon > 0$ such that, for all $x_0 \in S + \varepsilon\mathbb{B}$

$$\inf_{y \in \mathcal{S}} ||x(t) - y|| \to 0, \text{ for } t \to +\infty,$$

being $x(t)$ a solution of the system (2.8.1) with initial condition x_0.

In the case of nonlinear systems, like the model presented in this chapter, we can study local stability of periodic solutions by linearising the dynamics (2.8.1) in a neighborhood of a periodic trajectory $x(t)$ and getting the following linear system with periodic coefficients

$$\dot{x} = A(t)x = \begin{cases} A_1(t) & t \in [t_0, \Delta) \\ A_2(t - \Delta) & t \in [\Delta, T) \end{cases}, \tag{2.8.5}$$

where

$$A_1(t) = \frac{\partial f_1}{\partial x}\Big|_{x^p(t)}(t),$$
$$A_2(t) = \frac{\partial f_2}{\partial x}\Big|_{x^p(t)}(t),$$

and $A_1(\Delta) \neq A_2(\Delta)$. To simplify the study without affecting the system, we will replace $A(t) = A_3(t)$ for all $t \in [\Delta - \tau, \Delta + \tau]$ where $A_3(t)$ is a linear transformation such that $A_3(\Delta - \tau) = A_1(\Delta - \tau)$, $A_3(\Delta + \tau) = A_2(\Delta + \tau)$ and τ small enough.

The Floquet theory is useful to study the linear stability of periodic nonautonomous differential equations [188]. The Foquet theory aims to find a coordinate change that transforms the periodic system

$$\dot{x}(t) = A(t)x \tag{2.8.6}$$
$$x(t_0) = x_0, \ A(t) = A(t + T) \text{ for some } T > t_0, \ A \text{ continuous} \tag{2.8.7}$$

to a linear system with constant, real coefficients [189]. The main object of FLoquet theory is the *state transition matrix* $\Phi(t, t_0)$, a matrix such that

$$x(t) = \Phi(t, t_0)x_0, \ \forall \ t \geq t_0.$$

Since the dynamics (2.8.6) has a unique solution, also $\Phi(t, t_0)$ is uniquely determined. In particular, $\Phi(t, t_0)$ is called principal fundamental matrix of (2.8.6), since the following matrix differential equation is satisfied

$$\dot{\Phi}(t, t_0) = A(t)\Phi(t, t_0), \ \Phi(t_0, t_0) = I, \tag{2.8.8}$$

being I the identity matrix. The Floquet's theorem claims that $\Phi(t + T, t_0 + T) = \Phi(t, t_0)$. The matrix $M = \Phi(t+T, t)$ is known as the *Monodromy matrix*. The eigenvalues of a monodromy matrix are called the *characteristic multipliers*. As reported in [189], it can be proved that characteristic multipliers are time independent. This observation makes the study on characteristic multipliers crucial to study the stability properties of the linear system (2.8.6). In particular, the following result holds (see for example [190]).

Theorem 2.8.4. *The origin is uniformly stable for the linearised system* (2.8.6) *if and only if the characteristic multipliers are in the unitary disk and the multipliers on the boundary of the disk have multiplicity* 1*. As a consequence, the periodic trajectory is locally orbitally asymptotically stable.*

2.8.1 Computational results

Let us fix $[t_0, T] = [0, 24]$, $\Delta = 12$ and optimal soil conditions. The Monodromy matrix is computed by approximating the Jacobian by finite differences and solving the differential equation (2.8.8) through the classic Runge-Kutta method of 4th order. In the case of a trivial periodic orbit

$$x^p(t) = [a^*, 0, \gamma^p(t), n_0, p_0, a_n^*, a_p^*, f_r^*, 0, 0],$$

one can choose, without loss of generality, $a_{n,0} = 1,\ a_{p,0} = 1,\ f_{r,0} = 0.5$ and γ_0 as in (2.8.4). The Floquet multipliers are

$$\rho = [1;\ 2.7496e{-}11;\ 0.0437;\ 1;\ 2.7496e{-}11;\ 1;\ 1;\ 2.7496e{-}11;\ 0.9417;\ 0.9417].$$

Since there is more than one multiplier on the boundary of the unit disc, the Floquet theory cannot be used to address the stability of $x^p(t)$.

Remark. *The set*

$$\mathcal{S} = \{x^p(t) |\ x^p \text{ trivial periodic solution}\}$$

is a locally stable set. Indeed, choosing

$$\epsilon < \min\{\frac{\mu_l}{\eta}, \frac{\bar{r}_m s(0) b_l^{\min}}{p_h^{\max}}\},$$

it holds that

$$|s_0 - s_0^p| = s(0) < \epsilon \leq \frac{\mu_l}{\eta},$$
$$|b_{l,0} - b_{l,0}^p| = b_{l,0} < \epsilon \leq \frac{\bar{r}_m s(0) b_l^{\min}}{p_h^{\max}}.$$

Therefore, $s(t), b_l(t) \to 0$ *and* $x(t)$ *will tend to a periodic orbit* $z_\epsilon^p \in \mathcal{S}$ *whose components depend on* x_0*.*

In the case of the non-trivially periodic orbit $y^p(t)$, with starting point

$$y^p(0) = [6.1745,\ 1.5801,\ 0.6174,\ 82.2705,\ 8.1157,\ 0.2365,\ 0.4549,\ 0.2726,\ 0.1185,\ 0.0787],$$

the Floquet multipliers are

$$[1,\ 0.8791 + 0.0889i,\ 0.8791 - 0.0889i,\ 0.6057,\ 0.1520,\ 0.0726,\ 0,\ 0,\ 0,\ 0].$$

One multiplier is 1, as expected for the periodic orbits. The remaining ones are in the open unit disk. Therefore, $y^p(t)$ is locally orbitally asymptotically stable (see figure 2.14).

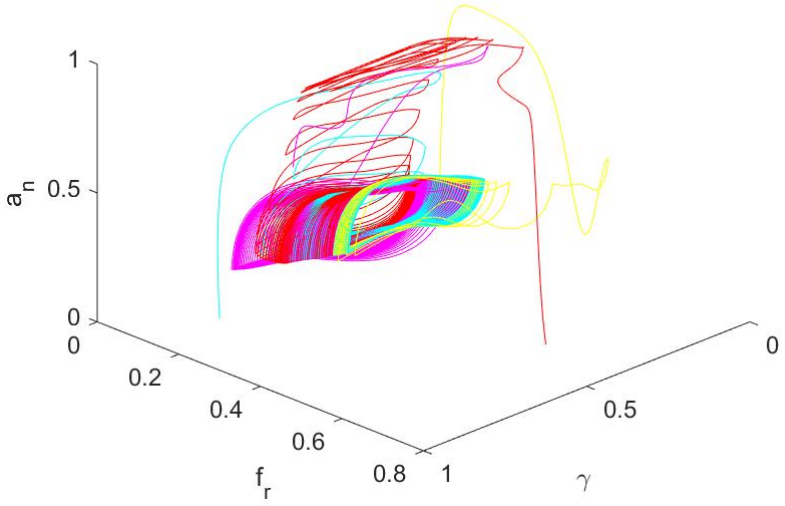

Figure 2.14: **Example of locally orbitally stable periodic solution**. Four different initial conditions are chosen and only three variables are showed. The orbit is reported in green.

2.9 DISCUSSION

The model presented in this chapter attempts to describe, even though with some simplifications, the whole plant system with a detailed overview of the key signals driving the growth. By signals, it is meant the products (e.g., starch, sucrose, nutrients) of key internal processes (e.g., photosynthesis, nutrients uptake, resource accumulation and consumption) that are activated as a growth strategy by the plants in response to external stimuli and internal conditions. The model is able to predict the dynamics of these internal signals which have been confirmed by biological data (see section 2.6). To test the robustness of the model, the biomass, sucrose dynamics, photosynthesis partitioning rate, uptake strength, and sink priorities are compared with a large data-set of biological data collected from the literature. All validation tests showed high accuracy in the results and very small errors (e.g., we obtained 3.52% as the maximum relative error in nutrient uptake comparisons (section 2.6.4) and 4.04% as a difference in estimating resources allocation in limiting soils (table 2.4)).

The model can be used to better define biological concepts and processes. It can become a powerful tool for the study and validation of biological hypothesis (which also might consider the introduction of additional dynamics, e.g., light, temperature, starch degradation, respiration or exudation), and it can describe and explain complex behaviours, thus helping to find the signals driving the plant plasticity.

The main result presented, is a novel definition for the plant efficiency (see section 2.7). In the literature, some equations compute the efficiency of the plant as the total biomass achieved given the amount of a nutrient into the soil. These formulations are used in agriculture to estimate the forage to seed to ensure a desired crop yield. Nevertheless, they do not consider many factors that affect the wellness of the plant, with possibly negative consequences both for plants and soils [8].

The novelty of the proposed definition is that it arises from a global view of the plant, taking into account the main external and internal factors affecting the growth. The formulation of this chapter has been thought to be easy to compute and, therefore, it is based on measurable quantities that could be gathered at the end of the growth period. Indeed, it measures the biomass and the resources stored with respect to the soil conditions. In addition, the formulation aims to describe the ability of the plant to exploit soil nutrients to grow up, to store resources to sustain the metabolism and to avoid to waste resources due to overfilled stocks. This novel definition of efficiency includes and extends the previous definitions (figure 2.11) and could be used both for agricultural and ecological issues. In agriculture, it can be used to better estimate the foraging, for example considering, at the same time, the consequences on the yield of the light, the nitrogen and the phosphorus. In ecological studies, the model can help to investigate how the efficiency of the growth is modified in limiting environments, analysing how to prevent damages to the plant. Finally, one could couple the model with genetic studies and compare different growing strategies modifying the internal signals (see section 2.7).

This novel definition of efficiency validates the idea that plants adapt their growing strategies aiming to reach an equilibrium among biomass and resources stored. Even if it is a reasonable conclusion, the proposed formulation is the first definition of efficiency able to take into account all the key processes during the growth and represents the first strong validation of this hypothesis. In addition, the novel definition of efficiency arises from biological assumptions linked in a mathematical model that has been strongly validated with the existing literature. It allows both biologists and mathematicians to further investigate the internal signals highlighted in the model and how they interact and affect the plant plasticity.

The model can now be extended and generalised in order to include additional dynamics.

Firstly, in the current model, it has neglected the water distribution which can be introduced in two manners: explicitly, coupling the model with a Richards' equation for the flow of water outside and inside the plant [29, 122]; implicitly, describing the effects of water into the soil on the accessibility to nutrients.

Secondly, it has assumed a homogeneous and non-limiting distribution of CO_2, humidity and temperature. All the three parameters affect the photosynthetic rate [191, 192], and their effects can be taken into account by

replacing the constant maximum photosynthetic rate of our model with specific functions [111, 112].

Thirdly, two nutrients (nitrogen and phosphorus) useful for plant growth are investigated. However, equations analogues to those of nitrogen and phosphorus can be adopted to include all other nutrients, with very few changes according to specific dynamics.

Moreover, due to the scarcity of data from the literature, the effects of tissues death and overproduction are not explicitly modelled. Nerveless, natural stop in biomass production in those conditions where intra-plant competition was emerging is observed.

Finally, the current model did not consider the spatial distribution of roots and leaves. The generalisation requires the introduction of partial differential equations to model the movement of each root or leaf as independent organs interacting with each other and it will be the topic of future works.

Nevertheless, the model is able to provide new information. For example, it can be used to forecast the optimal biomass with respect to specific soil conditions, or anticipate the sucrose production adaptation to changes in nutrients into the soil. In addition, it can be estimated the role (or affinity) of nitrogen on the phosphorus uptake and vice-versa or the role of both nitrogen and phosphorus on the photosynthesis. This model can thus also adopted to evaluate the reasons behind specific plant plasticity (e.g., why it is putting more effort in growing shoot instead of roots or vice versa).

Chapter 3

OPTIMAL CONTROL OF PLANT ROOT TIP DYNAMICS IN SOIL

3.1 INTRODUCTION

In Chapter 2, a mechanistic model is developed by looking at the internal and external signals driving the growth. The model proposed is then used to suggest a quantitative formulation for the plant efficiency that takes into account all the metabolic necessities of a plant during the growth. Applications of such a novel definition span from agriculture to ecology to genetics. Instead of studying the efficiency of a plant as a whole organism, one can focus on a specific organ of the plant or a peculiar movement or a single process. The aim could be to investigate what the plant is optimising while performing a task. In Section 1.5 we have reviewed some examples of this approach such as the optimal amount of sugar among organs or the survival of a species. In particular, the control theory has been already applied to investigate the optimal flowering time of a plant or the optimal curvature of a growing stem to avoid obstacles. Here, we propose a novel application of the optimal control theory to both investigate the efficiency of root's movements into the soil and translate such motions in robotic strategies for soil exploring devices.

Indeed, a plant root grows into the soil driven by attractive targets (e.g. nutrients or water) while avoiding obstacles [193]. Under non-stressful biological and chemical conditions, root growth mainly depends on the mechanical strength of the surrounding soil and the presence of obstacles at the root tip [194]. When exploring soil, a root apex must overcome the resistance of the surrounding environment [11].

It is well known that roots move by growing at the tip level and has been proven this strategy facilitates the soil penetration [135]. Also, to reduce the soil resistance, the root apex produces exudates and mucus [195], or it might adapts its morphology by reducing the elongation rate and increasing

the root diameter [196]. Furthermore, it has been hypothesised that, in roots, a characteristic motion strategy called circumnutation could be adopted to facilitate penetration and improve the seedling of the plant [197].

Circumnutation is a widespread motion strategy adopted by most plant roots and stems, who was first observed by Darwin [198]. It consists of elliptical, circular, pendulum-like or zigzag-shaped movements [199]. In the case of regular motions (circular or elliptical), we can distinguish the amplitude ρ, namely the radius of the movement, and the period T to complete one lap. Several studies have investigated the origin and biological processes driving this pattern of motion [10, 199]. It has been shown that circumnutation is induced by different growth rates along opposite sides of the organ [10], and it is thought to be driven by both gravitropism and internal periodic signals [200, 201, 202].

Recently, the ability of roots to efficiently move into the soil has inspired novel robotic technologies for soil exploration, penetration and monitoring [16, 136]. However, to accurately replicate a plant's growth dynamics in robotic devices, it is crucial to fully characterise the motion strategy employed by a root's apex to reduce soil friction and the role of circumnutation in performing this task. Nevertheless, circumnutation in roots is a process still poorly understood, mainly because of the lack of data.

Collection of experimental data is limited by two main factors. First, the response of soil to the forces actuated by a growing root is complex to characterise. Soil is a mixture of organic matter, minerals, gases, liquids and organisms, where the arrangement of these distinct components defines the soil type, its texture and behaviour, in response to external forces [203]. This makes the detailed description of the dynamics of an object moving in soil an open problem [204]. Second, plants have evolved differently in response to the environment, resulting in a wide diversity of genotype across species and phenotype over the same species. As a result, similar growth conditions can produce very different root behaviour [205, 206]. Hence, considering the complexity of soil composition and plant genotype and phenotyping, generalising such conditions for the characterisation of a specific pattern of motion such as root circumnutation remains challenging.

To reduce such a degree of complexity, previous studies have conducted direct experiments on plants using homogeneous media, such as agar or phytagel [207, 208, 209]. However, the results from these studies are difficult to generalise to real soil conditions, and are therefore not readily translatable to plant-inspired robotic systems. In a more recent study [12], it has been proposed an experimental framework to analyse the circumnutation of a robotic tip into topsoil. Here, the experimental setting confirmed that circumnutation, when applied to a robotic tip travelling into soil, reduces friction compared to straight penetration and, consequently, the energy spent by the plant-inspired robotic system.

Another way to study the root growth in real soil reducing previous limitations is represented by mathematical modelling. Models can help to investi-

gate the root growth and motion by describing the physical root-soil interactions. For example, in [11] the existing mathematical models of root growth in soils are combined with the macroscopic observations of root behaviours to estimate the magnitude of some of the frictional forces experienced by the root apex. The study has shown that the forces acting on the root flank can be neglected assuming a quasi-static root growth. They have also shown that the macroscopic root growth can be investigated looking at the water potential flow inside the cells.

However, these models are not suitable for the study of dynamical interactions between roots and soil, such as the ones described by oscillatory patterns of motion. In addition, models focused on cellular growth cannot be easily translated to robotic applications, because of the mechanical and macroscopic nature of engineering systems for soil penetration.

All the previous limitations make the study of specific movements, such as circumnutations, still an open question and a great challenge for modelling. Investigations on the patterns of motion during root growth can lead to solutions fundamental in agriculture to improve the uptake, in civil engineering and soil sciences to stabilise slopes and in robotics to design efficient penetration devices.

For the first time, in this paper we want to investigate and describe the dynamics of a root penetrating into the soil by approaching the problem with optimal control theory methods. In the model, the root moves under the action of a control signal, without any *a priori* assumption on the root's dynamics, and we study which motion of the root apex minimises the friction with the surrounding soil. We formulate the minimising control function defining the framework of forces acting at the tip and translating the physical constraints of the root-soil interaction into the constraints of the control problem. We then use the proposed model to estimate the dynamics of a root apex penetrating into the soil in the presence of different mechanical stresses. We demonstrate that the optimal motion strategy adopted by plant roots follows an oscillatory pattern similar to circumnutation movements.

In the following, we first introduce the framework in which the system is moving, the forces involved, and we formalise the optimal control problem we aim to solve (Section 3.2). We then validate the model (Section 3.3) and study the effects of soil compactness and tip shape on the energy consumption (the work done by the system) (Section 3.4.1). We finally investigate on the optimal trajectory emerging at different soil compactness (Section 3.4.2), and we conclude with final discussions and open questions (Section 3.5).

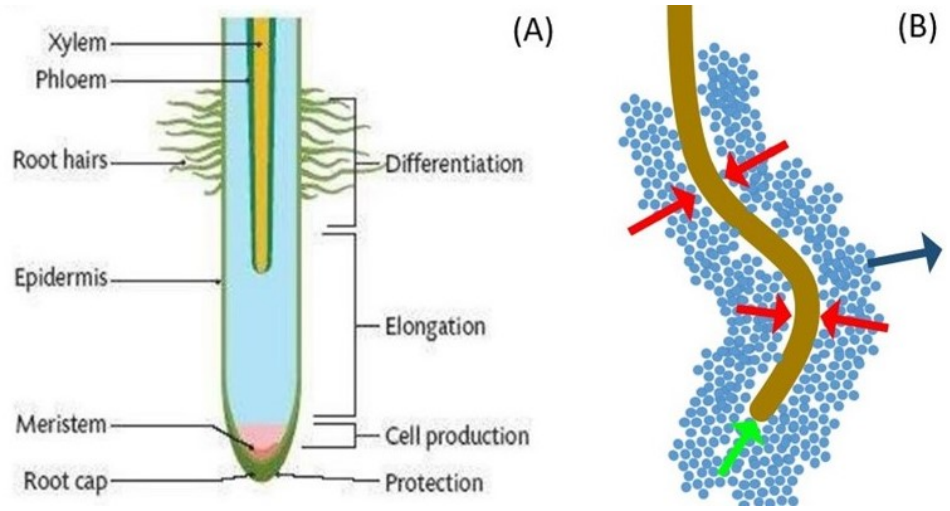

Figure 3.1: **Analysis of the root tip growth**. (A) Zonation of a generic root apex. In the elongation zone there is a fast growth. Into the meristem the growth is slower. Specialised cells are formed into the differentiation zone. The root cap protects the tip and senses the environmental stimuli. (B) In a homogeneous soil, the tip penetration affect the soil structure rearranging the soil particles (blue arrow). On the other side, the soil opposes to this rearrangement by exerting a lateral confinement (red arrows) and an axial friction (green arrow).

3.2 METHODS

3.2.1 Model setting

In this section, we will describe the root movement into the soil under the action of forces by using a system of ordinary differential equations (ODEs). To this aim, let us first observe that the forces acting on the root are relevant just at the tip (since plant roots move by growing from the tip [210]) and that root penetration tasks are better accomplished by conical or parabolic tip shapes [211, 212, 204], similar to the root apex (figure 3.1(A)).

Let us imagine a conical or parabolic device immersed into the soil for which the relevant variables are the diameter d, the height h and the axis of symmetry $a \in \mathbb{R}^3$. The shape of the device is assumed constant during all the time evolution, so that only the axis $a = a(t)$ will depend on time, according to the position of the device into the space. Let $x(t),\ v(t) \in \mathbb{R}^3$ and $u(t) \in U \subset \mathbb{R}^3$ be the position, the velocity of the vertex and the accelerating force, or control which drives the root growth, respectively. Here,

$$U := [-u_m, u_M]^2 \times [-u_m, u_M - g]$$

is the set of control values and $u_m,\ u_M > 0$ are the maximum deceleration and acceleration values that can be produced by the device and depend on its

physical and mechanical constraints. We use g to denote the vertical downward gravitational acceleration. The frictional forces are modeled assuming that the root tip has a regular external surface and that the soil produces a uniform friction on it when the root moves and grows. These assumptions are reasonable in the case of a continuous medium (when the root diameter is bigger than the average soil particle diameter) [11], but they may no longer be valid in heterogeneous soils.

When a conical or parabolic tip is moving into the soil, we can distinguish three main frictional forces. First, the axial friction (blue arrows in figure 3.1(B)), due to the soil resistance to penetration. Second, the lateral confinement (red arrows in figure 3.1(B)), as a result of the soil particles that oppose to being moved. Third, the drag force [213, 214], a dissipative and non-conservative force that acts on any object partially or totally immersed in a fluid or in a granular medium. The latter force is anti-parallel to the velocity. The axial friction and the lateral confinement oppose to the control $u(t)$, reducing the pushing acceleration driving the tip. Let $F_s^{\max}$ be the maximal resistance offered by a fully compressed soil. Then the control $u(t)$ is reduced in a real soil according to the relation

$$u(t)(1 - F_s(t)),$$

where

$$F_s(t) = F_s^{\max} \frac{k}{k^{\max}} R(t).$$

Here, k $[\frac{g}{cm^3}]$ labels the soil density, while $k^{\max}$ indicates the maximum density reached by the soil when compressed. Let us note that $F_s(t) = 1$ when the control is not able to overcome the soil friction. This is the case, for example, of a root tip that encounters an obstacle and cannot break it. Finally, as showed in [12], the soil friction is affected by rotations of the device during the soil penetration. These rotations rearrange particles and break up the granular structure, reducing the friction experienced by the tip. Here, we propose the following formulation in order to model the friction experienced by the tip:

$$R = \left(1 - \frac{\sqrt{v_1^2 + v_2^2}}{|v| + \mu}\right)^{\lambda_1 \frac{k}{k^{\max}}(1 - \frac{k}{k^{\max}})|cos\alpha|}.$$

In the previous equation (where we have neglected the time dependence to not burden the notation), $v = (v_1, v_2, v_3)$ is the velocity and $\lambda_1,\ \mu$ are parameters whose values are reported in table 3.1. The parameter $\mu << 1$ is used only to ensure the well-posedness the evolution equation (3.2.1) for velocity such that $|v| << 1$. The angle $\alpha \in [0, \pi]$, that the versor $a(t)$ forms with the vertical direction $-e_3 = (0, 0, -1)$, takes into account the interaction of the tip surface with the soil when the device is not directed along the vertical direction. The term

$$[1 - \frac{\sqrt{v_1^2 + v_2^2}}{|v| + \mu}]$$

measures the strength of the rotation (as showed in Section 3.3). The power exponent of R reduces its action when either the tip lateral surface which interacts with the soil is maximum (namely if $cos(\alpha) \to \pi/2$) or when the soil is compressed (and there are no particles to rearrange) or when the soil density is very low (and the rearrangement of soil structures has no evident effects). As for the drag force, it is a dissipative and non-conservative force that acts on any object that is partially or totally immersed in a fluid or a granular medium. Since the soil is a complex mixture of solid and fluid structures [215], the drag force should be a combination of these properties [204, 216]. In particular, in the case of an object immersed in a fluid with a speed $|v|$ relatively high with respect to the fluid velocity, the drag force is proportional to $|v|^2$ [204]. On the other hand, at relatively slow speed, namely when no turbulence phenomena occur, the drag force is linear with respect to v [217]. We will assume a linear dependence of the drag force on the velocity since the root moves relatively slow with respect to the water and the air flows into the soil. Furthermore, the experiment proposed in [12], and here used to estimate model parameters, provides a tool for studying a robotic tip that moves as fast as a root, thus the linearity assumption of the drag force with respect to v is still valid. Therefore the drag force F_d is a function depending on the velocity of the tip v, the lateral surface of the device S_l, the soil density k and the rearrangement of particles R that reduces the friction. These properties are expressed in the equation

$$F_d = R\lambda_2(k, k^{\max})\frac{S_l}{S_l^c}v,$$

where λ_2 is a parameter estimated in table 3.1. For a conical tip of height h and radius r, $S_l = \pi r\sqrt{(h^2 + r^2)}$, whereas for a parabolic tip, $S_l = (\pi r)((r^2 + 4h^2)^{(3/2)} - r^3)/(6h^2)$. $S_l^c = 2\pi rh + \pi r^2$ is the soil interacting surface of a cylinder of height h and radius r. The ratio S_l/S_l^c measures the tapering of the tip that results in a smaller experienced drag force [204]. Therefore, the resulting system for the dynamics of the tip (at the position $x(t)$ with velocity $v(t)$) in the time interval $[t_0, T_f]$ is

$$\begin{cases} \dot{x}(t) = v, \qquad t \in [t_0, T_f] \\ \dot{v}(t) = u(1 - F_s) - F_d \\ (x(t_0), v(t_0)) = (x_0, v_0) \in \mathbb{R}^6,\ t_0 \geq 0,\ T_f \geq t_0 \end{cases}, \tag{3.2.1}$$

being u the control, whose action is opposed by the soil frictional effect F_s, while the drag force F_d acts regardless of the presence of the accelerating force u.

In the previous equations, the choice of a control $u : [t_0, T_f] \to U$ will determine a specific trajectory $x(t)$ with velocity $v(t)$. In accordance with the usual definition of work *force*$\times$*displacement*, here we can compute the work performed by the control strategy $u(t)$ as

$$W = \int_{t_0}^{T_f} M^* |\langle u, v\rangle| ds.$$

Since $[u] = [cm^2/s^2]$, a scaling factor $[M^*] = [kg]$ is required in order to make the definition of the work W computed by the control $u(t)$ dimensionally consistent (see table 3.1 for the units of measurement). Furthermore, the absolute value is necessary to take into account the non-conservative nature of the forces acting on the root tip, thus avoiding negative work values.

3.2.2 Optimal control

The main contributions of this paper will be achieved by estimating the optimal trajectory for the tip that minimises the dissipated energy W. To be more precise, consider the control $u : [t_0, T_f] \to U$, the angle $\alpha : [t_0, T_f] \to [0, 2\pi]$ and the solution $y(t) = (x, v)(t)$ of (3.2.1) for a given initial position and velocity $y(0) = (x, v)(0) = (x_0, v_0)$. One can use $y(t) = y(u, \alpha)(t)$ for $t \in [t_0, T_f]$ to emphasise the dependence of $y(t)$ on the choices of the functions $u(t)$, $\alpha(t)$. Furthermore, one can regard W as a function whose value depends on the choice of the control $u(t)$, the angle $\alpha(t)$ and the related trajectory $y(t) = y(u, \alpha)(t)$. Accordingly, we will write $W = W(y, u, \alpha, T_f)$. Let us also introduce the closed set $\mathcal{T} \subseteq \mathbb{R}^3$, which represents the target that the device should reach during the soil penetration. For example, $\mathcal{T}$ could be a desired depth or, for roots, an underground pool of nutrients. The aim is to find both the optimal control $\bar{u}(t)$ and the optimal slope $\bar{\alpha}(t)$ such that the trajectory solution $\bar{y} = \bar{y}(t, \bar{u}, \bar{\alpha})$ of (3.2.1) reaches the target $\mathcal{T}$ minimising the cost function W in the time interval $[t_0, T_f]$.

It is equivalent to solve the optimal control problem (P), defined as:

$$
\begin{aligned}
(P) \qquad \min_{(u,\alpha)\in U\times[0,2\pi]} \{ & (W(y, u, \alpha, T_f)) \mid T_f \geq t_0,\ u : [t_0, T_f] \to U \text{ measurable}, \\
& y = (x, v) : [t_0, T_f] \to \mathbb{R}^6 \text{ solution of (3.2.1)}, \\
& (x(t_0), v(t_0)) = (x_0, v_0),\ x(T_f) \in \mathcal{T}\}.
\end{aligned}
$$

In the next sections, we will focus on the numerical solution of problem (P) by looking for the optimal couple $(u(t), \alpha(t))$ that minimises the total work (in reaching a given depth in the time $[t_0, T_f]$) only in the case of a parabolic tip.

To numerically solve the optimal control problem (P), we will use the direct method, being more stable with respect to other methods [218]. More precisely, the time interval $[t_0, T_f]$ is divided in n subintervals or stages. In any subinterval, the control is assumed to be a constant function. Starting from an initial guess of the control for any stage, the constrained optimisation method *fmincon* of Matlab is used to fix values of the control in all subintervals [219]. Both the dynamics and the cost function are converted in algebraic equations so that the resulting nonlinear programming problem can be solved by well established methods [220]. The optimisation variables are both the control u and the angle α. To speed up the convergence of the method, the initial guess can be chosen similar to a circumnutating control with a constant slope

α (since by evidences in section 3.4, the straight penetration is not expected to be the optimal solution). Namely, $u_0 \in \mathbb{R}^{3,n},\ \alpha_0 \in \mathbb{R}^n$ are like:

$$u_0 = (u_{0,1}cos(1:n), u_{0,2}sin(1:n), -u_{0,3});$$
$$\alpha_0 = u_{0,4}ones(1,n);$$

where $u_{0,i} \in \mathbb{R},\ i = 1 \dots 4$ are coefficients arbitrarily chosen. We have fixed $[t_0, T_f] = [0, 1]$, $n = 10$, $x_0 = (0, 0, 0)$, $v_0 = (0, 0, -v_{0,3})$. The integration of the ODE system in each stage is performed using the $ODE45$ solver of Matlab.

3.3 PARAMETER ESTIMATION

To validate the model, we verify if the dynamics (3.2.1) is able to capture motion behaviours of root-like intruders already observed and described in the literature.

Motivated by the results obtained in [207], we aim to investigate the role of the root circumnutation in reducing the soil friction. In [12], the mechanical work of a parabolic robotic tip (height $h = 3.3cm$ and diameter $d = 2cm$) is measured. The tip is reaching a depth of $x_M = 30cm$ in a real soil (topsoil) under three different densities: $k = 0.38,\ 0.4,\ 0.42 \frac{g}{cm^3}$ (see table 3.1 for the values of all variables).

To convert dimensional values in dimensionless numbers, we have used the following reference values: $T^* = 60s,\ L^* = 10cm,\ M^* = 1kg$. The parameter $\lambda_2(k, k^{\max})$ (used in the equation for the drag force F_d) is measured in $[1/s]$. It is the inverse of the characteristic time T^C $[s]$. To describe the meaning of the characteristic time, let us assume a cylinder (of height h and diameter d), with vertical initial velocity $v_0 = (0, 0, -v_{0,3})$, immersed into a given soil without any control u. The dynamics for the third component of the velocity will be

$$\dot{v}_3 = -F_d = -\lambda_2(k, k^{\max})v_3 = -v_3/T^C$$

and, thus,

$$v_3(t) = v_{0,3}exp(-t/T^C).$$

Therefore, T^C is the time necessary (according to the soil density) to have $v(T^C) = v_{0,3}e^{-1}$ (equivalent to a reduction of 63.22% of the initial velocity). By fitting data in [12], we obtained

$$\lambda_2(k, k^{\max}) = \max\left\{0, 15\frac{k}{k^{\max}} - 9\right\} 10^5 \ \left[\frac{1}{s}\right].$$

The dimensionless value will be $\lambda_2(k, k^{\max}) = \max\{0, 90(k/k^{\max}) - 54\}\, 10^6$. For example, when $k = 0.38$, it results $\lambda_2 = 5 \cdot 10^4$ and $T^C = 20\mu s$.

Finally, let us note that, if $F_s^{\max} = 1$ and the soil is maximally compressed (namely, $k = k^{\max}$), then the soil cannot be penetrated, since, regardless of the dynamics, one has $(1 - F_s) = 0$ and the speed of the device will tend to 0.

Table 3.1: **List of model variables**

Variable	Dimensional value	Dimensionless value	Significance
x_M	$30cm$	3	Maximum depth in [12]
$v_{0,3}$	$-0.06\frac{cm}{s}$	-0.36	Axial downward velocity in [12]
h	$3.3cm$	0.33	Height of the tip in [12]
d	$2cm$	0.2	Diameter of the tip in [12]
k_M	$0.6\frac{g}{cm^3}$	0.6	Maximum soil density due to compression (arbitrarily assumed)
k	$0.38\frac{g}{cm^3}$	0.38	Low soil density in [12]
k	$0.4\frac{g}{cm^3}$	0.4	Medium soil density in [12]
k	$0.42\frac{g}{cm^3}$	0.42	High soil density in [12]
$F_s^{\max}$	0.6	0.6	Maximum resistance offered by the soil
μ	$10^{-5}\frac{cm}{s}$	$6 \cdot 10^{-5}$	Regularising parameter
λ_1	3	3	Proportional parameter for function R

The condition $F_s^{\max} = 1$ is reasonable in the case in which one is studying the plant root evolution in those soil conditions in which the root growth strength cannot overcome the soil friction [11]. On the other hand, the case of $F_s^{\max} = 1$ is not interesting to study the effects of circumnutation in compressed soils (section 3.4.1). Therefore, as reported in the table 3.1, we have chosen to restrict our study to the case in which $F_s^{\max} < 1$. This kind of condition is more interesting for the purpose of our study, since we are interested in the root growth evolution when growth can occur.

In the experiment [12], the tip is forced to perform either a straight penetration or a circular circumnutation with a fixed slope (i.e. α introduced in Section 3.2) with respect to the vertical direction. We refer to section 2 in [12] for each detail about the experimental setup, the protocols and the acquisition of data.

Here, we will use the experiment in [12], in order to calibrate the free parameters of the dynamic equation (3.2.1), while in section 3.4.1 we will investigate the effects of both the compactness of the soil and the shape of the tip (section 3.4.1). Finally, we will derive the optimal control arising at different soil compactness values (section 3.4.2).

Simulations in this section and in section 3.4.1 are obtained by integrating the ODE system (3.2.1) with the Euler method (step of $\Delta x = 10^{-3}$) and computing the dissipated work W with the trapezoidal rule. It remains to evaluate the control $u(t)$ to perform the wished trajectory. At each step of the Euler method, the control $u(t)$ is computed by solving a nonlinear equation, as follows.

For the straight penetration, the control $u = u(t)$ solves:

$$\frac{d}{dt} v_u(t) = (0, 0, 0),$$

while for the circumnutation:

$$\frac{d}{dt} v_u(t) = -\rho\omega(cos(\omega t), \sin(\omega t), 0).$$

Here, the notation v_u indicates the dependence of the velocity v on the choice of the control $u(t)$. ρ and $\omega = 2\pi/T$ are the radius and the frequency of the helix, respectively, where T is the circumnutating period. Since the height h of the tip and its inclination (the angle α introduced in Section 3.2) are fixed, it follows $\rho = h\sin(\alpha)$. Furthermore, initial conditions are set coherently with the desired trajectory. For the straight penetration, the tip starts from the origin with a straight down velocity, namely $x(t_0) = (0, 0, 0)$ and $v(t_0) = (0, 0, -v_{0,3})$. For the circumnutation, the tip belongs to a helix with axis e_3. Therefore:

$$\begin{cases} x(t_0) = (\rho\cos(\omega t_0), \rho\sin(\omega t_0), 0) \\ v(t_0) = (-\rho\omega\sin(\omega t_0), \rho\omega\cos(\omega t_0), -v_{0,3}) \\ \left\langle \frac{v(t_0)}{|v(t_0)|}, -e_3 \right\rangle = \cos(\alpha) \end{cases} .$$

The authors in [12] conclude that the circumnutation could save up to the 33% of energy with respect to the straight penetration. Figure 3.2 shows the similar behaviour obtained by the two approaches (left from [12], right from the simulations) for the case of straight penetration (with $\alpha = 0°$) and for the case of different kinds of circumnutations ($\alpha \in \{10°, 20°\}$ and $T \in \{30s, 60s, 120s, 240s\}$).

Moreover, it is possible to characterise the helix resulting from the circular circumnutation by the lead angle ε which is defined as:

$$\varepsilon = \arctan\left(\frac{P_0}{2\rho\pi}\right),$$

where $P_0 = v_3 T$ is the pitch of the helix and v_3 is the downward velocity of the tip. In [12], it is shown that the circumnutation is more efficient than the straight penetration if, regardless of the soil density, the lead angle is in the range $\varepsilon \in [45°, 63°]$ (fig 4.2(A)). To verify this condition, we simulated the total work W done by the intruder at different lead angles ε in the range

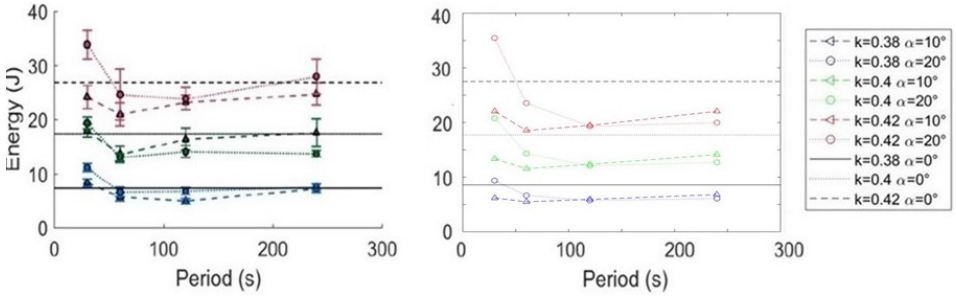

Figure 3.2: **Circumnutation vs straight penetration**. On the left, results in [12]. On the right, the behaviour of the model.

$[20°, 90°]$ within the three different soil densities as in [12]. The simulations (figures 4.2(B)-(D)) are in agreement with the experimental results in [12], and confirmed the presence of an optimal value for the lead angle such that the energy is minimised. In section 3.2, we have estimated the strength of the rotation by the term $\sqrt{v_1^2 + v_2^2}/|v|$ (neglecting the regulating parameter μ since the velocity is assumed to be greater than 0). In [12], authors have showed that the reduction of frictional forces due to the rotation is directly affected by $cos(\varepsilon)$. The formulation here proposed is more general, since we are comparing any possible motion in the soil and, thus, the lead angle ε is not always easy to characterise. Nevertheless, for the circular circumnutation (as in [12]), the velocity is $v = (-\rho\omega\sin(\omega t), \rho\omega\cos(\omega t), -v_3)$ and the two terms coincide:

$$cos(\varepsilon) = \frac{1}{\sqrt{1+\tan\varepsilon^2}} = \frac{1}{\sqrt{1+(\frac{P_0}{d\pi})^2}} = \frac{\omega\rho}{\sqrt{(\omega\rho)^2+v_3^2}} = \frac{\sqrt{v_1^2+v_2^2}}{|v|}.$$

In particular, in [12], the authors couple the $cos(\varepsilon)$ with two varying parameters to take into account the effects of different soils and different inclinations of the tip. Here, we estimate this effect for any inclination of the tip by introducing the exponent in the formulation of R.

3.4 RESULTS

3.4.1 Circumnutation vs straight penetration

Effects of soil compactness

It has been conjectured that the circumnutation movement could rearrange the particles into the soil and breaks up the granular structure reducing the soil compactness effects [12]. Indeed, as it has already been noted in [221], the inclination of the root apex plays a fundamental role in facilitating the soil penetration.

When the root apex encounters an obstacle or a very dense layer of soil, two strategies can be adopted by the tip: either it changes the growth direction,

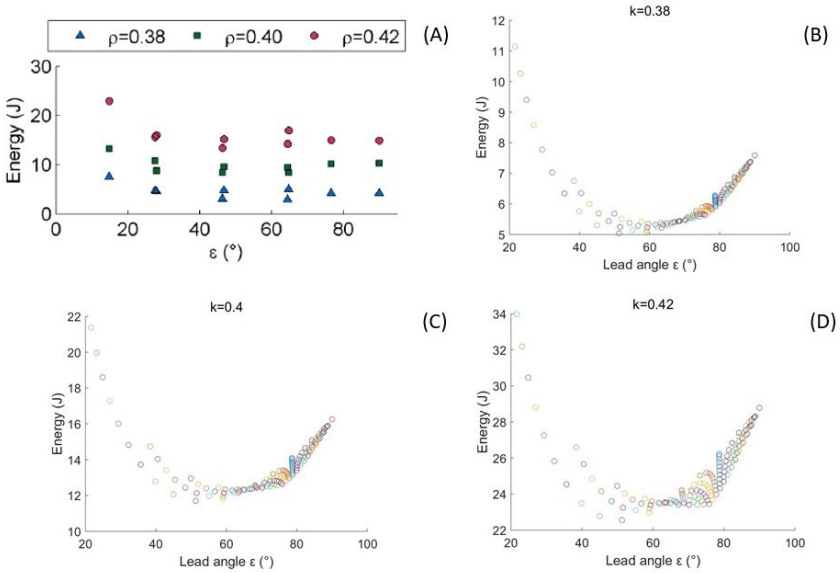

Figure 3.3: **Optimal values of the lead angle** ε. (A) Results in [12]. (B)-(D) Values of the energy simulated with the model at three different soil densities.

sliding along the obstacle, or it promotes the radial growth to overcome the increased mechanical stress [11].

The adoption of either of these two strategies by roots suggests that, when the density increases, the circumnutation is no longer efficient. To investigate this condition, we compared the instantaneous energy between the straight penetration and the penetration performed by the root with circumnutation, in the case of a high soil density ($k = 0.42$) and with a non-compressible soil (arbitrarily assumed in the model as $k^{\max} = 0.6$), as showed in figure 3.4(A). Figure 3.4(B) shows the instantaneous energy of both the straight penetration and the circumnutation when the soil is composed of different soil layers: a topsoil (up to $-1.5cm$) at density $k = 0.38$, a second layer (up to $-3.5cm$) with density increasing from $k = 0.4$ to $k = 0.42$, a third layer (up to $-4.5cm$) with density increasing from $k = 0.56$ to $k = 0.6$ and the latter layer of non-compressible soil ($k = 0.6$). It is interesting to notice that, when the soil density increases, the rearrangement of particles becomes more difficult (if not impossible) to achieve, making the circumnutation a less efficient strategy in soils with high density.

Effects of tip shape

The dimension of the robotic tips can affect the efficiency of a penetrometer [222, 204], as well as its shape [211, 212, 204]. According to [204], a conical body that is moving into a granular medium feels a smaller drag force in the cases in which it is more tapered. In figure 3.5, the total work in a low dense soil ($k = 0.38$) is plotted when the tip becomes more and more

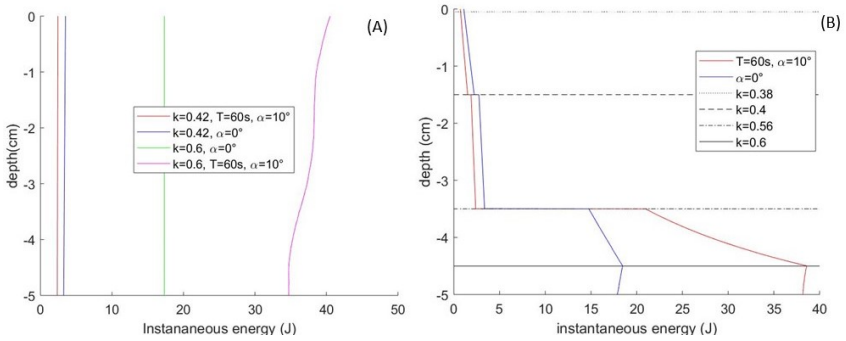

Figure 3.4: **Instantaneous energy**. Comparison between straight penetration and circumnutation in the case of (A) a non-compressible soil and (B) a stratified soil.

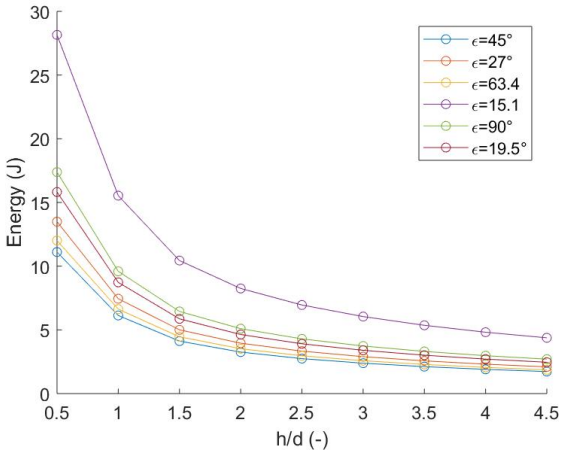

Figure 3.5: **The shape of the tip**. Total work of the tip in a low dense soil when the ratio h/d increases. Notice that the asymmetries in the oscillations

tapered (i.e., the height-diameter ratio h/d increases). For each h/d ratio, both the straight penetration (lead angle $\varepsilon = 90°$) and the circumnutation at different periods and the amplitudes are performed. The simulations show a behaviour in agreement with results in [204], where it has been observed that the drag force and, consequently, the frictional force and the energy dissipated to perform the motion, decrease with an increment of the h/d ratio, but with less evident benefits at high ratios.

3.4.2 Optimal control

In this section we will investigate the best strategy for an intruder to penetrate in a medium such that the total work W is minimised. Following the work in [12], in the previous section 3.4.1 we have imposed and compared two different strategies: a straight penetration and a penetration performed with circumnutations. In this section, we extend previous results by evaluating

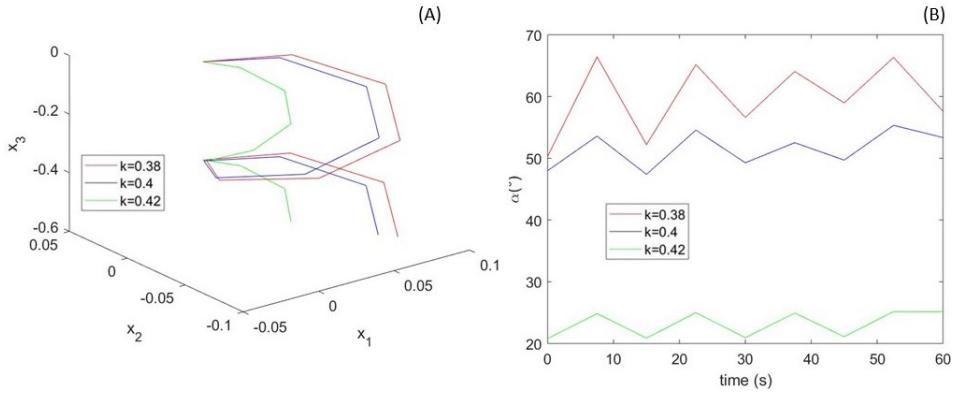

Figure 3.6: **Optimal control**. (A) The optimal trajectory for three different soils. (B) The values for α for the optimal solution in each soil.

which strategy emerges from the simulation without fixing *a priori* any path for the trajectory $x(t)$ or any value for the inclination angle α of the tip with respect to the vertical axis $-e_3$. We use here the direct method (see section 3.2.2) to compute the best strategy that minimises the total work in three different soil densities cases ($k = 0.38,\ 0.4,\ 0.42$).

Figure 3.6(A) shows that the optimal penetration strategy is an oscillatory trajectory for each soil density. In particular, in section 3.3, in the case of soil density $k = 0.42$, the most efficient motion has been observed to be a circumnutation with $\alpha = 10°$ and $T = 60s$. The optimal control performed by the direct method allows to save the 0.16% of W with respect to the previous circumnutation when the depth to reach is fixed to $5cm$, even if better results could be obtained by improving the accuracy of the direct method.

Since with the direct method also the slope α is a variable to optimise, we evaluated the behaviour for this parameter for each soil density (figure 3.6(B)). It is worth noting that:

- In each soil, the optimal angle α tends to continuously oscillate around an average value, without reaching a constant.
- This average value decreases in more dense soils. This behaviour is in agreement with the experimental results in [207].
- Oscillations are greater in the low dense soil and this observation agrees with previous evidences [221].

To summarise, two main results are here obtained: I) an oscillatory trajectory (circumnutation-like motion) as the optimal, without imposing a prescribed behaviour to the control, and II) a dynamics of α in agreement with the few experimental observations available in the literature. These results strongly validate the model and its accuracy in describing the root tip-soil interaction; while at the same time, they strengthen the hypothesis that circumnutation helps plant roots in reducing soil friction during penetration [207, 12].

From these results, one can deduce that circumnutation can emerge from the mechanical interaction between the root tip and the impeding medium, as the outcome of an adapting strategy of roots to reduce the total work.

3.5 DISCUSSION

In this paper, we investigated the role of circumnutation in plant roots and the advantages of replicate circumnutating movements in autonomous systems. Following the idea in [12], we hypothesise that circumnutation can reduce the friction experienced by a system during penetration of a medium. To this aim, we proposed a mathematical model to describe the movement of an autonomous device and the frictional forces experienced by a root tip-like intruder in soil.

Previous experiments [12] showed that circumnutation could reduce the energy in vertical soil penetration. However, the complexity of the soil, the genetic diversity in plants and the lack of biological data make difficult to generalise these results to plants in real soils.

Here, we described the dynamics of a root tip-like object moving into granular soil at different density and compactness coefficients, modelling the physical phenomenon and considering only the frictional forces acting at the tip, while neglecting the existence of a body above the tip where other forces, not involved in the motion, may act. This assumption was made possible by the ability of plant roots to move in soil by growing at their apical level [210], with no relative motion between soil and the mature part of the root, avoiding this way the perception of lateral friction on such a region [135]. We at first estimated model parameters using data in [12], and obtained results in agreement with the existing literature (see section 3.4.1). By fixing different circumnutation amplitudes, we demonstrated that in non-compressed soils, the circumnutation can reduce the mechanical friction of the soil with respect to a straight penetration.

Borrowing tools from the optimal control theory, we then evaluated the optimal penetrating strategy for an intruder in soils which reduces the mechanical work. The resulting optimal trajectory confirmed the presence of oscillatory patterns matching circumnutation movements performed by the tip (section 3.4.2). Moreover, looking at the optimal slope α of the tip (the amplitude of the circumnutation motion), we observed greater amplitude for less dense soils and smaller amplitude in more dense soils, a behaviour already verified by experimental results [221].

The work showed that the circumnutation is a mechanical behaviour induced by frictional forces into the soil that helps root tips to save energy during growth. In particular, the optimal control based approach has successfully demonstrated that the circumnutation is the most efficient penetrating strategy among an infinite combination of possible penetrating motions. Since the dimension of the system penetrating in soil can be easily changed, the model

can also provide the most efficient strategy for soil exploration in autonomous systems forecasting the optimal control that minimise the mechanical work.

As far as we know, this is the first attempt to model the root dynamics by adopting an optimal control based approach. We believe this mathematical tool could be successfully applied to investigate many others plant growing processes as well as the interactions among roots. For example, the dynamics (3.2.1) can be generalised to more than one root tip to investigate the complex plant root system development in a real soil. Furthermore, if the cost function W is modified to take into account the metabolic needs of a plant, then the optimal control based approach could help to unveil growth mechanisms and resource allocation patterns in plants.

Beside the biological implications, such an approach can suggest optimal strategies to design efficient robotic devices for soil exploration. Indeed, the model can help to estimate forces in soils, forecast the requirements for the robots and identify the most convenient trajectory to follow.

In particular, the framework presented in [223] can be used to generalise the results here proposed. Indeed, if the soil cannot be assumed homogeneous all around the tip, one could average the local soil frictional effects, getting an integro-differential equation whose well-posedness is investigated in [223] (and reported in Chapter 4).

Furthermore, if the robotic tip moves so fast that the drag force F_d may not depend anymore linearly on the speed, the formulation here proposed for the drag force could be modified in the following one

$$F_d = R\lambda_2(k, k^{\max})\frac{S_l}{S_l^c}f(|v|)\frac{v}{|v|},$$

where $f(|v|)$ is a nonlinear function to be defined. It is worthy to note that this framework is not anymore Lipschitz and the existence of a minimum solution is studied in [223].

As a future step, we mean to increase the complexity of the proposed model by adding more variables to be optimised. For example, the optimal shape could be investigated as well as the radial expansion of roots, or the interaction among multiple tropisms (directional growth responses to environmental stimuli [224]). Moreover, as a further step, we aim to insert into the dynamics (3.2.1) a stochastic term to simulate the random search of root tips and unveiling how the root's need to explore and exploit the soil affects the need of minimising the energy dissipation.

Chapter 4

HAMILTON-JACOBI-BELLMAN EQUATION FOR CONTROL SYSTEMS WITH FRICTION

4.1 INTRODUCTION

In Chapter 3 it has been proposed a model to study the movement of a device into the soil under the action of forces that are relevant only at the tip. The model has allowed the study of a peculiar movement in roots: the circumnutation. The model parameters have been estimated by fitting data in [12], in which a parabolic tip moves into an homogeneous soil. In these conditions, the frictional forces can be approximated as proposed in Chapter 3. To study cases in which these assumptions are not valid, we propose here a more general framework.

In greater details, this Chapter deals with the dynamical friction between two or more solid bodies that are moving one relative to the other and rub together along parts of their surfaces. Modelling dynamic friction in control systems is not an easy task since it concerns the study of, possibly discontinuous, dynamic equations. On one hand, the dissipative structure of the system still yields well-posedness of the control system: for a given input $u(t)$ and a given initial condition $x(t_0) = x_0$ at time t_0, the system has a unique state $x(t)$ for all $t \geq t_0$. Moreau's Sweeping Process [225, 226] is a notable example of dynamical systems in which the dynamic friction phenomenon occurs between a rigid body and a moving, perfectly indeformable, active constraint. On the other hand, the dynamics is described by a new class of upper semicontinuous differential inclusions and the characterisation of the optimal trajectory requires the derivation of different techniques with respect to the literature. The Chapter focuses on this characterisation.

To generalise the model of Chapter 3, assume that a solid body $\mathcal{B}$ has

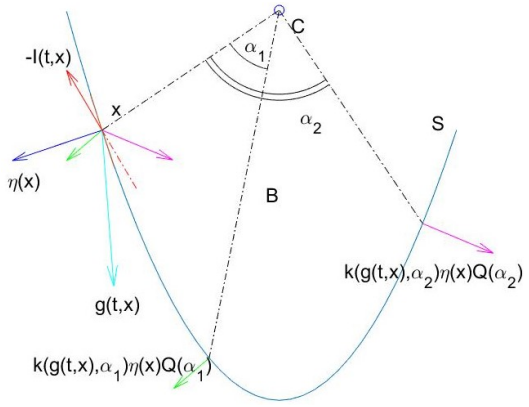

Figure 4.1: **An example generating the studied model**. $\mu = \delta_{\alpha_1} + \delta_{\alpha_2}$ and $k(g, \alpha_i) = \lambda_i > 0$ for $i = 1, 2$. Therefore, the total friction at x will be $-I(t, x)$, affecting $g(t, x)$.

a region of contact S with another external body. The aim is to derive the friction produced at a point $x \in S$, when a vector field g is applied to $\mathcal{B}$ at x. Suppose that the family of normal vectors to $\mathcal{B}$ is described by the mapping $\alpha \mapsto \eta(x) \cdot Q(\alpha)$, where $\eta(x)$ is the normal to $\mathcal{B}$ at x and $\alpha \mapsto Q(\alpha)$ is a matrix transporting $\eta(x)$ along S. Then, one can approximate the resulting vector field at the point $x \in S$ as the vector field g minus the *averaged friction* at x, namely (see Figure 4.1)

$$g(t, x) - \int_A k(g(t, x), \alpha)\eta(x) \cdot Q(\alpha)\mu(d\alpha) =: g(t, x) - I(t, x).$$

Here, $k(g(t, x), \alpha)$ is a coefficient measuring the strength of response to the vector field g at the point x, while the integral over A sums up the total averaged dynamic friction. Motivated by such a physical intuition, one then can consider the controlled differential inclusion

$$\dot{x} \in g(t, x, u) - \int_A k(t, x, u, \alpha)\partial_x \varphi(x, \alpha)\mu(d\alpha), \tag{4.1.1}$$

where now the control u determines the choice of a vector field, the strength to the response k also depends on the control and the measure μ is allowed to choose the relevant, averaging points over S through A. φ will be a possible non-smooth function and ∂_x is a suitable sub-gradient.

More than the result in chapter 3, differential equations with discontinuous right-hand side has been used for several tasks such as to model electric circuits, hysteresis phenomena, mechanical constraints (see, e.g. [227, 228, 229]) and, more recently, the growth of stems and vines (see, e.g., [110, 230]).

Furthermore, this dynamics has some strong connections with the controlled perturbed sweeping process $\dot{x} \in g(t, x, u) - N_C(x)$ where C is a set and $N_C(x)$ is a suitable normal cone to C at x. In fact, when the strength to the response k in (4.1.1) is sufficiently large and $\varphi(x, \alpha) = d(x, C(\alpha))$ (where

$d(\cdot, C(\alpha))$ is the distance function from $C(\alpha)$), then the model (4.1.1) can be regarded as a perturbed, *averagely swept*, sweeping process.

Note that the averaging occurring in (4.1.1) has a quite different character compared to the one presented in the Riemann-Stiltjies control literature (see, e.g. [18], [20], [19]), since the averaging in (4.1.1) occurs in the dynamics and not in the cost. Similar results to what described in the following sections have been derived in [231, 232, 233] in the case in which optimal stopping and optimal exit time are considered and the dynamics is Lipschitz continuous. However, since the control system (4.1.1) does not have such a property, the characterization of the value function as the unique viscosity solution of an Hamilton-Jacobi equation does not follow from the standard theory and requires different techniques [234, 235].

4.2 PRELIMINARIES AND NOTATIONS

In this section, we will recall some useful notations and concepts which will be used throughout the whole chapter. Let us use $\mathbb{B}$ to denote the open, unit ball. For a given closed set $C \subseteq \mathbb{R}^n$ and a point $x \in C$, the proximal normal cone to C at x is

$$N_C^P(x) := \{p \in \mathbb{R}^n : \exists\, M > 0 \text{ s.t. } \langle p, y - x\rangle \leq M|y - x|^2 \quad \forall y \in C\}\ . \tag{4.2.1}$$

For a given lower semi-continuous function $f : \mathbb{R}^n \to \mathbb{R}$, the domain of f is $\mathrm{dom}(f) := \{x \in \mathbb{R}^n : \ f(x) < \infty\}$. The proximal sub-differential of f at $x \in \mathrm{dom}(f)$ is

$$\partial_P f(x) = \left\{v \in \mathbb{R}^n : \ (v, -1) \in N^P_{\mathrm{epi}(f)}(x, f(x))\right\},$$

where $\mathrm{epi}(f) = \{(x, \alpha) \in \mathbb{R}^{n+1} : \ f(x) \leq \alpha\}$. An equivalent characterization (see, e.g., [17], Proposition 4.4.1) of proximal the sub-differential is the following: $\xi \in \partial_P f(x)$ if there exist $M > 0$ and $\varepsilon > 0$ such that

$$\langle \xi, y - x\rangle \leq f(y) - f(x) + M|x - y|^2, \tag{4.2.2}$$

for each $y \in x + \bar{\mathbb{B}}$. Furthermore, if $f : \mathbb{R}^n \to \mathbb{R}$ is Lipschitz continuous, with constant $L > 0$, then the relation (4.2.2) is satisfied with $\varepsilon = \infty$ (see, e.g., [17], Proposition 4.4.2) and $\partial_P f(x) \subseteq L\bar{\mathbb{B}}$ for each $x \in \mathrm{dom}(f)$. If $f : \mathbb{R}^n \to \mathbb{R}$ is lower semi-continuous and convex, then $\mathrm{epi}(f)$ is closed and convex. In particular this implies that $\partial_P f(x) \neq \emptyset$ for each $x \in \mathrm{dom} f$. Further, if f is convex, then the proximal sub-differential $\partial_P f(x)$ coincides with the set

$$\partial f(x) := \{\xi \in \mathbb{R}^n : f(z) \geq f(x) + \langle \xi, z - x\rangle \quad \forall z \in \mathrm{dom}(f)\} \tag{4.2.3}$$

and we will simply refer to it as subdifferential. It will be also helpful to define a notion of proximal super-differential. For a given upper semi-continuous

function $f : \mathbb{R}^n \to \mathbb{R}$ and $x \in \mathrm{dom}\,(f)$, the proximal super-differential of f at x is

$$\partial^P f(x) = \left\{ v \in \mathbb{R}^n : \ (-v, 1) \in N^P_{\mathrm{hypo}(f)}(x, f(x)) \right\},$$

where $\mathrm{hypo}(f) = \{(x, \alpha) \in \mathbb{R}^{n+1} : \ f(x) \geq \alpha\}$. Given $\Omega \subseteq \mathbb{R}^k$ and $M : \Omega \rightsquigarrow \mathbb{R}^r$, M has closed graph if $\mathrm{Gr}\, M = \{(x, v) : \ v \in M(x),\ x \in \Omega\}$ is closed. It is well known that if a multifunction is bounded and has closed graph, then M is upper semicontinuous. M is said one-sided Lipschitz (OSL) if there is a constant $L \geq 0$ such that

$$\langle w - v, y - x \rangle \leq L|x - y|^2,$$

for every $x, y \in \mathbb{R}^k$, $v \in M(x)$ and $w \in M(y)$. Given a finite Radon measure μ and a μ-measurable set A, let us define

$$L^1(A; \mu) := \left\{ g : A \to \mathbb{R}^n \ \mu-\mathrm{meas.} : \ \int_A |g(\alpha)|\, \mu(d\alpha) < \infty \right\}. \tag{4.2.4}$$

Given a multifunction $\tilde{\Gamma} : \Omega \times A \rightsquigarrow \mathbb{R}^r$, the parametrised integration of $\tilde{\Gamma}$ (see, e.g., [236], [237], [238]) is a new multifunction $\Gamma(x) := \int_A \tilde{\Gamma}(x, \alpha)\mu(d\alpha)$ where

$$\begin{aligned} \int_A \tilde{\Gamma}(x, \alpha)\mu(d\alpha) := \Big\{ & \int_A \gamma(\alpha)\mu(d\alpha) : \ \gamma(\alpha) \\ & \mu-\text{measurable selection of } \tilde{\Gamma}(x, \cdot) \Big\}. \end{aligned} \tag{4.2.5}$$

4.3 THE GENERAL SETTING

This chapter is focused on studying the following free-time optimal control problem

$$(P) \begin{cases} \text{Minimize } W(T, x(T)) \\ \text{over } \ T \geq t_0 \ \text{ and } \ (x, u) \in AC([t_0, T]; \mathbb{R}^n) \times \mathcal{U} \ \text{ s.t.} \\ \dot{x}(t) \in F(t, x, u), \quad a.e.\ t \in [t_0, T] \\ u(t) \in U \subset \mathbb{R}^m, \quad a.e.\ t \in [t_0, T] \\ x(t_0) = x_0 \in \mathbb{R}^n \\ (T, x(T)) \in \mathrm{Gr}\, \mathcal{T} \subseteq \mathbb{R}^{1+n} \end{cases}, \tag{4.3.1}$$

the data comprise an initial time $t_0 \in \mathbb{R}$, an initial state $x_0 \in \mathbb{R}^n$, a cost function $W : \mathbb{R}^{1+n} \to \mathbb{R}$, a set $\mathcal{U}$ of measurable control functions u defined on $[t_0, +\infty)$ and taking values in a compact set $U \subset \mathbb{R}^m$, a controlled, non-empty multifunction $F : \mathbb{R}^{1+n} \times U \rightsquigarrow \mathbb{R}^n$ and a non-empty multifunction $\mathcal{T} : \mathbb{R} \rightsquigarrow \mathbb{R}^n$. In particular, one can consider the case in which the controlled multifunction F is defined as

$$F(t, x, u) = g(t, x, u) - \int_A k(t, x, u, \alpha)\partial_x \varphi(x, \alpha)\mu(d\alpha), \tag{4.3.2}$$

where A is a given compact set, $k : \mathbb{R}^{1+n} \times U \times A \to \mathbb{R}^+$, $g : \mathbb{R}^{1+n} \times U \to \mathbb{R}^n$, $\varphi : \mathbb{R}^n \times A \to \mathbb{R}$ are given functions and μ is a finite Radon measure over A. Sometimes, to emphasize the dependence on the initial condition, the notation $(P)_{(t_0,x_0)}$ will be used to denote the optimal control problem (P) with initial condition $x(t_0) = x_0$. The following standing hypothesis **(SH)** are assumed:

H_1: The maps $(t, x, u, \alpha) \mapsto k(t, x, u, \alpha)$, $(t, x, u) \mapsto g(t, x, u)$ and $(x, \alpha) \mapsto \varphi(x, \alpha)$ are continuous.

H_2: There exist constants $L, C > 0$ such that

$$\begin{aligned} &|g(t,x,u) - g(s,y,u)| \leq L\left(|t-s| + |x-y|\right), \\ &|\varphi(x,\alpha) - \varphi(y,\alpha)| \leq L|x-y|, \\ &|k(t,x,u,\alpha) - k(s,y,u,\alpha)| \leq L\left(|t-s| + |x-y|\right), \\ &0 \leq k(t,x,u,\alpha),\ |g(t,x,u)| \leq C. \end{aligned} \tag{4.3.3}$$

for every (t, x), $(s, y) \in \mathbb{R}^{1+n}$, $u \in U$ and $\alpha \in A$.

H_3: for each $\alpha \in A$, the mapping $x \mapsto \varphi(x, \alpha)$ is convex.

H_4: the set-valued map $\bar{F}(t, x) := \cup_{u \in U} F(t, x, u)$ takes convex values for each $(t, x) \in \mathbb{R}^{1+n}$.

H_5: the multifunction $\mathcal{T} : \mathbb{R} \rightsquigarrow \mathbb{R}^n$ has closed graph.

H_6: the function $W : \mathbb{R}^{1+n} \to \mathbb{R}$ is locally Lipschitz continuous in $\mathrm{Gr}\,\mathcal{T} + \varepsilon\mathbb{B}$, for some $\varepsilon > 0$.

4.4 BASIC PROPERTIES OF THE MODEL

In this section, we will formally prove some important properties of the free-time optimal control problem (P). To this purpose, let us introduce the set-valued function

$$I(t, x, u) = \int_A k(t, x, u, \alpha),\ \partial_x \varphi(x, \alpha)\mu(d\alpha) \tag{4.4.1}$$

and the set-valued map

$$\bar{F}(t, x) = \bigcup_{u \in U} \{g(t, x, u) - I(t, x, u)\},$$

for each $(t, x) \in \mathbb{R}^{1+n}$. The maps F and $\bar{F}$ satisfy the following conditions:

Proposition 4.4.1. Assume conditions H_1-H_3. Then the map $(t, x) \rightsquigarrow \bar{F}(t, x)$ is non-empty, compact and upper semi-continuous. Furthermore, for each $x \in \mathbb{R}^n$, the map $t \rightsquigarrow \bar{F}(t, x)$ is Lipschitz continuous and, for each

$(t,u) \in \mathbb{R} \times U$, the map $x \to F(t,x,u)$ is OSL. In particular, there exists a constant $L_{\bar{F}}$ such that for every $y_1 = (t_1, x_1),\ y_2 = (t_2, x_2) \in \mathbb{R}^{1+n}$, one has

$$\begin{aligned} &\sup_{v \in \bar{F}(y_1)} \langle v, x_1 - x_2 \rangle - \\ &\qquad - \sup_{w \in \bar{F}(y_2)} \langle w, x_1 - x_2 \rangle \leq L_{\bar{F}} |y_1 - y_2|^2 \end{aligned} \tag{4.4.2}$$

.

Proof. In view of the hypothesis H_2-H_3 on φ, one has that $\partial_x \varphi(x,\alpha)$ is non-empty, bounded and convex for each $(x,\alpha) \in \mathbb{R}^n \times A$. The continuity of φ with respect to α ensures that the graph of $\alpha \mapsto \partial_x \varphi(x,\alpha)$ is closed. Therefore, the map $\alpha \mapsto \partial_x \varphi(x,\alpha)$ admits a measurable selection for each $x \in \mathbb{R}^n$ (see, e.g., Theorem 2.3.11 [17]) and $\bar{F}(t,x)$ is non-empty for each $(t,x) \in \mathbb{R}^{1+n}$. Furthermore, $\bar{F}$ is bounded in view of H_2.

Since U is compact and in view of H_1-H_2, one can prove that the mapping $(t,x) \mapsto I(t,x,u)$ has closed graph for each $u \in U$. In fact, fix $u \in U$, take $(t_k, x_k) \in \mathbb{R}^{1+n}$ converging to (t,x) and $v_k \in I(t_k, x_k, u)$ for each $k \in \mathbb{N}$, converging to some v. It needs to show that $v \in I(t,x,u)$. It follows from the definition of parametrized integration that

$$\begin{aligned} I(t_k, x_k, u) = \big\{ &\textstyle\int_A k(t_k, x_k, u, \alpha) \xi_k(\alpha) \mu(d\alpha) : \\ &\xi_k(\alpha)\ \mu\text{−measurable selection of } \partial_x \varphi(x_k, \cdot) \big\} \end{aligned} . \tag{4.4.3}$$

Hence any μ-measurable sequence $\xi_k(\alpha) \in \partial_x \varphi(x_k, \alpha)$ weakly converges in $L^1(A;\mu)$ to a μ-measurable selection $\xi(\alpha) \in \partial_x \varphi(x,\alpha)$ (see, e.g., Theorem 1, pg. 125, [239]). Furthermore, in view of H_2, one easily obtains

$$\max_{U \times A} |k(t_k, x_k, u, \alpha) - k(t, x, u, \alpha)| \leq L \left(|t_k - t| + |x_k - x| \right). \tag{4.4.4}$$

Call $\epsilon_k = \int_A k(t,x,u,\alpha) \left(\xi_k(\alpha) - \xi(\alpha) \right) \mu(d\alpha)$ and observe that, $\epsilon_k \to 0$ since $\xi_k(\alpha)$ weakly converges in $L^1(A;\mu)$ to $\xi(\alpha)$. In particular in view of (4.4.4), one easily obtains

$$\begin{aligned} \textstyle\int_A k(t_k, x_k, u, \alpha) \xi_k(\alpha) \mu(d\alpha) &\in \textstyle\int_A k(t,x,u,\alpha) \xi(\alpha) \mu(d\alpha) \\ &\quad + \left(|\epsilon_k| + L^2 \mu(A) \left(|t_k - t| + |x_k - x| \right) \right) \bar{\mathbb{B}} \\ &\subset I(t,x,u) + \left(|\epsilon_k| + L^2 \mu(A) \left(|t_k - t| + |x_k - x| \right) \right) \bar{\mathbb{B}} \end{aligned} \quad , \tag{4.4.5}$$

which implies that $(t,x) \rightsquigarrow I(t,x,u)$ has closed graph for each $u \in U$. Since $I(t,x,u)$ is also bounded, one has that the map $(t,x) \rightsquigarrow I(t,x,u)$ is upper semi-continuous for each $u \in U$. To prove that $F(t,x,u)$ is upper semi-continuous for each $u \in U$ is straightforward.

This in particular implies that, for each $u \in U$ fixed, for any $(t,x) \in \mathbb{R}^{1+n}$ and for every neighborhood $\mathcal{N}_u$ of $F(t,x,u)$, there exists a neighborhood $\mathcal{O}_u$ of (t,x) such that $F(s,y,u) \subset \mathcal{N}_u$ for any $(s,y) \in \mathcal{O}_u$. Now, observe that $\mathcal{N} := \cup_{u \in U} \mathcal{N}_u$ can be regarded as an open arbitrary neighborhood of $\bar{F}(t,x)$ and that $\bar{F}(s,y) \subseteq \mathcal{N}$, for every $(s,y) \in \mathcal{O} := \cup_{u \in U} \mathcal{O}_u$. This shows that $\bar{F}$

is upper semi-continuous. Furthermore, the Lipschitz continuity of the map $t \rightsquigarrow \bar{F}(t,x)$ easily follows from the Lipschitz continuity conditions H_2.

It is then possible to prove that F is one-sided Lipschitz w.r.t. $x \in \mathbb{R}^n$, uniformly w.r.t. $(t,u) \in \mathbb{R} \times U$. Fix any $(t,x,u),(t,y,u) \in \mathbb{R}^{1+n} \times U$. For every $v \in F(t,x,u)$, $w \in F(t,y,u)$ there exist measurable selections $\eta_x(\alpha) \in \partial_x \varphi(x,\alpha)$ and $\eta_y(\alpha) \in \partial_y \varphi(y,\alpha)$, μ-a.a. $\alpha \in A$, such that

$$
\begin{aligned}
v &= g(t,x,u) - \int_A k(t,x,\alpha,u)\eta_x(\alpha)\mu(d\alpha), \\
w &= g(t,y,u) - \int_A k(t,y,\alpha,u)\eta_y(\alpha)\mu(d\alpha).
\end{aligned}
$$

Therefore, one can derive the following inequalities:

$$
\begin{aligned}
\langle x-y, v-w\rangle \leq L|x-y|^2 + \\
\textstyle\int_A k(t,y,u,\alpha)\,\langle \eta_y(\alpha), x-y\rangle\,\mu(d\alpha) + \\
\textstyle\int_A k(t,x,u,\alpha)\,\langle \eta_x(\alpha), y-x\rangle\,\mu(d\alpha) \leq \\
L|x-y|^2 + \textstyle\int_A k(t,y,u,\alpha)(\varphi(x,\alpha)-\varphi(y,\alpha))\mu(d\alpha) - \\
\textstyle\int_A k(t,x,u,\alpha)(\varphi(x,\alpha)-\varphi(y,\alpha))\mu(d\alpha) \leq \\
L|x-y|^2 + L|x-y| \textstyle\int_A |k(t,y,u,\alpha)-k(t,x,u,\alpha)|\mu(d\alpha) \\
\leq \Big(L + L^2\mu(A)\Big)|x-y|^2 = L_F|x-y|^2
\end{aligned}
\qquad , \qquad (4.4.6)
$$

for each $x,y \in \mathbb{R}^n$, $t \in \mathbb{R}$, $u \in U$, where, in turns, the characterization (4.2.3) of the proximal sub-differential was used, together with the hypothesis H_2 and the positivity of k. This shows that F is OSL w.r.t. x, uniformly w.r.t. to $t \in \mathbb{R}$, $u \in U$.

In order to prove (4.4.2), let $u \in U$ and $v_1 \in F(t_1,x_1,u)$ be such that

$$
\sup_{v \in \bar{F}(t_1,x_1)} \langle v, x_1 - x_2\rangle = \langle v_1, x_1 - x_2\rangle .
$$

Fix any $v_2 \in F(t_2,x_2,u)$ and choose $w \in F(t_1,x_2,u)$ such that

$$
|w - v_2| \leq L|t_1 - t_2|.
$$

Then one can easily estimate

$$
\begin{aligned}
&\sup_{v \in \bar{F}(t_1,x_1)} \langle v, x_1 - x_2\rangle - \sup_{w \in \bar{F}(t_2,x_2)} \langle w, x_1 - x_2\rangle \leq \\
&\langle v_1, x_1 - x_2\rangle - \langle v_2, x_1 - x_2\rangle = \\
&\langle v_1 - w, x_1 - x_2\rangle + \langle w - v_2, x_1 - x_2\rangle \leq \\
&L_F|x_1 - x_2|^2 + |w - v_2||x_1 - x_2| \leq \\
&L_F|x_1 - x_2|^2 + L|t_1 - t_2||x_1 - x_2| \leq \\
&(L_F + L)|(t_1,x_1) - (t_2,x_2)|^2 = L_{\bar{F}}|(t_1,x_1) - (t_2,x_2)|^2,
\end{aligned}
$$

where $L_{\bar{F}} = (L_F + L)$. This shows relation (4.4.2) and concludes the proof. $\square$

Now, consider the control system

$$\begin{cases} \dot{x}(t) \in F(t,x,u), \quad u \in \mathcal{U}, \quad a.e.\ t \in [t_0, +\infty) \\ x(t_0) = x_0 \in \mathbb{R}^n \end{cases} . \tag{4.4.7}$$

Remark 4.4.2. Notice that, as a consequence of the one-sided Lipschitz property (4.4.2), for every solution of (4.4.7) $x_1(\cdot)$, $x_2(\cdot)$, respectively starting from $x(t_1) = x_1$, $x(t_2) = x_2$ with a given control $u \in \mathcal{U}$, then one has

$$|x_1(t) - x_2(t)| \leq e^{2L_{\bar{F}}(t-t_0)} |x_1(t_0) - x_2(t_0)|, \tag{4.4.8}$$

for all $t \geq \max\{t_1, t_2\} =: t_0$. In particular (4.4.8) implies that

$$\begin{array}{l} |x_1(t) - x_2(t)| \leq e^{2L_{\bar{F}}(t-t_0)} \left(|x_1(t_0) - x_1| + \right. \\ \qquad\qquad \left. + |x_2 - x_2(t_0)| + |x_1 - x_2|\right) \leq \\ \leq e^{2L_{\bar{F}}(t-t_0)} 2 \left(C(1 + L\mu(A))|t_1 - t_2| + |x_1 - x_2|\right) \\ \leq \lambda(t) |(t_1, x_1) - (t_2, x_2)| \end{array} , \tag{4.4.9}$$

where $C, L > 0$ are the constants appearing in H_2 and

$$\lambda(t) := 2e^{2L_{\bar{F}}t} \max\{C(1 + L\mu(A)), 1\} > 1$$

An important consequence of Proposition 4.4.1 is that the control system (4.4.7) is well-posed, as it is stated in the following result.

Theorem 4.4.3. Assume the hypotheses H_1-H_4. For a given $(t_0, x_0) \in \mathbb{R}^{1+n}$ and $u \in \mathcal{U}$, there exists a unique solution to (4.4.7).

Proof. Proposition 4.4.1 ensures that $\bar{F}$ is upper semi-continuous with nonempty compact convex values. The same properties are satisfied by the multifunction F, for each $u \in \mathcal{U}$. Theorem 10.1.3 in [240] guarantees the existence of a global Caratheodory solution to (4.4.7). Moreover, in view of the relation (4.4.9), the uniqueness property of the solution of (4.4.7) easily follows. □

Furthermore, one can show that the set of trajectories generated by the dynamics (4.4.7) is equivalent to the set of solutions of

$$\begin{cases} \dot{x}(t) \in \bar{F}(t,x), \quad a.e.\ t \in [t_0, +\infty) \\ x(t_0) = x_0 \in \mathbb{R}^n \end{cases} . \tag{4.4.10}$$

One has the following result:

Proposition 4.4.4. Let us assume H_1-H_4. Fix $(t_0, x_0) \in \mathbb{R}^{1+n}$. Then the set of solutions of (4.4.7) with initial condition $x(t_0) = x_0$ is equal to the set of solutions of (4.4.10) with initial condition $x(t_0) = x_0$.

Proof. If $x(\cdot)$ is a solution of (4.4.7) with initial condition $x(t_0) = x_0$, then it is trivially also a solution of (4.4.10) with the same initial condition. Take $x(\cdot)$, solution of (4.4.10) such that $x(t_0) = x_0$. In what follows, $L^1(A;\mu)$ is equipped with its natural weak topology. Consider the multifunction $\Sigma : [t_0,\infty) \rightsquigarrow L^1(A;\mu) \times U$ defined as

$$\Sigma(t) := \{(\xi(\cdot), u) : \ u \in U, \ \xi(\cdot) \\ \mu-\text{measurable selection of } \partial_x \varphi(x(t), \cdot)\}$$

and the mapping $\tilde{g} : [t_0,\infty) \times U \times L^1(A;\mu) \to \mathbb{R}^n$ defined as

$$\tilde{g}(t,u,\xi) := g(t,x(t),u) - \int_A k(t,x(t),u,\alpha)\xi(\alpha)\mu(d\alpha).$$

It is a straightforward matter to check that Σ is non-empty (in view of H_3) and has weakly closed graph (in view of the compactness of U and of the upper-semicontinuity and convexity of the sub-differential). Furthermore, in view of H_1, H_2, the map $\tilde{g}$ is weakly continuous. Notice also that the relation

$$\dot{x}(t) \in \{\tilde{g}(t,u,\xi) : \quad (u,\xi) \in \Sigma(t)\}, \qquad \text{a.e. } t \in [t_0,\infty)$$

is clearly satisfied.

So one can apply a well-known selection theorem (see, e.g. Theorem III.38, [239]), which provides the existence of a measurable selection $(\xi(t), u(t)) \in \Sigma(t)$ such that $\dot{x}(t) = \tilde{g}(t,u(t),\xi(t))$, a.e. $t \in [t_0,\infty)$. This concludes the proof. □

4.5 EXISTENCE OF MINIMIZERS AND PROPERTIES OF THE VALUE FUNCTION

Fix $(t_0,x_0) \in \mathbb{R}^{1+n}$. Let us now define the reachable set generated by the dynamics (4.4.10) and starting from the point $x(t_0) = x_0$, evaluated at $s \geq t_0$ (in view of Proposition 4.4.4, one can regard any trajectory of (4.4.10) as a trajectory of (4.4.7) and vice-versa):

$$R(s;t_0,x_0) = \left\{x(s) : \ \dot{x} \in \bar{F}(t,x), \ t \in [t_0,s], \ x(t_0) = x_0\right\}.$$

The set of points of $\operatorname{Gr}\mathcal{T}$ reached by a trajectory of (4.4.7) starting from $x(t_0) = x_0$ is defined as

$$\mathcal{A}_{(t_0,x_0)} = \{(s,y) \in \operatorname{Gr}\mathcal{T} : \ y \in R(s;t_0,x_0), \ s \geq t_0\},$$

while the set of initial conditions for which a feasible trajectory exists is denoted by

$$\mathcal{D} = \left\{(t_0,x_0) \in \mathbb{R}^{1+n} : \ \mathcal{A}_{(t_0,x_0)} \neq \emptyset\right\}.$$

In order to guarantee the existence of a minimizer, one has to assume further conditions, characterizing the behaviour of the cost function W when the end-time $T > t_0$ tends to infinity. In what follows, assume the following growth condition holds:

(GC) Fix $(t_0, x_0) \in \mathbb{R}^{1+n}$. For every $(T_k, x_k) \in \mathcal{A}_{(t_0,x_0)}$ such that $T_k \to +\infty$, one has that $W(T_k, x_k) \to +\infty$.

Clearly, if W is a function coercive w.r.t. t, uniformly w.r.t. x, then the condition **(GC)** is trivially satisfied. The existence of a minimizer for the optimal control problem (P) easily follows.

Theorem 4.5.1. Assume hypothesis **(SH)** and that condition **(GC)** is satisfied. Then, for any $(t_0, x_0) \in \mathcal{D}$, there exists a minimizer for the free-time optimal control problem (P).

Proof. Fix $(t_0, x_0) \in \mathcal{D}$. Let $(T_n, x_n)_{n\in\mathbb{N}}$ be a minimising sequence in $\mathcal{A}_{(t_0,x_0)}$. In particular, $(T_n, x_n) \in \mathrm{Gr}\,\mathcal{T}$ and T_n has to be bounded. In fact, if T_n were not bounded, there would exist a subsequence such that $W(T_n, x(T_n)) \to +\infty$, providing a contradiction with the definition of minimising sequence. Let $M > 0$ be such that $T_n \leq M$ for each n. By standard compactness arguments $T_n \to T^*$ and $x_n(\cdot) \to x^*(\cdot)$ uniformly on $[t_0, M]$ (here, one can consider trajectories x_n, x^* extended on $[t_0, M]$ such that $x_n(t) = x_n(T_n)$ for $T_n \leq t \leq M$ and $x^*(t) = x^*(T^*)$ for $T^* \leq t \leq M$). It follows from Proposition 4.4.1 and assumptions H_4-H_5 that the set $R(s; t_0, x_0)$ is compact for every $t_0 \leq s \leq M$ (see, e.g., Proposition 2.6.1, [17]). Since W is continuous in $\mathrm{Gr}\mathcal{T}$, this concludes the proof. □

One can introduce, for all $(t_0, x_0) \in \mathbb{R}^{1+n}$, the value function of the free-time optimal control problem (P) as

$$V(t_0, x_0) = \inf \left\{ W(T, x) : \ (T, x) \in \mathcal{A}_{(t_0,x_0)} \right\}. \tag{4.5.1}$$

Notice that $V(t_0, x_0) = \infty$ if $(t_0, x_0) \notin \mathcal{D}$. The standard dynamic programming principle for the optimal control problem (P) can be stated as follows:

Proposition 4.5.2. For any $(t, x) \in \mathcal{D}$, take $y : [t, +\infty) \to \mathbb{R}^n$ such that $y(t) = x$ solution of (4.4.7) with a control $u \in \mathcal{U}$. Then, for any $s \in [t, \infty)$ the value function satisfies

$$V(t, x) \leq V(s, y(s)).$$

Furthermore, consider $\bar{y} : [t, +\infty) \to \mathbb{R}^n$ such that $(\bar{T}, \bar{y}(\cdot))$ is a minimizer for $(P)_{(t,x)}$. Then for any $t \leq s \leq \bar{T}$, one has

$$V(t, x) = V(s, \bar{y}(s)).$$

If the growth condition **(GC)** on W is satisfied, one can easily derive also a related growth condition on the value function.

Proposition 4.5.3. Assume **(SH)** and that condition **(GC)** is satisfied. Then the following growth condition holds:

(GC)$_V$ For every $(t_k, x_k) \in \mathcal{D}$ such that $t_k \to \infty$, one has that $V(t_k, x_k) \to \infty$.

Proof. Take $(t_k, x_k) \in \mathcal{D}$ such that $t_k \to \infty$. It follows from the definition of value function that for each $\varepsilon_k > 0$, there exists $(T_{\varepsilon_k}, y_{\varepsilon_k}) \in \mathcal{A}_{(t_k,x_k)}$ such that

$$W(T_{\varepsilon_k}, y_{\varepsilon_k}) \leq V(t_k, x_k) + \varepsilon_k. \tag{4.5.2}$$

Assume that $\varepsilon_k \to 0$. Since $T_{\varepsilon_k} \geq t_k$, then also $T_{\varepsilon_k} \to \infty$ for $k \to \infty$. It follows from the condition **(GC)** on W that

$$\infty = \lim_{k\to\infty} W(t_{\varepsilon_k}, y_{\varepsilon_k}) \leq \lim_{k\to\infty} V(t_k, x_k). \tag{4.5.3}$$

This concludes the proof. □

In order to derive the Hamilton-Jacobi equation for the problem (P), it will be helpful to impose conditions which guarantee the locally Lipschitz continuous regularity in $\mathcal{D}$ of the value function. To this aim, it is necessary to extend to the one-sided Lipschitz case some results provided in [241]. Assume the following inward pointing condition on $\operatorname{Gr}\mathcal{T}$:

(IPC) For any compact set $G \subseteq \mathbb{R}^{1+n}$ there exists $\rho > 0$ such that, for all $(t, x) \in \partial(\operatorname{Gr}\mathcal{T}) \cap G$,

$$\min_{\xi\in\bar{F}(t,x)} \left\{ l^0 + \langle l, \xi\rangle \right\} \leq -\rho$$
$$\forall\ (l^0, l) \in N^P_{\operatorname{Gr}\mathcal{T}}(t, x),\ |(l^0, l)| = 1.$$

It is then possible to prove the following technical result:

Proposition 4.5.4. *Assume H_1-H_5 hold and $\operatorname{Gr}\mathcal{T}$ satisfies **(IPC)**. Then, for any compact set $K \subseteq \mathbb{R}^{1+n}$, there exist $\varepsilon_K,\ L_K > 0$ such that for all $(t_0, x_0) \in \operatorname{Gr}\mathcal{T} \cap K + \varepsilon_K\bar{\mathbb{B}}$*

$$d((t_0, x_0), \mathcal{A}_{(t_0,x_0)}) \leq L_K d((t_0, x_0), \operatorname{Gr}\mathcal{T}). \tag{4.5.4}$$

Proof. Given a closed set $\mathcal{C} \subseteq \mathbb{R}^{1+n}$ and $v \in \mathbb{R}^{1+n}$,

$$\mathcal{P}_{\mathcal{C}}(v) = \{w \in \mathcal{C}|\ |v - w| = d(v, \mathcal{C})\}$$

denotes the set of all projections of v on $\mathcal{C}$. On the other hand, according to ([17], Proposition 4.2.2), given $w \in \mathcal{C}$, the proximal normal cone $N^P_{\mathcal{C}}(w)$ is characterised as

$$N^P_{\mathcal{C}}(w) = \{v \in \mathbb{R}^m|\ \exists\ \alpha > 0 \text{ s.t. } w \in \mathcal{P}_{\mathcal{C}}(w + \alpha v)\}.$$

Define the lower Dini derivative of a function $\psi : \mathbb{R}^{1+n} \to \mathbb{R}$ in the direction of $(1, y)$ as

$$D^-\psi(t, x; 1, y) := \liminf_{h\to 0^+} \frac{\psi(t + h, x + hy) - \psi(t, x)}{h}$$

and fix $K \subset \mathbb{R}^{1+n}$ a compact set. Define $\mathcal{O}_\theta = \mathrm{Gr}\mathcal{T} \cap K + \theta\mathbb{B}$ for some $\theta > 0$ and $G = \bar{\mathcal{O}}_1$. Let $[\tau_1, \tau_2] = \mathrm{co}\mathcal{P}_{\mathbb{R}}(G)$. Fix θ such that

$$\theta < \min\left\{0.5, \frac{1}{L_G + 1}\right\},$$

where L_G is such that $|F(t,x,u)| \leq L_G$ for all $(t,x,u) \in [\tau_1, \tau_2] \times \mathbb{R}^n \times U$. With the choice of $G = \bar{\mathcal{O}}_1$, let us take $\rho > 0$ such that **(IPC)** holds true. Define, for each $(t,x) \in \mathbb{R}^{1+n}$, the functions

$$\begin{aligned} \psi(t,x) &= d((t,x), \mathrm{Gr}\mathcal{T}) \\ \varphi(t,x) &= \begin{cases} (L_F + L)\psi(t,x) - \rho & (t,x) \notin \mathrm{Gr}\mathcal{T} \text{ and} \\ & (t,x) \in \mathcal{O}_\theta \\ +\infty & \text{otherwise} \end{cases}, \end{aligned}$$

where L_F is the one-sided Lipschitz constant of F, and the multifunction $\Phi : \mathbb{R}^{1+n} \rightsquigarrow \mathbb{R}^n$ defined as

$$\Phi(t,x) = \left\{y \in \bar{F}(t,x) |\ D^-\psi(t,x;1,y) \leq \varphi(t,x)\right\}. \tag{4.5.5}$$

It is a straightforward matter to check that $\varphi(t,x)$ is upper semi-continuous. Furthermore, by possibly reducing the size of ρ, it is not restrictive to suppose that there exists $0 < \rho < 1$ satisfying **(IPC)** with the choice $G = \bar{\mathcal{O}}_1$.

It is necessary to check that $\Phi(t,x) \neq \emptyset$ for every $(t,x) \in \mathbb{R}^{1+n}$. If $(t,x) \in \mathrm{Gr}\mathcal{T}$ or $(t,x) \notin \mathcal{O}_\theta$, then $\Phi(t,x) = \bar{F}(t,x) \neq \emptyset$. Otherwise, define

$$(l^0, l) = \frac{(t - \bar{t}, x - \bar{x})}{|(t,x) - (\bar{t}, \bar{x})|} \in N^P_{\mathrm{Gr}\mathcal{T}}(\bar{t}, \bar{x}),\ |(l^0, l)| = 1$$

for any $(\bar{t}, \bar{x}) \in \mathcal{P}_{\mathrm{Gr}\mathcal{T}}(t,x)$. Being $(\bar{t}, \bar{x})$ a projection of (t,x) on $\mathrm{Gr}\mathcal{T}$, then $(\bar{t}, \bar{x}) \in \partial\mathrm{Gr}\mathcal{T}$ and one has

$$|(\bar{t}, \bar{x}) - (t,x)| = d((t,x), \mathrm{Gr}\mathcal{T}) < \theta < 1.$$

In particular this implies $(\bar{t}, \bar{x}) \in G \cap \partial\mathrm{Gr}\mathcal{T}$. In view of **(IPC)** there exists $\bar{\xi} \in \bar{F}(\bar{t}, \bar{x})$ (and then $\bar{u} \in U$ for which $\bar{\xi} \in F(\bar{t}, \bar{x}, \bar{u})$) such that

$$l^0 + \left\langle l, \bar{\xi} \right\rangle \leq -\rho.$$

Take any $\xi \in F(t,x,\bar{u})$. Then one can obtain the following estimates:

$$\begin{aligned} &l^0 + \left\langle l, \bar{\xi} - \xi + \xi \right\rangle = l^0 + \langle l, \xi \rangle + \left\langle l, \bar{\xi} - \xi \right\rangle \leq -\rho \implies \\ &l^0 + \langle l, \xi \rangle \leq -\rho + \left\langle l, \xi - \bar{\xi} \right\rangle = -\rho + \tfrac{\left\langle x - \bar{x}, \xi - \bar{\xi} \right\rangle}{d((t,x), \mathrm{Gr}\mathcal{T})}. \end{aligned} \tag{4.5.6}$$

Choose $\xi^* \in F(\bar{t}, x, \bar{u})$ such that $|\xi^* - \xi| \leq L|\bar{t} - t|$. It is then possible to estimate the right hand side of (4.5.6) as follows:

$$\begin{aligned}
&\frac{\langle x - \bar{x}, \xi - \bar{\xi} \rangle}{d((t,x), \mathrm{Gr}\mathcal{T})} = \\
&\frac{\langle x - \bar{x}, \xi - \xi^* \rangle}{d((t,x), \mathrm{Gr}\mathcal{T})} + \frac{\langle x - \bar{x}, \xi^* - \bar{\xi} \rangle}{d((t,x), \mathrm{Gr}\mathcal{T})} \leq \\
&\frac{|x - \bar{x}||\xi - \xi^*|}{d((t,x), \mathrm{Gr}\mathcal{T})} + \frac{L_F |x - \bar{x}|^2}{d((t,x), \mathrm{Gr}\mathcal{T})} \leq \\
&\frac{L|t - \bar{t}||x - \bar{x}|}{d((t,x), \mathrm{Gr}\mathcal{T})} + \frac{L_F |x - \bar{x}|^2}{d((t,x), \mathrm{Gr}\mathcal{T})} \leq \\
&\frac{L|(t,x) - (\bar{t}, \bar{x})|^2}{d((t,x), \mathrm{Gr}\mathcal{T})} + \frac{L_F |(t,x) - (\bar{t}, \bar{x})|^2}{d((t,x), \mathrm{Gr}\mathcal{T})},
\end{aligned}$$

where, in turns, it has used the one-sided Lipschitz property of $x \mapsto F(t, x, u)$, uniformly w.r.t. $(t, u) \in \mathbb{R} \times U$, and the Lipschitz continuity of the mapping $t \mapsto F(t, x, u)$, uniformly w.r.t. $(x, u) \in \mathbb{R}^n \times U$. This analysis shows that

$$l^0 + \langle l, \xi \rangle \leq -\rho + (L_F + L) d((t,x), \mathrm{Gr}\mathcal{T}).$$

Let us show that $\xi \in \Phi(t, x)$. Since $(\bar{t}, \bar{x}) \in \mathrm{Gr}\mathcal{T}$ and $(t, x) \notin \mathrm{Gr}\mathcal{T}$, then $\psi(t, x) > 0$ and one can compute

$$\begin{aligned}
&D^- \psi(t, x; 1, \xi) = \\
&\liminf_{h \to 0^+} \frac{\psi^2(t + h, x + h\xi) - \psi^2(t, x)}{h(\psi(t + h, x + h\xi) + \psi(t, x))} \leq \\
&\liminf_{h \to 0^+} \frac{|(t + h - \bar{t}, x + h\xi - \bar{x})|^2 - |(t - \bar{t}, x - \bar{x})|^2}{h(\psi(t + h, x + h\xi) + \psi(t, x))} = \\
&\frac{t - \bar{t} + \langle x - \bar{x}, \xi \rangle}{\psi(t, x)} = l^0 + \langle l, \xi \rangle \leq \varphi(t, x).
\end{aligned}$$

Thus, $\xi \in \Phi(t, x)$. Fix $\varepsilon > 0$ such that

$$\varepsilon < \min \left\{ 1 - \theta(L_G + 1), \frac{\theta\rho}{C}, \frac{\theta(1 - \rho)}{C} \right\},$$

where $C = \exp\left(\int_{\tau_1}^{\tau_2} L_F + L ds \right)$. Let $(t_0, x_0) \in \bar{\mathcal{O}}_\varepsilon = \mathrm{Gr}\mathcal{T} \cap K + \varepsilon\bar{\mathbb{B}}$.

If $(t_0, x_0) \in \mathrm{Gr}\mathcal{T}$, then (4.5.4) is trivially satisfied. Alternatively, observe that $(t_0, x_0) \in \bar{\mathcal{O}}_\varepsilon \subseteq G$ and $x_0 \in \mathcal{P}_{\mathbb{R}^n}(G)$. Define $T = t_0 + \theta$. Therefore, for any solution $x(\cdot)$ of (4.4.7) starting from (t_0, x_0) with control $u(\cdot)$ it holds

$$|x(t) - x_0| \leq \int_{t_0}^{t} |F(t, x, u)| \leq L_G |t - t_0| \leq L_G \theta$$

and $(t, x(t)) \in (t_0, x_0) + (L_G + 1)\theta\bar{\mathbb{B}}$ for all $t \in [t_0, T]$.

Since $\theta(L_G+1)<1-\varepsilon<1$, then $(t,x(t))\in G$ for all $t\in[t_0,T]$. Then, in view of well known selection theorems (see [241], Proposition 2.1) there exists a solution to

$$\dot{x}(t)\in\Phi(t,x(t)),\ x(t_0)=x_0,\ t\in[t_0,T]. \tag{4.5.7}$$

Define $\bar{T}\in[t_0,\infty)$ as the first time such that a given solution $x(\cdot)$ of (4.5.7) satisfies either $(\bar{T},x(\bar{T}))\in \mathrm{Gr}\mathcal{T}$ or $(\bar{T},x(\bar{T}))\in\partial\mathcal{O}_\theta$. If there is not such a $\bar{T}$, fix $\bar{T}:=t_0+\theta=T$. Setting $\tilde{d}(t)=d((t,x(t)),\mathrm{Gr}\mathcal{T})$, it follows from the relation (4.5.5) that, for all $t\in[t_0,\bar{T}]$, $\tilde{d}(t)$ satisfies

$$\begin{aligned}&\dot{\tilde{d}}(t)=D^-\psi(t,x(t);1,\dot{x}(t))\le(L_F+L)\tilde{d}(t)-\rho\\&\tilde{d}(t_0)=d((t_0,x_0),\mathrm{Gr}\mathcal{T})\le\varepsilon.\end{aligned}$$

The definitions of τ_1,τ_2 imply that $\tau_1\le t_0\le t_0+\theta\le\tau_2$. Using Gronwall's Lemma, then one easily estimates

$$\tilde{d}(t)\le\exp\left(\int_{\tau_1}^{\tau_2}L_F+Lds\right)\tilde{d}(t_0)-(t-t_0)\rho= \tag{4.5.8}$$

$$C\tilde{d}(t_0)-(t-t_0)\rho<C\varepsilon-(t-t_0)\rho. \tag{4.5.9}$$

Recall that the differential equation for $\tilde{d}(\cdot)$ is studied on $[t_0,\bar{T}]$ so that, since $C\varepsilon<C\varepsilon/\rho\le\theta$, one has that $\tilde{d}(t)<\theta$ for all $t\in[t_0,\bar{T}]$. Hence, $(t,x(t))\in\mathcal{O}_\theta$ for all $t\in[t_0,\bar{T}]$. In particular, $\tilde{d}(t)=0$ if

$$t=t_0+\frac{C\tilde{d}(t_0)}{\rho}<t_0+\theta\implies t-t_0=\frac{C\tilde{d}(t_0)}{\rho}<\theta. \tag{4.5.10}$$

This shows that $\bar{T}\in[t_0,\infty)$ has to be such that $(\bar{T},x(\bar{T}))\in\mathrm{Gr}\mathcal{T}$ and $(\bar{T},x(\bar{T}))\in\mathcal{A}_{(t_0,x_0)}$. Furthermore one can obtain the following estimate:

$$\tilde{d}((t_0,x_0),\mathcal{A}(t_0,x_0))\le|(t_0,x_0)-(\bar{T},x(\bar{T}))|\le \tag{4.5.11}$$

$$|t_0-\bar{T}|+|x_0-x(\bar{T})|\le\frac{C\tilde{d}(t_0)}{\rho}+L_G|t_0-\bar{T}|\le \tag{4.5.12}$$

$$\frac{C(L_G+1)}{\rho}\tilde{d}(t_0)=L_K\tilde{d}(t_0) \tag{4.5.13}$$

where in the last two steps we have used the relation (4.5.10). This concludes the proof. □

Proposition 4.5.5. Assume conditions **(SH)** and **(GC)** hold. Suppose that $\mathrm{Gr}\,\mathcal{T}$ satisfies **(IPC)**. Then $\mathcal{D}\subseteq\mathbb{R}^{1+n}$ is an open set and $V(t_k,x_k)\to+\infty$ for all $(t_k,x_k)\in\mathcal{D}$ such that $(t_k,x_k)\to(t_0,x_0)\in\partial\mathcal{D}$.

Proof. Firstly, show that $\mathcal{D}^{\mathsf{c}}$, the complement of $\mathcal{D}$, is closed. Let (t_n,x_n) be a sequence in $\mathcal{D}^{\mathsf{c}}$ converging to (t,x). It is enough to prove that $(t,x)\in\mathcal{D}^{\mathsf{c}}$. By contradiction, assume that $(t,x)\in\mathcal{D}$. By definition of $\mathcal{D}$, there exist

$(T, y) \in \mathcal{A}_{(t,x)}$, a control $u_x \in \mathcal{U}$ and $x(\cdot)$ solution of (4.4.7) with control $u_x \in \mathcal{U}$ such that $x(t) = x,\ x(T) = y,\ T \geq t$ and $(T, y) \in \operatorname{Gr} \mathcal{T}$. One can take $\varepsilon_n > 0$, $\varepsilon_n \to 0$ such that

$$|(t, x) - (t_n, x_n)| < \varepsilon_n$$

Let us consider two different cases:

CASE 1: $T = t$**.** Let $K \subseteq \mathbb{R}^{1+n}$ be a compact set containing $(t, x) = (T, y) \in \operatorname{Gr} \mathcal{T}$. Then

$$d((t_n, x_n), \operatorname{Gr}\mathcal{T}) < |(t_n, x_n) - (T, y)| = |(t_n, x_n) - (t, x)| < \varepsilon_n$$

and $(t_n, x_n) \in \operatorname{Gr} \mathcal{T} \cap K + \varepsilon_n \bar{\mathbb{B}}$. In view of Proposition 4.5.4, there exist $\varepsilon_K,\ L_K > 0$ and, for n sufficiently large, $\varepsilon_n \leq \varepsilon_K$ holds.

CASE 2: $T > t$**.** Taking n sufficiently large, one can assume that $t_n < T$. Let $x_n(\cdot)$ be the unique trajectory of (4.4.7) when $u(\cdot) = u_x(\cdot)$ with initial condition $x(t_n) = x_n$. In view of relation (4.4.9), one has that

$$|x_n(T) - x(T)| < \lambda(T)\varepsilon_n \tag{4.5.14}$$

where $\lambda(\cdot)$ is the function appearing in condition (4.4.9), Remark 4.4.2. Fix $K \subseteq \mathbb{R}^{1+n}$ a compact set containing $(T, y) = (T, x(T))$ and choose $\varepsilon_K,\ L_K$ such that the statement Proposition 4.5.4 is satisfied. For all $\varepsilon_n < \frac{\varepsilon_K}{\lambda(T)}$ it follows $(T, x_n(T)) \in \operatorname{Gr} \mathcal{T} \cap K + \varepsilon_K \bar{\mathbb{B}}$.

In both **CASES 1-2**, it follows, in view of Proposition 4.5.4

$$d((t_n, x_n), \mathcal{A}_{(t_n,x_n)}) \leq L_K d((t_n, x_n), \operatorname{Gr} \mathcal{T})$$

Since $(t_n, x_n) \notin \mathcal{D}$, then $\mathcal{A}_{(t_n,x_n)} = \emptyset$, implying that $d((t_n, x_n), \mathcal{A}_{(t_n,x_n)}) = +\infty$, which yields a contradiction. The next step is to prove that the value function $V(t, x)$ tends to infinity when (t, x) approaches $\partial\mathcal{D}$. Fix $\{(t_k, x_k)\}_k \subseteq \mathcal{D}$, $(t_k, x_k) \to (t_0, x_0) \in \partial\mathcal{D}$. Let $x_k(\cdot)$ be a trajectory of (4.4.10) with initial condition $x_k(t_k) = x_k$.

Assume by contradiction that $|V(t_k, x_k)| < \bar{M}$ for all k and some $\bar{M} > 0$. It follows from the definition of value function that, for all $\varepsilon_k > 0$, there exists $(T_k, y_k) \in \mathcal{A}_{(t_k,x_k)}$ such that

$$W(T_k, x_k) \leq V(t_k, x_k) + \varepsilon_k$$

Hence, $|W(T_k, x_k)| < +\infty$. In view of **(GC)**, T_k has to be bounded by a constant M. Hence, in view of the hypothesis H_2, also y_k is uniformly bounded and one can arrange along a subsequence (not relabelled) that $(T_k, y_k) \to (T_0, y_0) \in \operatorname{Gr} \mathcal{T}$. Arguing as in Theorem 4.5.1, one can find a subsequence of trajectories of (4.4.10) such that $x_k(\cdot) \to \tilde{x}(\cdot)$ uniformly on $[0, M]$. In particular, $x_k = x_k(t_k) \to \tilde{x}(t_0) = x_0$. Hence $\tilde{x}(\cdot)$ is a trajectory starting from (t_0, x_0), such that $\dot{\tilde{x}} \in \bar{F}(t, \tilde{x})$ a.e. $t \in [t_0, M]$ and $(T_0, y_0) = (T_0, \tilde{x}(T_0)) \in \operatorname{Gr} \mathcal{T}$. Then $\mathcal{A}_{(t_0,x_0)} \neq \emptyset$, which is impossible since $\mathcal{D}$ is open and $(t_0, x_0) \in \partial\mathcal{D}$. This concludes the proof. □

The existence of a minimizer, together with **(IPC)** and **(GC)** conditions guarantee the locally Lipschitz continuity of the value function on $\mathcal{D}$.

Theorem 4.5.6. Assume that conditions **(SH)**, **(GC)** hold and that $\mathrm{Gr}\,\mathcal{T}$ satisfies **(IPC)**. Then V is locally Lipschitz on $\mathcal{D}$.

Proof. Firstly, show that, for any $(t_0, x_0) \in \mathcal{D}$, there exist $\varepsilon_V,\ L_V > 0$ such that for all $(t_1, x_1),\ (t_2, x_2) \in \mathcal{O}_{\varepsilon_V} := (t_0, x_0) + \varepsilon_V \mathbb{B}$, one has

$$|V(t_1, x_1) - V(t_2, x_2)| \leq L_V |(t_1, x_1) - (t_2, x_2)|.$$

Let $L_W > 0$ be the Lipschitz constant of W and $\varepsilon_W > 0$ the neighbourhood radius in which the Lipschitz property of W is verified.

Fix $\rho > 0$ and $(t_0, x_0) \in \bar{\mathcal{O}}_\rho \subset \mathcal{D}$. Define

$$\bar{T} := \sup \left\{ T :\ (T, x(\cdot)) \text{ minimizer of } (P)_{(t,x)},\ (t, x) \in \bar{\mathcal{O}}_\rho \right\}$$

Since $\bar{\mathcal{O}}_\rho \subset \mathcal{D}$, then $\bar{T} < \infty$. Let $(T_0^*, x_0^*(\cdot))$ be the minimizer of the optimal control problem $P_{(t_0,x_0)}$. In view of the hypothesis H_2, for all $(t, x) \in \bar{\mathcal{O}}_\rho$, one has

$$|(T^*, x^*(T^*)) - (T_0^*, x_0^*(T_0^*))| \leq 2(\bar{T}C + \rho + \bar{T}) =: R,$$

where $(T^*, x^*(\cdot))$ is the minimizer of the optimal control problem $(P)_{(t,x)}$.

Hence, one can fix both $K = (T_0^*, x_0^*(T_0^*)) + R\bar{\mathbb{B}}$ and ε_K, L_K such that the statement of Proposition 4.5.4 is satisfied for all $(t, x) \in \mathrm{Gr}\mathcal{T} \cap K + \varepsilon_K \bar{\mathbb{B}}$. Fix $\varepsilon_V > 0$ such that

$$\varepsilon_V \leq \min \left\{ \rho, \frac{\min\{\varepsilon_K, \varepsilon_W\}}{2\lambda(\bar{T})(L_K + 1)} \right\}$$

where $\lambda(\cdot)$ is the function introduced in Remark 4.4.2.

Take $(t_1, x_1),\ (t_2, x_2) \in \mathcal{O}_{\varepsilon_V}$ such that $V(t_1, x_1) > V(t_2, x_2)$. Let $u_2(\cdot)$ be the optimal control starting from (t_2, x_2) with trajectory $x_2(\cdot)$ and optimal time T_2. Then $(T_2, x_2(T_2)) \in \mathrm{Gr}\mathcal{T} \cap K$, since $\mathcal{O}_{\varepsilon_V} \subseteq \mathcal{O}_\rho$. It is convenient to distinguish the two cases $T_2 > t_2$ and $T_2 = t_2$:

CASE 1: If $T_2 > t_2$, then it is not restrictive to assume also $T_2 > t_1$ (it is sufficient to reduce the size of ε_V). Let $x_1(\cdot)$ be the trajectory of (4.4.7) starting from (t_1, x_1) with control $u_2(\cdot)$. Proposition 4.5.2 ensures $V(t_2, x_2) = W(T_2, x_2(T_2))$ and $V(t_1, x_1) \leq V(T_2, x_1(T_2))$. In view of (4.4.9), one has that

$$\begin{aligned} &|(T_2, x_2(T_2)) - (T_2, x_1(T_2))| \leq \\ &\qquad \leq |(t_1, x_1) - (t_2, x_2)| \lambda(T_2) \leq 2\varepsilon_V \lambda(\bar{T}) < \varepsilon_K \end{aligned}$$

where $\lambda(\cdot)$ is the function introduced in Remark 4.4.2.

Therefore $(T_2, x_1(T_2)) \in \mathrm{Gr}\mathcal{T} \cap K + \varepsilon_K \bar{\mathbb{B}}$. Set $(\bar{t}, \bar{x}) := (T_2, x_1(T_2))$ and take $\bar{x}_1(\cdot)$ be a solution of the differential inclusion (4.5.7) starting from $(\bar{t}, \bar{x})$. Then, in view of the relation (4.5.9), there exists a time $\bar{T}_1 \geq \bar{t}$ such that $(\bar{T}_1, \bar{x}_1(\bar{T}_1)) \in \mathrm{Gr}\mathcal{T}$. In particular, one obtains the inequality $V(t_1, x_1) \leq W(\bar{T}_1, \bar{x}_1(\bar{T}_1))$. It then follows from such a construction the estimate

$$V(t_1, x_1) - V(t_2, x_2) \leq W(\bar{T}_1, \bar{x}_1(\bar{T}_1)) - W(T_2, x_2(T_2)). \tag{4.5.15}$$

Furthermore, observe that

$$|(\bar{T}_1, \bar{x}_1(\bar{T}_1)) - (T_2, x_2(T_2))| \leq \tag{4.5.16}$$
$$|(\bar{T}_1, \bar{x}_1(\bar{T}_1)) - (\bar{t}, \bar{x})| + |(\bar{t}, \bar{x}) - (T_2, x_2(T_2))| \leq \tag{4.5.17}$$
$$|(\bar{T}_1, \bar{x}_1(\bar{T}_1)) - (\bar{t}, \bar{x})| + \lambda(\bar{T})|(t_1, x_1) - (t_2, x_2)| \tag{4.5.18}$$

where the relation (4.4.9) was used in the last inequality. Using now the relation (4.5.10) in (4.5.16) (as it is done in (4.5.13)), one obtains

$$|(\bar{T}_1, \bar{x}_1(\bar{T}_1)) - (\bar{t}, \bar{x})| \leq \tag{4.5.19}$$
$$L_K d((\bar{t}, \bar{x}), \mathrm{Gr}\mathcal{T}) \leq L_K |(\bar{t}, \bar{x}) - (T_2, x_2(T_2))|. \tag{4.5.20}$$

So one can obtain from (4.5.16) and (4.5.19) the relevant estimates

$$|(\bar{T}_1, \bar{x}_1(\bar{T}_1)) - (T_2, x_2(T_2))| \leq \tag{4.5.21}$$
$$(L_K + 1)\lambda(\bar{T})|(t_1, x_1) - (t_2, x_2)| \leq \tag{4.5.22}$$
$$2\lambda(\bar{T})(L_K + 1)\varepsilon_V \leq \varepsilon_W \tag{4.5.23}$$

f where in the first inequality the relation (4.4.9) was used again.

CASE 2: If $T_2 = t_2$ then $|(t_2, x_2) - (t_1, x_1)| \leq 2\varepsilon_V < \varepsilon_K$ and $(t_1, x_1) \in \mathrm{Gr}\mathcal{T} \cap K + \varepsilon_K \bar{\mathbb{B}}$. Set $(\bar{t}, \bar{x}) = (t_1, x_1)$ and, as in the previous case, take a solution $\bar{x}_1(\cdot)$ of (4.5.7) starting from $(\bar{t}, \bar{x})$ and a time $\bar{T}_1 \geq \bar{t}$ such that $(\bar{T}_1, \bar{x}_1(\bar{T}_1)) \in \mathrm{Gr}\mathcal{T}$. Using the same argument employed in **CASE 1**, one can obtain the relations (4.5.15) and (4.5.21).

Therefore, in both **CASES 1-2**, the hypothesis H_6 can be invoked and it follows from the estimates (4.5.15) and (4.5.21) that

$$\begin{aligned}
&V(t_1, x_1) - V(t_2, x_2) \leq W(\bar{T}_1, \bar{x}_1(\bar{T}_1)) - W(T_2, x_2(T_2)) \leq \\
&L_W |(\bar{T}_1, \bar{x}_1(\bar{T}_1)) - (T_2, x_2(T_2))| \leq \\
&L_W C_1 |(t_1, x_1) - (t_2, x_2)| := L_V |(t_1, x_1) - (t_2, x_2)|
\end{aligned}$$

where $C_1 = 2\lambda(\bar{T})(L_K + 1)$ if $T_2 > t_2$ and $C_1 = L_K + 1$ if $T_2 = t_2$. This concludes the proof. □

Remark 4.5.7. The growth condition **(GC)** permits to the optimal trajectory $\bar{x}(\cdot)$ of problem $(P)_{(t_0,x_0)}$ to reach the point in $\mathcal{A}_{(t_0,x_0)}$ which minimizes the cost function W. In general, $\bar{x}(\cdot)$ *does not* stop when the target is reached, as it is the case in which one considers a problem (P) in which the parameter to minimize is the time. In fact, the related cost function in the minimum time problem satisfies the stronger condition:

- **(LGC)**. For any $K \subseteq \mathbb{R}^{n+1}$ compact, there exists $\gamma > 0$ such that

$$W(t', x') \geq W(t, x) + \gamma(t' - t)$$

for all $(t, x) \in K$ and $(t', x') \in \mathcal{A}_{(t,x)}$

This particular feature of the problem of study is also reflected in the formulation of the Hamilton-Jacobi equation.

4.6 DYNAMIC PROGRAMMING AND INVARIANCE PRINCIPLES

In this section, the dynamic programming principle in Proposition 4.5.2 is linked to the weak and strong invariance principles for the epigraph and the hypograph of the value function w.r.t. a suitable, augmented dynamics. To this aim, introduce the augmented differential inclusion

$$(AD)_{y_0} \ \{\dot{y}(t) \in \Gamma(y(t)), \quad a.e.\ t \in [0, +\infty), y(0) = y_0\} \tag{4.6.1}$$

where $y(t) = (\tau(t), x(t), a(t))$, $y_0 = (\tau_0, x_0, a_0) \in \mathbb{R}^{1+n+1}$ and $\Gamma(\tau, x, a) = \{1\} \times \bar{F}(\tau, x) \times \{0\}$. It is easy to check that all of the properties stated in Proposition 4.4.1 for $\bar{F}$ are still valid for Γ.

Definition 4.6.1. Suppose $\mathcal{O} \subseteq \mathbb{R}^{1+n+1}$ is open, $y_0 \in \mathcal{O}$ and $y(\cdot)$ solution of $(AD)_{y_0}$. Then $T > 0$ is an escape time from $\mathcal{O}$ (in which case it writes $\mathrm{Esc}(y(\cdot), \mathcal{O}) := T$), provided at least one of the following conditions occurs:

a) $T = \infty$ and $y(t) \in \mathcal{O}$ for all $t \geq 0$;

b) $y(t) \in \mathcal{O}$ for all $t \in [0, T)$ and $||y(t)|| \to \infty$ as $t \to T$.

c) $T < \infty$, $y(t) \in \mathcal{O}$ for all $t \in [0, T)$ and $d(y(t), \mathcal{O}^c) \to 0$ as $t \to T$.

In the following, the basic definitions of invariance principles are recalled. In particular, the weak invariance principle is stated in a local version.

Definition 4.6.2. *Take a closed set $\mathcal{C} \subseteq \mathbb{R}^{1+n+1}$ and an open set $\mathcal{O} \subseteq \mathbb{R}^{1+n+1}$. $\mathcal{C}$ is weakly invariant w.r.t. the set-valued dynamics $\dot{y} \in \Gamma(y)$ in $\mathcal{O}$ (and it writes $(\mathcal{C}, \Gamma)$ weakly invariant in $\mathcal{O}$) if and only if, for any initial condition $y_0 \in \mathcal{C} \cap \mathcal{O}$ and for some $T > 0$ the Cauchy problem $(AD)_{y_0}$ admits a solution $y(t) \in \mathcal{C} \cap \mathcal{O}$ for all $t \in [0, T)$.*

Definition 4.6.3. *A closed set $\mathcal{C} \subseteq \mathbb{R}^{1+n+1}$ is strongly invariant w.r.t. the set-valued dynamics $\dot{y} \in \Gamma(y)$ (and it writes $(\mathcal{C}, \Gamma)$ strongly invariant) if and only if, for any $y_0 \in \mathcal{C}$, $T \geq 0$ and $y : [0, T] \to \mathbb{R}^{1+n+1}$ solution of $(AD)_{y_0}$, one has $y(t) \in \mathcal{C}$ for all $t \in [0, T]$.*

The existence of an optimal trajectory can be reformulated as both a weak invariance principle for the epigraph of V and a strong invariance principle for the hypograph of V. Such properties will be captured by the next propositions.

Remark 4.6.4. Fix $y_0 = (\tau_0, x_0, a_0) \in \mathbb{R}^{1+n+1}$. Any solution $y(t) = (\tau(t), x(t), a(t))$ of $(AD)_{y_0}$ is such that $\tau(t) = t + \tau_0$. The inverse function of $\tau(t)$ is $t(\tau) = \tau - \tau_0$. Furthermore, one can observe that $z(\tau) := x(t(\tau))$ satisfies $\dot{z}(\tau) \in \bar{F}(\tau, z(\tau))$ a.e. $\tau \in [\tau_0, \infty)$ and $z(\tau_0) = x_0$.

Proposition 4.6.5. Assume that **(SH)**, **(IPC)** and **(GC)** hold true and V is bounded below and lower semi-continuous. Fix $\mathcal{E} = \mathrm{epi}(V)$, where

$$\mathrm{epi}(V) = \{(\tau, x, \beta) \in \mathbb{R}^{1+n+1} : V(\tau, x) \leq \beta\}$$

and the set $\mathcal{O} = (\Omega^{\mathsf{c}} \cap \mathcal{D}) \times \mathbb{R}$, where

$$\Omega = \{(\tau, x) \in \mathrm{Gr}\, \mathcal{T} : \ V(\tau, x) = W(\tau, x)\}.$$

Then $(\mathcal{E}, \Gamma)$ is weakly invariant in $\mathcal{O}$

Proof. Since V is lower semi-continuous, $\mathcal{E}$ is a closed set. Furthermore, $\mathcal{O}$ is an open set in view of Proposition 4.5.3. Fix $(\tau_0, x_0, \beta_0) \in \mathcal{E} \cap \mathcal{O}$. Then $V(\tau_0, x_0) \leq \beta_0 < \infty$.

Theorem 4.5.1 ensures the existence of an optimal solution $z^*(\tau)$ and an optimal time $S^* > \tau_0$ to the free-time optimal control problem (P) with initial condition $z^*(\tau_0) = x_0$ and such that $(S^*, z^*(S^*)) \in \mathrm{Gr}\mathcal{T}$ (here, in view of Proposition 4.4.4, $z^*(\cdot)$ is thought as a solution of (4.4.10) with initial condition $z^*(\tau_0) = x_0$).

By the optimality principle, for all $\tau \in [\tau_0, S^*]$,

$$V(\tau, z^*(\tau)) = V(\tau_0, z(\tau_0)) \leq \beta_0$$

In view of Proposition 4.5.5, $(\tau, z^*(\tau)) \in \mathcal{D}$ for all $\tau \in [\tau_0, S^*]$. Furthermore, one has that $\tau_0 < \mathrm{Esc}((\cdot, z^*(\cdot), V((\cdot, z^*(\cdot))), \Omega^{\mathsf{c}} \times \mathbb{R}) \leq S^*$ since $V(S^*, z^*(S^*)) = W(S^*, z^*(S^*))$. For all $t \geq 0$, define $\tau(t) = t + \tau_0$. Therefore $\dot{\tau}(t) = 1$ and $\tau(0) = \tau_0$. Define $x^*(t) = z^*(\tau(t))$ and observe that $y^*(t) = (\tau(t), x^*(t), \beta_0)$ is a solution of (4.6.1) with initial conditions $(\tau(0), x^*(0), \beta(0)) = (\tau_0, x_0, \beta_0)$.

Hence, there exists $T^* = S^* - \tau_0 \geq 0$ such that

$$V(\tau(t), x^*(t)) \leq \beta_0$$

for all $t \in [0, T^*]$. Furthermore, one has that $(\tau(t), x^*(t)) \in \mathcal{D}$ for all $t \in [0, T^*]$ and that $0 < \mathrm{Esc}((\tau(\cdot), x^*(\cdot), V(\tau(\cdot), x^*(\cdot))), \Omega^{\mathsf{c}} \times \mathbb{R}) \leq T^*$ since $V(\tau(T^*), x^*(T^*)) = W(\tau(T^*), x^*(T^*))$. This concludes the proof. □

Proposition 4.6.6. Assume that H_1-H_4 are satisfied and that V is upper semi-continuous. Define $\mathcal{H} = \mathrm{hypo}(V)$, that is

$$\mathrm{hypo}(V) = \{(\tau, x, \beta) \in \mathbb{R}^{1+n+1} : V(\tau, x) \geq \beta\}$$

Then $(\mathcal{H}, \Gamma)$ is strongly invariant.

Proof. Since V is upper semi-continuous, then $\mathcal{H}$ is a closed set. Fix $(\tau_0, x_0, \beta_0) \in \mathcal{H}$. If $(\tau_0, x_0) \notin \mathcal{D}$, then the thesis is trivially satisfied. Assume that $(\tau_0, x_0) \in \mathcal{D}$. Then $V(\tau_0, x_0) \geq \beta_0$.

In view of Remark 4.6.4, given any trajectory of (4.6.1), namely $y(t) = (\tau(t), x(t), \beta_0)$, with initial condition $y(0) = (\tau_0, x_0, \beta_0)$, it is possible to define

$t(\tau) = \tau - \tau_0$ and $z(\tau) = x(t(\tau))$, trajectory of $\dot{z}(\tau) \in \bar{F}(\tau, z(\tau))$ a.e. $\tau \in [\tau_0, +\infty)$, with initial condition $z(\tau_0) = x_0$. Observe that the value function V is non decreasing along $z(\tau)$ so that, for all $S \geq \tau_0$ and $\tau \in [\tau_0, S]$

$$\beta_0 \leq V(\tau_0, x_0) \leq V(\tau, z(\tau))$$

Finally, for any solution $y(t)$ of (4.6.1) with initial condition $y(t_0) = (\tau_0, x_0, \beta_0)$ and for any $T \geq 0$, one can set $S = T + \tau_0 \geq \tau_0$. Hence

$$\beta_0 \leq V(\tau_0, x_0) \leq V(\tau(t), x(t))$$

for all $t \in [0, T]$. This concludes the proof. □

4.7 HAMILTON-JACOBI-BELLMAN INEQUALITIES

It is finally possible to characterise the value function (4.5.1) as the unique viscosity solution of the Hamilton-Jacobi related to the problem (P). Define the maximized and minimized Hamiltonians for Γ.

Definition 4.7.1. *Fix $\eta, y \in \mathbb{R}^{1+n+1}$, $y = (\tau, x, a)$, $\eta = (\eta_1, \eta_2, \eta_3)$. The minimized Hamiltonian is defined as*

$$h_\Gamma(y, \eta) = \min_{v \in \Gamma(y)} \langle v, \eta \rangle = \min_{v \in \bar{F}(\tau, x)} \langle (1, v, 0), (\eta_1, \eta_2, \eta_3) \rangle ;$$

the maximized Hamiltonian is defined as

$$H_\Gamma(y, \eta) = \max_{v \in \Gamma(y)} \langle v, \eta \rangle = \max_{v \in \bar{F}(\tau, x)} \langle (1, v, 0), (\eta_1, \eta_2, \eta_3) \rangle .$$

Therefore, the weak invariance and strong invariance principle can be characterised in Hamiltonian forms. Firstly, observe that, since the set-valued map Γ inherits the same properties of $\bar{F}$ (summarised in Proposition 4.4.1 and hypothesis H_4), then the following result holds true ([242], Theorem 3.1):

Proposition 4.7.2. Assume H_1-H_4 are satisfied, V is lower semi-continuous and $\mathcal{O} \subseteq \mathbb{R}^{1+n+1}$ is an open set. Then the following statements are equivalent:

i) $(\mathrm{epi}(V), \Gamma)$ is weakly invariant in $\mathcal{O}$;

ii) For all $(\tau, x, a) \in \mathrm{epi}(V) \cap \mathcal{O}$,
$h_\Gamma((\tau, x, a), \eta) \leq 0$ for all $\eta \in N^P_{\mathrm{epi}(V)}(\tau, x, a)$.

Since Γ also satisfies the relation (4.4.2), then one can invoke a strong invariance principle proved in ([235], Corollary 5).

Proposition 4.7.3. Assume H_1-H_4 are satisfied and V is upper semi-continuous. Then the following statements are equivalent:

i) $(\mathrm{hypo}(V), \Gamma)$ is strongly invariant

ii) For all $(\tau, x, a) \in \mathrm{hypo}(V)$ and $\eta \in N^P_{\mathrm{hypo}(V)}(\tau, x, a)$,
$\limsup_{(\tau', x', a') \to_\eta (\tau, x, a)} H_\Gamma((\tau', x', a'), \eta) \leq 0$.

In the previous proposition, given $z \in \mathbb{R}^{1+n+1}$ and a non-zero vector $\eta \in \mathbb{R}^{1+n+1}$, $z' \to_\eta z$ is equivalent to say that $z' \to z$ and $(z' - z)/|z' - z| \to \eta/|\eta|$.

In what follows, it is proved a comparison principle result characterizing any continuous function that exhibits the same qualitative properties of the value function V. Precisely:

Proposition 4.7.4. Assume that **(SH)** hold and that **(GC)** and **(IPC)** are satisfied. Let $\Theta : \mathbb{R}^{1+n} \to \mathbb{R}$ be a continuous, bounded below function such that:

a) $\Theta(t, x) \leq W(t, x)$ for each $(t, x) \in \mathrm{Gr}\, \mathcal{T}$;

b) $\Theta(t, x) = +\infty$ for all $(t, x) \notin \mathcal{D}$;

c) $\Theta(t_k, x_k) \to +\infty$ for all $(t_k, x_k) \in \mathcal{D}$ such that $(t_k, x_k) \to (t, x) \in \partial\mathcal{D}$;

d) For every $(t_k, x_k) \in \mathcal{D}$ such that $t_k \to \infty$, then $\Theta(t_k, x_k) \to \infty$.

Then one has that:

i) If $(\mathrm{epi}(\Theta), \Gamma)$ is weakly invariant in $\mathcal{O} = (\Omega^c \cap \mathcal{D}) \times \mathbb{R}$, where

$$\Omega = \{(\tau, x) \in \mathrm{Gr}\, \mathcal{T} : \ \Theta(\tau, x) = W(\tau, x)\},$$

then one has that $V(t, x) \leq \Theta(t, x)$.

ii) if $(\mathrm{hypo}(\Theta), \Gamma)$ is strongly invariant. Then one has $V(t, x) \geq \Theta(t, x)$

Proof. i). Given any $y_0 = (t_0, x_0, a_0) \in \mathrm{epi}(\Theta) \cap \mathcal{O}$, let us define

$$\begin{aligned} T_{max} := \sup \{T > 0 : \ \exists\, y(\cdot) \text{ solution of } (AD)_{y_0} \\ \text{s.t. } y(t) \in \mathrm{epi}(\Theta) \cap \mathcal{O} \ \text{ for all } t \in [0, T)\} \end{aligned} \tag{4.7.1}$$

Since the couple $(\mathrm{epi}(\Theta), \Gamma)$ is weakly invariant in $\mathcal{O}$, the supremum in (4.7.1) is taken over a non-empty set. In what follows, it will be shown that the supremum in (4.7.1) is actually a maximum. In fact, take a maximizing sequence of trajectories $y_n(\cdot)$ of $(AD)_{y_0}$ and the related T_n such that $y_n(t) \in \mathrm{epi}(\Theta) \cap \mathcal{O}$ for all $t \in [0, T_n)$. If $T_n \to \infty$, then one would easily get a contradiction from the weak invariance of the couple $(\mathrm{epi}(\Theta), \Gamma)$ and from the condition d) on Θ. Furthermore, by standard compactness arguments (see, e.g. Proposition 2.6.1, [17]), $y_n(\cdot) \to y(\cdot)$ uniformly on $[0, T_{max}]$, where $y(\cdot)$ is a trajectory of $(AD)_{y_0}$. This implies that the supremum in (4.7.1) is a maximum and that there exists a solution $y(t) = (\tau(t), x(t), a_0)$ to (4.6.1) with initial condition $y(0) = (t_0, x_0, a_0)$ (where $\tau(t) = t + t_0$) such that $\Theta(\tau(t), x(t)) \leq a_0$ for all $t \in [0, T_{max})$.

Fix $a_0 = \Theta(t_0, x_0)$ and one can show that $T_{max} = \mathrm{Esc}(y(\cdot), \mathcal{O})$. In fact, if $T_{max} \neq \mathrm{Esc}(y(\cdot), \mathcal{O})$, this implies that $y(t) \in \mathrm{epi}(\Theta) \cap \mathcal{O}$ for all $t \in [0, T_{max}]$ and that $y(T_{max} + \varepsilon) \notin \mathrm{epi}(\Theta)$, $y(T_{max} + \varepsilon) \in \mathcal{O}$ for every $\varepsilon > 0$ sufficiently small. However, using again the weak invariance principle of the couple $(\mathrm{epi}(\Theta), \Gamma)$, one could construct a new trajectory $\tilde{y}(\cdot) = (\tilde{\tau}(\cdot), \tilde{x}(\cdot), \tilde{a})$ defined on $[T_{max}, \tilde{T})$ for some $\tilde{T} > T_{max}$, with initial condition $\tilde{y}(T_{max}) = y(T_{max})$ such that $\Theta(\tilde{\tau}(t), \tilde{x}(t)) \leq \Theta(\tau(T_{max}), x(T_{max})) = \Theta(t_0, x_0)$ for every $t \in [T_{max}, \tilde{T})$, which is clearly a contradiction with the definition of T_{max}.

These arguments show that there exists a trajectory $y(\cdot)$ solution of (4.6.1) such that $y(0) = (t_0, x_0, a_0)$ and $y(t) \in \mathrm{epi}(\Theta) \cap \mathcal{O}$ for every $t \in [0, \mathrm{Esc}(y(\cdot), \mathcal{O}) = T_{max})$. In particular this implies that

$$\Theta(\tau(t), x(t)) \leq \Theta(t_0, x_0) \tag{4.7.2}$$

for every $t \in [0, T_{max})$. It is easy to observe that, in view of condition c) on Θ and on relation (4.7.2), one has that $T_{max} = \mathrm{Esc}(y(\cdot), \mathcal{O}) = \mathrm{Esc}(y(\cdot), \Omega^c \times \mathbb{R})$.

One then easily obtains that $(\tau(T_{max}), x(T_{max})) \in \mathrm{Gr}\mathcal{T}$ and that

$$W(\tau(T_{max}), x(T_{max})) = \lim_{t \to T_{max}} \Theta(\tau(t), x(t)) \leq \Theta(t_0, x_0). \tag{4.7.3}$$

Hence $V(t_0, x_0) \leq \Theta(t_0, x_0)$

ii). The couple $(\mathrm{hypo}(\Theta), \Gamma)$ is strongly invariant. This implies that, given any $(t_0, x_0, a_0) \in \mathrm{hypo}(\Theta)$ and $T \geq 0$, any solution $y(t) = (\tau(t), x(t), a_0)$ of (4.6.1) with initial condition $y(0) = (t_0, x_0, a_0)$ remains in $\mathrm{hypo}(\Theta)$ for all $t \in [0, T]$.

If $(t_0, x_0) \notin \mathcal{D}$, then $+\infty = V(t_0, x_0) = \Theta(t_0, x_0)$ in view of condition b) on Θ. For $(t_0, x_0) \in \mathcal{D}$, fix $(\bar{S}, \bar{x}) \in \mathcal{A}_{(t_0, x_0)}$. Then there exists a solution $z(\tau)$ such that $\dot{z}(\tau) \in \bar{F}(\tau, z(\tau))$ for all $\tau \in [t_0, \bar{S}]$, $z(t_0) = x_0$ and $z(\bar{S}) = \bar{x}$. Define $\tau(t) = t + t_0$, $x(t) = z(\tau(t))$ and $T = \bar{S} - t_0$. Then $y(t) = (\tau(t), x(t), a_0)$ is a solution of (4.6.1) for all $t \in [0, T]$ with initial condition $y(0) = (t_0, x_0, a_0)$.

Choose $a_0 = \Theta(t_0, x_0)$. It follows from the strong invariance principle and the condition a) on Θ that

$$W(\bar{S}, \bar{x}) \geq \Theta(\tau(T), x(T)) \geq a_0 = \Theta(t_0, x_0)$$

Hence $\Theta(t_0, x_0) \leq V(t_0, x_0)$. This concludes the proof. □

To characterize the value function as the unique continuous, viscosity solution of a set of Hamilton-Jacobi inequalities one should note that the following result holds:

Theorem 4.7.5. Assume hypotheses **(SH)** and that conditions **(GC)**, **(IPC)** are satisfied. Then the value function V is the unique continuous, bounded below, locally Lipschitz in $\mathcal{D}$ function which satisfies the following properties:

i) $V(t, x) \leq W(t, x)$ for each $(t, x) \in \mathrm{Gr}\,\mathcal{T}$;

ii) $V(t, x) = +\infty$ for all $(t, x) \notin \mathcal{D}$;

iii) $V(t_k, x_k) \to +\infty$ for all $(t_k, x_k) \in \mathcal{D}$ such that $(t_k, x_k) \to (t, x) \in \partial\mathcal{D}$;

iv) For every $(t_k, x_k) \in \mathcal{D}$ such that $t_k \to \infty$, then $V(t_k, x_k) \to \infty$;

Consider the no-characteristic set

$$\Omega = \{(\tau, x) \in \operatorname{Gr} \mathcal{T} : \ V(\tau, x) = W(\tau, x)\}.$$

Then:

v) take $\mathcal{O} := \Omega^c \times \mathbb{R}$. For every $(t, x, a) \in \operatorname{epi}(V) \cap \mathcal{O}$ one has

$$\min_{v \in \bar{F}(t,x)} (1, v, 0) \cdot p \leq 0 \qquad \forall p \in N^P_{\operatorname{epi}(V)}(t, x, a); \tag{4.7.4}$$

vi) for every $(t, x, b) \in \operatorname{hypo}(V)$, one has

$$\limsup_{(t',x',b') \to_p (t,x,b)} \max_{v \in \bar{F}(t',x')} (1, v, 0) \cdot p \leq 0, \tag{4.7.5}$$

for all $p \in N^P_{\operatorname{hypo}(V)}(t, x, b)$;

vii) for every $(t, x) \in \mathcal{D} \cap (\Omega^c)$ one has

$$p_t + \min_{v \in \bar{F}(t,x)} v \cdot p_x \leq 0, \quad \forall\ (p_t, p_x) \in \partial_P V(t, x); \tag{4.7.6}$$

viii) for every $(t, x) \in \mathcal{D}$, one has

$$q_t + \liminf_{x' \to_{-q_x} x} \left\{ \min_{v \in \bar{F}(t,x')} v \cdot q_x \right\} \geq 0 \tag{4.7.7}$$

for every $q = (q_t, q_x) \in \partial^P V(t, x)$

Proof. Conditions i)-vi) follow from Propositions 4.5.3, 4.5.5-4.7.4. Furthermore, in view of Proposition 4.5.5 and Theorem 4.5.6, V is locally Lipschitz continuous in $\mathcal{D}$ and continuous in $\mathbb{R}^{1+n}$.

Theorem 4.5.1 assures that V is bounded below. If either $\partial_P V(t, x) = \emptyset$ or $\partial^P V(t, x) = \emptyset$, then, respectively, condition vii) and condition viii) are satisfied. It remains to show conditions vii)-viii) in the other cases to conclude the proof.

It follows from an easy application of ([17], Proposition 4.3.4) that

$$\begin{aligned} &N^P_{\operatorname{epi}(V)}(t, x, V(t, x)) = \\ &\qquad \{(\lambda p, -\lambda) : \ \lambda > 0, \quad p \in \partial_P V(t, x)\} \cup \{(0, 0)\} \\ &N^P_{\operatorname{hypo}(V)}(t, x, V(t, x)) = \\ &\qquad \{(-\lambda q, \lambda) : \ \lambda > 0, \quad q \in \partial^P V(t, x)\} \cup \{(0, 0)\} \end{aligned} \tag{4.7.8}$$

for every $(t, x) \in \mathcal{D}$.

Let $p = (p_t, p_x) \in \partial_P V(t,x)$. Then $(\lambda p, -\lambda) \in N^P_{\mathrm{epi}(V)}(t,x,V(t,x))$ for every $\lambda > 0$. It follows from condition v) that, rescaling w.r.t. $\lambda > 0$, one obtains

$$\begin{aligned}
&\min_{v\in\bar F(t,x)} (1,v,0)\cdot(\lambda p,-\lambda) \le 0 \implies\\
&\lambda \min_{v\in\bar F(t,x)} (1,v)\cdot(p_t,p_x) \le 0\\
&\implies p_t + \min_{v\in\bar F(t,x)} v\cdot p_x \le 0
\end{aligned}$$

for every $(t,x) \in \mathcal{D} \cap (\Omega)^c$, for every $(p_t, p_x) \in \partial_P V(t,x)$.

Similarly, if $q = (q_t, q_x) \in \partial^P V(t,x)$ then $(-\lambda q, \lambda) \in N^P_{\mathrm{hypo}(V)}(t,x,V(t,x))$ for every $\lambda > 0$. Hence, setting $\bar q = (-\lambda q, \lambda) \in N^P_{\mathrm{hypo}(V)}(t,x,V(t,x))$, it follows from condition vi) that

$$\limsup_{(t',x',a')\to\bar q(t,x,V(t,x))} \max_{v\in\bar F(t',x')} (1,v,0)\cdot(-\lambda q,\lambda) \le 0 \implies \tag{4.7.9}$$

$$\limsup_{(t',x')\to -q(t,x)} \max_{v\in\bar F(t',x')} (1,v)\cdot(-\lambda q_t,-\lambda q_x) \le 0 \implies \tag{4.7.10}$$

$$\limsup_{(t',x')\to -q(t,x)} \{-\lambda \min_{v\in\bar F(t',x')} (1,v)\cdot(q_t,q_x)\} \le 0 \implies \tag{4.7.11}$$

$$\liminf_{(t',x')\to -q(t,x)} \left\{ q_t + \min_{v\in\bar F(t',x')} v\cdot q_x \right\} \ge 0 \tag{4.7.12}$$

for every $(t,x) \in \mathcal{D}$ and $(q_t, q_x) \in \partial^P V(t,x)$. Since the map $t \rightsquigarrow \bar F(t,x)$ is Lipschitz continuous for each x, one easily obtains condition viii) from (4.7.12). This concludes the proof. □

Remark 4.7.6. Some implications of Theorem 4.7.5 deserve to be commented. First of all, observe that condition vii) of Theorem 4.7.5 implies that, for every $(t,x) \in \mathcal{D} \cap (\Omega)^c$ and $p = (p_t, p_x) \in \partial_P V(t,x)$, one has

$$p_t + \liminf_{x'\to -p_x x} \left\{ \min_{v\in\bar F(t,x')} v\cdot p_x \right\} \le 0$$

Now, take $(t,x) \in \mathcal{D}$ and assume that V is differentiable in a neighborhood of (t,x). Then $\partial_P V(t,x) \cap \partial^P V(t,x) = \{\nabla_{t,x} V(t,x)\} = (\eta_t, \eta_x) = \eta$. If $(t,x) \notin \mathrm{Gr}\mathcal{T}$, then conditions vii)-viii) provide the Hamilton-Jacobi equation

$$\eta_t + \liminf_{x'\to -\eta_x x} \left\{ \min_{v\in\bar F(t,x')} v\cdot \eta_x \right\} = 0 \tag{4.7.13}$$

On the other hand, when $(t,x) \in \mathrm{Gr}\mathcal{T}$, conditions vii)-viii) together with condition i) yield the following Hamilton-Jacobi equation

$$\min\left\{ (W-V)(t,x), \eta_t + \liminf_{x'\to -\eta_x x} \left\{ \min_{v\in\bar F(t,x')} v\cdot \eta_x \right\} \right\} = 0 \tag{4.7.14}$$

While the equation (4.7.13) reflects the need of hitting the target $\mathrm{Gr}\mathcal{T}$ (as it happens in the minimum time problems), the equation (4.7.14) is motivated by the search of a minimum point of W in $\mathrm{Gr}\mathcal{T}$.

The conditions v)-viii) characterise the value function V as the unique, continuous, bounded below viscosity solution of the Hamilton-Jacobi equation (4.7.13) when $(t,x) \notin \mathrm{Gr}\,\mathcal{T}$, and of the Hamilton-Jacobi equation (4.7.14) when $(t,x) \in \mathrm{Gr}\,\mathcal{T}$.

4.8 A TOY EXAMPLE

Consider the following optimal control problem

$$(P_{ex}) \begin{cases} \text{Minimize } W(T, v(T)) \\ \dot{v}(t) \in \ u - \frac{u^2}{2}\partial_v\varphi(v), \ \text{a.e. } t \in [t_0, T] \\ u(t) \in [-2, 2] \qquad \text{a.e. } t \in [t_0, T] \\ v(t_0) = v_0 \in \mathbb{R}, \\ (T, v(T)) \in \mathrm{Gr}\mathcal{T} \subseteq \mathbb{R}^2 \end{cases} \tag{4.8.1}$$

in which $t_0 \in \mathbb{R}$, $\mathcal{T} : \mathbb{R} \rightsquigarrow \mathbb{R}^+$, $\mathcal{T}(t) = [r, +\infty)$, $W(t,v) = Ct + (1/v^2)$ for some constants C, $r > 0$ such that $Cr^3 \leq 1$ and

$$\varphi(v) = \begin{cases} 0 & v < 0 \\ v & v \geq 0 \end{cases}$$

It is easy to see that (P_{ex}) is a special case of the general optimal control problem (P), in which the data are defined as $g(t,v,u) = u$, $k(t,v,u,\alpha) = u^2\alpha$, $A = [0,1]$, $\mu(\alpha) = \delta_{\frac{1}{2}}(\alpha)$ and

$$F(t,v,u) = u - \frac{u^2}{2}\partial_v\varphi(v)$$

Furthermore, a straightforward computation shows that

$$\bar{F}(t,v) = \cup_{u\in U} F(t,v,u) = \begin{cases} [-4, \ \frac{1}{2}] & v > 0 \\ [-4, \ 2] & v = 0 \\ [-2, \ 2] & v < 0 \end{cases}$$

and that hypothesis H_1-H_6 and condition **(GC)** are satisfied (notice that the Lipschitz continuity of the cost function W is required merely in a neighborhood of the target).

Furthermore, by definition of $t \rightsquigarrow \mathcal{T}(t)$, $(\bar{t}, \bar{v}) \in \partial\mathrm{Gr}\mathcal{T}$ if and only if $(\bar{t}, \bar{v}) = (\bar{t}, r)$ for some $\bar{t} \in \mathbb{R}$. It follows that $(l^0, l) \in N^P_{\mathrm{Gr}\mathcal{T}}(\bar{t}, r)$, $|(l^0, l)| = 1$ if and only if $(l^0, l) = (0, -1)$. Hence, **(IPC)** is satisfied because, for any compact $G \subseteq \mathbb{R}^2$ and any $(\bar{t}, r) \in \partial\mathrm{Gr}\mathcal{T} \cap G$, one has

$$\min_{\xi \in \bar{F}(\bar{t}, r)} (l^0 + \langle l, \xi \rangle) = -\frac{1}{2} < 0$$

The problem (P_{ex}) is describing the velocity $v(t)$ of an object that is moving, assuming that the friction acts only in one direction (see Figure 4.2). When the velocity is negative, one can choose the control without taking into account the effect of the friction. When the velocity is positive, the friction reduces the velocity and one has to choose the control providing the maximum of the difference between velocity and friction.

The target describes a minimum velocity requirement for the optimal solution to the problem.

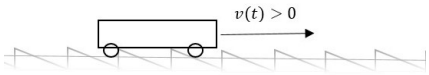

Figure 4.2: Example of a one side friction framework

It is natural to guess that the optimal control will be $\bar{u}(t) = 2$ for all t such that $v(t) \leq 0$. Furthermore, when $v(t) > 0$ and $v(t) < r$, the optimal control should be positive (to reach the target region) and related to the maximum velocity (in order to minimise the time in the cost function). Hence

$$\begin{aligned} &\partial_u \left\{ u - \frac{u^2}{2} \partial_v \varphi(v) \right\} = \partial_u \left\{ u - \frac{u^2}{2} \right\} = 0 \\ &\rightarrow \ |u| = 1 \ \rightarrow \ \bar{u}(t) = 1 \end{aligned}$$

Furthermore, (P_{ex}) is an example in which the optimal solution does not stop as soon as the target is reached. Let us study the behaviour of $W(t, \bar{v}(t))$, when $\bar{v}(t) > 0$ and $\dot{\bar{v}}(t) \in F(t, \bar{v}, \bar{u}) = F(t, \bar{v}, 1) = \frac{1}{2}$:

$$\frac{d}{dt} W(\bar{t}, v(\bar{t})) = C - \frac{1}{\bar{v}(\bar{t})^3} = 0 \ \leftrightarrow \ \bar{v}(\bar{t}) = v^* = \sqrt[3]{\frac{1}{C}} \geq r$$

where the last inequality holds since $Cr^3 \leq 1$. On the other hand, if Cr^3 were larger than 1, then $v^* \notin \mathcal{T}(t)$ and the optimal solution would stop as soon as it reaches the $\operatorname{Gr} \mathcal{T}$. The previous analysis shows that the guessed optimal control is

$$\bar{u}(t) = \begin{cases} 2 & v(t) \leq 0 \\ 1 & 0 < v(t) \leq v^* \\ 0 & v(t) > v^* \end{cases}$$

and, for any $(t_0, v_0) \in \mathbb{R}^2$, one can also guess that the value function is

$$V(t_0, v_0) = \begin{cases} Ct_0 + \frac{1}{v_0^2} & v_0 \geq v^* \\ 2Cv^* - 2Cv_0 + Ct_0 + \frac{1}{v^{*2}} & 0 \leq v_0 < v^* \\ 2Cv^* - C\frac{v_0}{2} + Ct_0 + \frac{1}{v^{*2}} & v_0 < 0 \end{cases} \tag{4.8.2}$$

One can now verify that the Hamilton-Jacobi inequalities of Theorem 4.7.5 are satisfied by the guessed value function (4.8.2). In fact, if V is differentiable at $(t_0, v_0) \in \mathbb{R}^2$, then $\partial_t V(t_0, v_0) = C$ and

$$\partial_x V(t_0, v_0) = \begin{cases} -\frac{2}{v_0^3} & v_0 \geq v^* \\ -2C & 0 < v_0 \leq v^* \\ -\frac{C}{2} & v_0 < 0 \end{cases}$$

Of course, the value function is differentiable at each point except at the origin. If $v_0 \geq v^*$, one can show that (4.7.14) is satisfied. In fact, in this case $\bar{F}(t_0, v_0) = [-4,\ \frac{1}{2}]$, $V(t_0, v_0) = W(t_0, v_0)$ and

$$\partial_t V(t_0, v_0) + \min_{w \in \bar{F}(t_0, v_0)} (w \cdot \partial_v V(t_0, v_0)) =$$
$$C + \frac{1}{2} \cdot (-\frac{2}{v_0^3}) \geq C - \frac{1}{v^{*3}} = 0$$

When $0 < v_0 \leq v^*$, then $\bar{F}(t_0, v_0) = [-4,\ \frac{1}{2}]$, $V(t_0, v_0) \leq W(t_0, v_0)$ and

$$\partial_t V(t_0, v_0) + \min_{w \in \bar{F}(t_0, v_0)} (w \cdot \partial_v V(t_0, v_0)) =$$
$$C + \frac{1}{2} \cdot (-2C) = 0,$$

showing that both equation (4.7.14) (which is valid when v_0 is in the target, namely $r \leq v_0 \leq v^*$) and equation (4.7.13) (valid outside the target) are satisfied.

If $v_0 < 0$, then $\bar{F}(t_0, v_0) = [-2,\ 2]$ and

$$\partial_t V(t_0, v_0) + \min_{w \in \bar{F}(t_0, v_0)} (w \cdot \partial_v V(t_0, v_0)) =$$
$$C + 2 \cdot (-\frac{C}{2}) = 0$$

showing that (4.7.13) is satisfied.

It remains to check what happens at the points in $(t_0, v_0 = 0)$, $t_0 \in \mathbb{R}$. In particular, it is easy to check that $\partial_P V(t_0, 0) = \emptyset$ for all $t_0 \in \mathbb{R}$. Then it is enough to check that condition viii) of Theorem 4.7.5 is verified. Observe that

$$\partial^P V(t_0, 0) = \left\{ q \in \mathbb{R}^{n+1} |\ q = (C, q_x),\ q_x \in \left[-2C, -\frac{C}{2} \right] \right\} \tag{4.8.3}$$

Take $(C, q_x) \in \partial^P V(t_0, 0)$. Since $x' \to_{-q_x} 0$ if and only if $x' > 0$ and $\bar{F}(t_0, x') = [-4, \frac{1}{2}]$, relation viii) of Theorem 4.7.5 is

$$C + \liminf_{x' \to -q_x 0} \left\{ \min_{v \in [-4, \frac{1}{2}]} v \cdot q_x \right\} = C + \frac{q_x}{2} \geq 0$$

for all $q_x \in [-2C, -\frac{C}{2}]$. In view of Theorem 4.7.5, one can conclude that (4.8.2) is the value function of the optimal control problem (P_{ex}).

4.9 DISCUSSION

The main result of this chapter is a characterisation of the value function of a free time optimal control problem subject to a controlled differential inclusion as unique, continuous viscosity solution of a related Hamilton-Jacobi equation. The dynamics arises from a class of systems in which the friction is represented by an averaged, upper semi-continuous, controlled differential inclusion. Under general assumptions, we show that the dynamic equation is well-posed and that the related optimal control problem admits solutions. Several theoretical questions (such as controllability, necessary optimality conditions etc.) and algorithmic considerations related to the present framework can be considered as future research directions. Furthermore, the theory provided in this chapter will be useful to describe a wide class of phenomena, in which a mechanical constraint producing friction is concerned, such as climbing plants.

Chapter 5

CONCLUSIONS AND OPEN QUESTIONS

It is staggering how strongly humans and all other life on Earth depend on plants. Firstly, plants supply food and maintain the atmosphere by continuously producing oxygen and absorbing carbon dioxide. Beside the agricultural and ecological importance, plants play a crucial role in biogeochemical cycles (for example the nitrogen fixation in peas), provide chemical compounds to synthesise medicines (aspirin, morphine, reserpine, etc...) and are sources of substances for the manufacturing industry (buildings, clothes, musical instruments, essential oils and soaps). In addition, the ability of plants to move by growing and to adapt to any environment by changing their morphology has inspired a new technology of growing robots, opening new frontiers in bio-inspired engineering.

To support this research field it is important to investigate plants movements and behaviors like the nutation, the exploring strategies, the resource allocation, the competition among neighbors, that are still poorly understood. The reasons of such a lack of knowledge is due to both the genetic diversity of plants, the huge number of external and internal stimuli that independent organs (leaves and roots) manage without a central brain and the complexity of soil that makes difficult the setting of experiments.

A crucial tool to mitigate the previous limitations is mathematical modelling. In Chapter 1 we have reviewed the main approaches proposed in the literature, the biological behaviors that each mathematical framework can address and the main drawbacks of each modelling technique. This thesis aims to further investigate plant behavior by focusing on the efficiency of the plant's movements and growing strategies. In Chapter 2, it is provided a new formulation for the efficiency of a growing strategy, by looking at the metabolic needs of the plant. Also, the efficiency function proposed is easy to compute and could be useful in ecological and agricultural studies, for example improving foraging strategies in crops.

Since the plant actively affects the environment and its growth to optimise this efficiency function, we can study plants by an optimal control approach.

The optimal control theory can be applied to investigate many behaviours of plants and in this thesis we propose two applications on the root movements into the soil.

In particular, in Chapter 3, the focus is on the root circumnutation. By using an optimal control based approach, the circumnutation motion is showed to be the most efficient dynamics to reduce the energy dissipation during the soil penetration. Also, it is possible to characterise the design of efficient autonomous robots for soil exploration. Finally, in Chapter 4, we generalise the framework of Chapter 3. A free-time optimal control problem is derived, whose dynamics is described by a new class of upper-semicontinuous controlled differential inclusions. They could be useful to model phenomena in which mechanical constraints producing friction are concerned. The value function for such a class of optimal control problems is characterised under general and mild hypothesis.

Two are the key aspects that characterise the thesis: the biological reliability of models proposed and the attention given to the engineering applications. Thus, the estimation of parameters and the validation with independent data and experiments is a crucial step in the thesis. Also, to support the bio-inspired engineering applications, it has been necessary to couple the mechanistic and the optimality approach. The former has been used to investigate the growing mechanisms of the plant system to provide tools that are system-free, and therefore, independent from the cellular interactions and hormone patterns. The optimal control based approach provides tools that engineers can easily translate into robotic algorithms.

The approach proposed in the thesis is novel and still at an early stage. Many open questions could be addressed and further biological, engineering and mathematical investigations are required.

Indeed, the framework in Chapter 3 and 4 is deterministic. For example, one could introduce a stochastic control $u + dw$ (being dw a Wiener process, i.e. a standard Brownian motion), to simulate the random exploration of the soil. If the Wiener process is introduced into the coefficients of soil frictional forces, then the model could estimate the effects on the motion due to the randomness of soil structures. It is expected the resulting dynamics will be a controlled differential inclusion with a multiplicative noise

$$dx(t) \in A(t, x, u)dt + B(t, x, u)dw$$

where A, B can be computed from $F(t, x, u)$ (see the dynamics in Chapter 4). Stochastic optimal control problems when the dynamics is Lipschitz have been recently investigated in [243, 244], but the existence of minimisers for the one-sided Lipschitz differential inclusion remains an open question.

The stochastic dynamics above could estimate the threshold between the exploration and the minimisation of energy dissipated, a crucial issue in robotic devices designed to explore the soil. On the other hand, the roots of the same plant have to face another issue: the competition among them. The investi-

gation of this issue could suggest information about the development of root architecture. In particular, the need for exploring the soil while minimising resource consumption due to the growth of roots. Or, also, the need for exploiting available nutrients (by increasing the roots in richer soil zones) while avoiding the negative effects of segregation. This problem could be addressed in two steps: firstly, replicating the dynamics in Chapters 3 or 4 as many times as the number of roots. Secondly, introducing dynamical state constraints to avoid the overlapping of a growing tip with the existing roots. In particular, recall that the dynamics in Chapter 4 is close to a sweeping process. In this case, the state constraint will not be a convex set, making the problem still different with respect to a recent result [234].

Far away from biological and engineering applications, it is worthy to note that the free-time optimal control problem in Chapter 4 cannot be completely replaced by an end-time problem. More specifically, the existence of a minimiser in the end-time problem can be proved as in the case of the free-time problem. However, in the end-time problem, both the growth condition and the invariance principles do not hold anymore. Therefore the characterisation of the value function is still an open question since it cannot be addressed as in the case of the free-time problem.

Finally, the framework presented in Chapter 2 can be further analysed. Indeed, several internal and external signals interact with each other to drive the growth of a plant. The mechanistic model proposed in the chapter aims to identify the main stimuli of this complex network and has allowed the formulation of a novel efficiency function depending on the metabolic needs of a plant. Such a formulation is suggested by what the plant is optimising during the growth and it has been thought to be easily measurable for agricultural and ecological studies. Nevertheless, the model depends on many variables and its coupling with other biological studies is not an easy task. Therefore, one could identify some control signals in the plant and rewrite the mechanistic model as an optimal control problem. For example, assuming as controls the resource allocation signal f_r, the nitrogen uptake signal a_n and the phosphorus uptake signal a_p, the model in Chapter 2 can be formulated as

$$\dot{x} = f(t, x) + g(t, x)u,$$

where x are the state variables in Chapter 2 except for $f_r,\ a_n,\ a_p$ and $u = (f_r, a_n, a_p)$. Assuming a smooth change from day to night, $f(t, x)$ and $g(t, x)$ can be written as continuous and periodic functions. The controllability and observability of such models are well established [245, 246]. Such a nonlinear control system can be used to propose new formulations for the efficiency function $\mathcal{E}$ proposed in Chapter 2. Indeed, one could couple the previous control system with a goal function (for example quadratic in the control) and compare the optimal trajectory with the solution of the accurate mechanistic model in Chapter 2.

The purpose is to propose a control system that well reproduce the mech-

anistic model but simplifying the efficiency function or reducing the number of signals to simulate. A simpler model is crucial to couple metabolic needs (namely the efficiency function) with other biological processes like models that describe the motion of plants. As an example, one could investigate the circumnutation (namely the dynamics in Chapters 3 and 4) while taking into account the metabolic needs of the plant, especially when many interacting roots of the same organism are studied.

To conclude, many other biological processes like stem climbing, branching development, interactions with neighbors and fungi, survival of plants, seedlings and fruit production can be investigated by an optimal control approach where the goal function is mainly related to the efficiency function.

Appendix A

List of Parameters in Chapter 2

Parameter	Value	Source	Significance
λ_c	see below	calibration	Feedback on photosynthesis
τ_{as}^{max}	$6\frac{\mu molC_6}{gFW \cdot h}$	[116]	maximum starch degradation rate
p_h^{max}	$12.7\frac{\mu molC_6}{gFW \cdot h}$	[116]	maximum rate of photosynthesis
n_{ph}	$5.75\frac{\mu molN}{gFW}$	[111]	minimum nitrogen for photosynthesis
$\mathcal{O}$	$10\frac{\mu molN}{\mu molP}$	[15]	optimal stoichiometry ratio
s^{max}	$2\frac{\mu molC_6}{gFW}$	[138]	maximum sucrose content in leaves
s^{min}	$1.3\frac{\mu molC_6}{gFW}$	[116]	sucrose starvation threshold
a_{min}	$0.15\frac{\mu molC_6}{gFW}$	[118]	minimum amount of starch at dawn
λ_{sdr}	$0.25\frac{1}{h}$	calibration	frequency parameter in γ dynamics
λ_{sdi}	$0.1\frac{1}{h}$	calibration	frequency parameter in γ dynamics
λ_{sni}	see below	calibration	frequency parameter in γ dynamics
b_l^{min}	b_l	arbitrarily chosen for Floquet analysis	minimum amount of leaf biomass to start photosynthesis
$\mu_l,\ \mu_r$	$5e-6\frac{1}{h}$	arbitrarily chosen for Floquet analysis	Death rate of leaf and root tissues

Parameter	Value	Source	Significance
$\delta_l,\ \delta_r$	$5e-6\frac{1}{hgFW}$	arbitratrily chosen for Floquet analysis	parameters for leaf and root competition
λ_{sb}	see below	calibration	conversion parameter from sucrose to biomass
λ_f	$0.066\frac{1}{h}$	calibration	conversion parameter in nutrients dynamics
r_A	$0.58\frac{\mu molC_6}{\mu molN}$	[111]	cost of nitrogen assimilation in biomass
λ_{csn}	0.0267	calibration	proportional parameter in nitrogen assimilation in biomass
λ_g	0.65	calibration	parameter for the computation of the cost r_g
λ_k	50	calibration	frequency weight in $a_n,\ a_p$ dynamics
I_n^{max}	$6.44\frac{\mu molN}{gFW\cdot h}$	[160]	Michaelis-Menten parameter for nitrogen uptake
k_n	$0.125\frac{\mu molN}{cm^3}$	[160]	Michaelis-Menten parameter for nitrogen uptake
I_p^{max}	$0.4\frac{\mu molP}{gFW\cdot h}$	[156]	Michaelis-Menten parameter for phosphorus uptake
k_p	$0.006736\frac{\mu molP}{cm^3}$	[156]	Michaelis-Menten parameter for phosphorus uptake
D	4	[112]	memory of the plant
r_m	$0.79\frac{1}{h}$	[148]	respiration frequency
η	$1.98\frac{1}{h}$	[148]	frequency of loading sucrose
p_c	$0.308\frac{\mu molC_6}{\mu molP}$	[121]	sucrose consumption in phosphorus uptake
$\bar{r}^t$	0.0035	[121]	sucrose consumption in transporting nutrients
n_c	$0.68\frac{\mu molC_6}{\mu molN}$	calibration	sucrose consumption in nitrogen uptake
$\bar{n}_s$	$12\frac{\mu molN}{cm^3}$	[169]	optimal nitrogen soil content
$\bar{p}_s$	$0.15\frac{\mu molP}{cm^3}$	[159]	optimal phosphorus soil content
μ_s	$5e-3$	calibration	sucrose losses

As explained in chapter 2, some parameters depend on the photoperiod. They are reported in table A and have been estimated, for each day-length, by fitting data in [138]:

	$4h$	$6h$	$8h$	$12h$	$18h$
λ_c $[-]$	0.82	0.79	0.67	0.62	0.55
λ_{sni} $[\frac{1}{h}]$	0.16	0.15	0.13	0.08	0.004
λ_{sb} $[\frac{gFW}{\mu molC_6}]$	0.00344	0.00413	0.00515	0.00578	0.00524

Table A.1: List of photoperiod-dependent parameters

Appendix B

Comparison of Starch Degradation Function with the Literature

In the chapter 2 it has been outlined a new function for starch degradation. In [118], a detailed function to describe this behaviour is proposed, and the complexity of starch degradation is highlighted. The function obtained does not depend on the starch level stored at dusk and, according to the length of dark period, it could consider starch degradation during the period of light. To compare their approach with the one proposed in this thesis, it has first reproduced the model in [118] by fixing p_h and γ according to their values and assuming no sucrose consumption for transport and uptake. The light period for the simulation has been fixed to $8h$. The results of the starch and sucrose dynamics (Fig B.1) are consistent with the plots of their paper. To

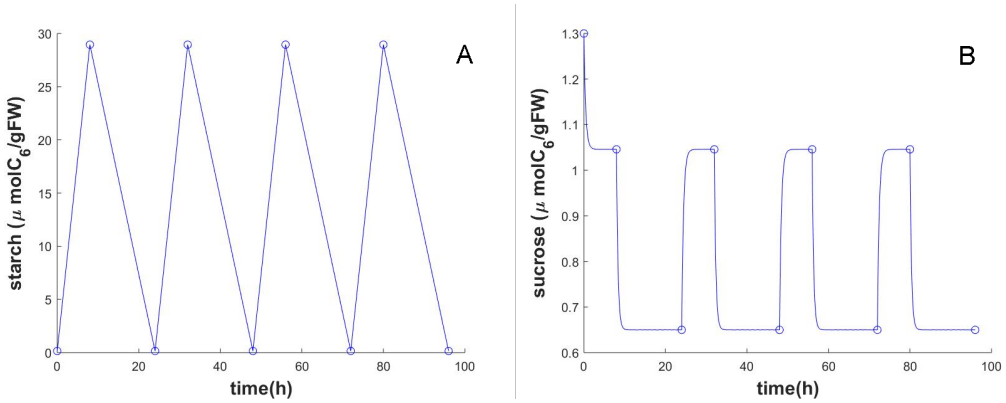

Figure B.1: **Integration in the model of the starch degradation rate proposed by [118].** See the equations ($S17$) and ($S22$) in the supplementary material of [118]. Results reported here are for the simulations performed with $8h$ of light. (A) Starch dynamics. (B) Sucrose dynamics.

simulate the experimental data in [138], it has been estimated the value of

the photosynthetic rate from [116] (see the list in the appendix A). γ is still approximated as in [118] ($\gamma = 0.6$). With these parameters, the model does not approximate well the behaviour of the experimental data (Fig B.2(A) and B.2(B)).

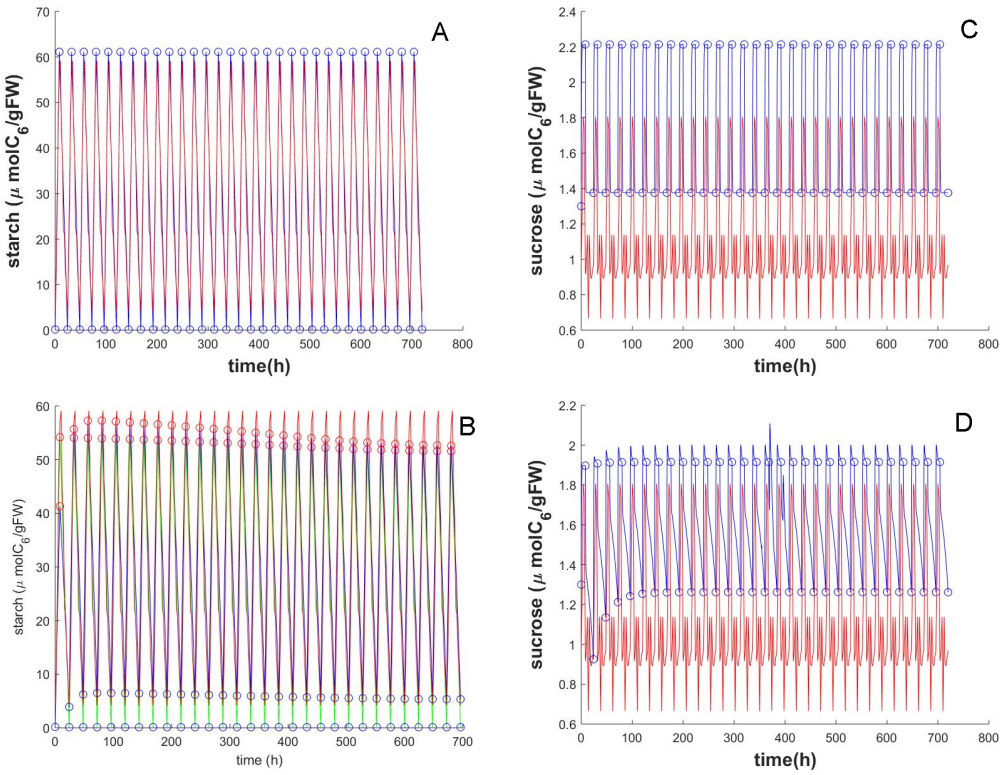

Figure B.2: **Sucrose and starch dynamics**(A) Starch comparison with $\gamma = 0.6$. (B) Sucrose comparison with $\gamma = 0.6$. (C) Starch comparison with $\gamma = 0.6$, which also includes the results from our original model. (D) Sucrose comparison with $\gamma = 0.68$. The blue curve represents the model simulation according to the degradation rate proposed by [118], while the red curve is the fitting among experimental data in [138], and the green line is the simulation due to the model as proposed in chapter 2. The day is fixed to $8h$.

The behaviour is worse if, according to [148], for $8h$ photoperiods $\gamma = 0.68$ instead of $\gamma = 0.6$ (Fig B.2(D)).

A better behaviour can be ascertained if the photosynthesis is no longer constant and both uptake and transport sucrose costs are inserted again (Fig B.3). In particular, the starch degradation function in [118] works by assuming

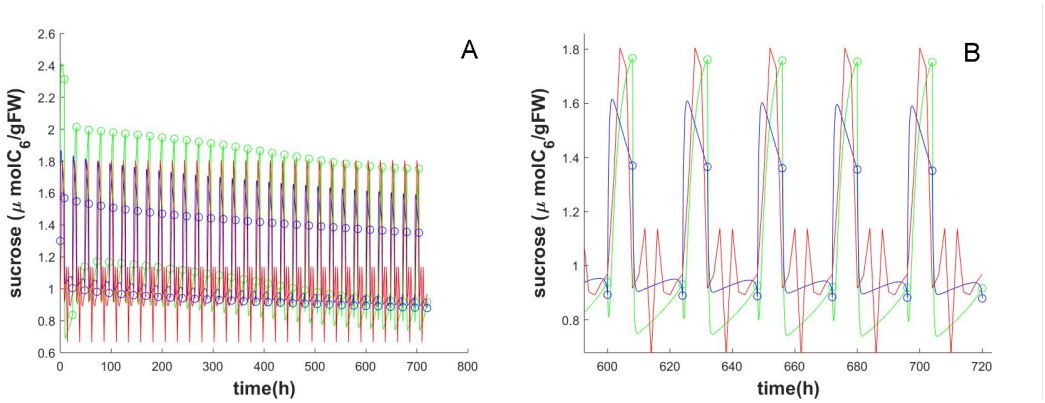

Figure B.3: **Sucrose comparison with** $\gamma = 0.6$. The red curve is the fitting with experimental data, the blue line is the simulation of our complete model with the starch degradation proposed by [118] and for $\gamma = 0.6$; the green curve is the simulation by the model in chapter 2.

a constant rate of photosynthesis. Two options are possible:

- photosynthesis can vary in time according to equations in chapter 2 when the function in [118] is integrated in the model;
- photosynthesis is fixed to a maximum value when computing the function in [118], but it varies according to equations in chapter 2 when computed in the rest of the model.

The former case provided the best result for $\gamma = 0.6$ and it is reported only the best behaviour (Fig B.3). The latter case provided the best result for $\gamma = 0.68$, as shown in Fig B.4(A) for sucrose dynamics. The differences between the two models are more evident in $12h$ days (Fig B.4(B) and B.4(C)). In conclusion, starch degradation is more complex than the model proposed in this thesis can simulate and needs further investigations. However, even if simpler, the behaviour obtained still provides a good approximation (and sometimes better) when compared with more complete functions already available from literature. A further integration between the model proposed in this thesis and the literature could lead to a sharper behaviour.

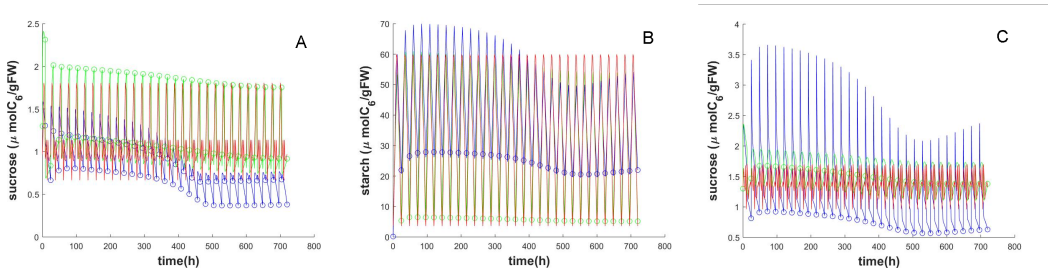

Figure B.4: **Sucrose and starch dynamics**(A) Sucrose comparison with $\gamma = 0.68$ and a day of $8h$. (B) Starch comparison with $\gamma = 0.6$ and a day of $12h$. (C) Sucrose comparison with $\gamma = 0.6$ and a day of $12h$. The red curve is the fitting with experimental data, and the blue line is the simulation of the model in chapter 2 with the starch degradation proposed by [118] when $\gamma = 0.6$ with variable photosynthesis; the green curve is the simulation of the model in chapter 2.

Appendix C

Dynamics of $\mathcal{E}$

Tables from C.1 to C.4 summarise, for each soil condition, the efficiency $\mathcal{E}$ and the total cost $\mathcal{C}$ computed after 40 days at $12h$ of light when the starch partition γ, the sucrose allocation f_r, and the nitrogen affinity a_n are kept constants one at a time. All of them are compared with $\bar{\mathcal{E}}$ and $\bar{\mathcal{C}}$, that are computed when no given dynamics is forced for the previous signals.

Table C.1 reports the values when both the nitrogen and the phosphorus are optimal into the soil. Table C.2 and C.3 show the situation of low nitrogen and phosphorus soil contents. In red are highlighted the values such that $\mathcal{E} \geq \bar{\mathcal{E}}$. All these values can reach a greater efficiency, but consuming more resources during the growth. Table C.4 shows the values for rich soils. Since the toxic effects of a high level of nitrogen are not modelled, only the phosphorus is higher than the optimal value. Also in this case, in red there are the values more efficient than $\bar{\mathcal{E}}$ but with higher costs. Finally, in blue, the only case in which the efficiency is higher than $\bar{\mathcal{E}}$, still having a lower cost. The reason could be that in richer soils the metabolism is reduced because it is easier to recover the nutrients. Therefore some values in the formulation of $\mathcal{C}$ should be changed to take into account this effect.

Table C.1: **NORMAL SOIL CONDITIONS**. The nitrogen into the soil is fixed at $12\frac{\mu molN}{cm^3}$. The soil phosphorus is $0.15\frac{\mu molP}{cm^3}$. The model gives $\bar{\mathcal{E}} = 3.061$ and $\bar{\mathcal{C}} = 402.1874$

Constant value	Efficiency $\mathcal{E}$	Cost $\mathcal{C}$
$\gamma = 0$	0.7424	654.6573
$\gamma = 0.1$	1.6126	649.0499
$\gamma = 0.2$	2.2042	652.8426
$\gamma = 0.3$	2.7305	652.1368
$\gamma = 0.4$	3.0272	535.082
$\gamma = 0.5$	3.0524	350.5144
$\gamma = 0.6$	2.9246	573.5625
$\gamma = 0.7$	2.6359	686.22
$\gamma = 0.8$	2.1067	922.8842
$\gamma = 0.9$	1.6386	938.2356
$\gamma = 1$	1.3649	940.9895
$f_r = 0$	0.0614	692.8741
$f_r = 0.1$	0.7807	798.4255
$f_r = 0.2$	1.5122	759.0151
$f_r = 0.3$	2.3517	485.2384
$f_r = 0.4$	3.0407	330.5974
$f_r = 0.5$	2.269	281.5307
$f_r = 0.6$	1.8271	271.1407
$f_r = 0.7$	1.6111	271.2217
$f_r = 0.8$	1.4907	268.2308
$f_r = 0.9$	1.4194	262.8242
$f_r = 1$	1.3777	258.6315
$a_n = 0$	0	44.1339
$a_n = 0.1$	0.1198	763.9592
$a_n = 0.2$	0.4739	761.4077
$a_n = 0.3$	1.108	748.3867
$a_n = 0.4$	1.9028	674.965
$a_n = 0.5$	2.6771	441.0439
$a_n = 0.6$	3.0234	369.3087
$a_n = 0.7$	2.4723	372.8219
$a_n = 0.8$	2.1014	402.2465
$a_n = 0.9$	1.8928	421.3757
$a_n = 1$	1.7639	446.1778

Table C.2: **POOR SOIL CONDITIONS**. The nitrogen into the soil is fixed at $9\frac{\mu molN}{cm^3}$. The soil phosphorus is $0.08\frac{\mu molP}{cm^3}$. The model gives $\bar{\mathcal{E}} = 2.9411$ and $\bar{\mathcal{C}} = 386.9829$

Constant value	Efficiency $\mathcal{E}$	Cost $\mathcal{C}$
$\gamma = 0$	1.9989	650.5305
$\gamma = 0.1$	2.6814	647.6121
$\gamma = 0.2$	2.9409	643.1252
$\gamma = 0.3$	3.0191	640.2454
$\gamma = 0.4$	2.9982	573.5694
$\gamma = 0.5$	2.902	258.1251
$\gamma = 0.6$	2.7377	463.9242
$\gamma = 0.7$	2.3039	613.0463
$\gamma = 0.8$	1.3305	607.8384
$\gamma = 0.9$	1.0671	887.0242
$\gamma = 1$	1.0007	910.1092
$f_r = 0$	0.0436	749.4585
$f_r = 0.1$	0.5559	761.4409
$f_r = 0.2$	0.9452	678.591
$f_r = 0.3$	1.4814	371.8798
$f_r = 0.4$	2.5654	369.761
$f_r = 0.5$	2.9112	382.3552
$f_r = 0.6$	3.0051	400.9119
$f_r = 0.7$	3.0104	415.7068
$f_r = 0.8$	2.9853	422.9904
$f_r = 0.9$	2.9536	425.8267
$f_r = 1$	2.9259	419.9589
$a_n = 0$	0	41.935
$a_n = 0.1$	0.1226	737.4998
$a_n = 0.2$	0.4024	698.0843
$a_n = 0.3$	0.8465	577.3882
$a_n = 0.4$	1.5348	289.3621
$a_n = 0.5$	2.3807	306.9095
$a_n = 0.6$	2.7392	344.9178
$a_n = 0.7$	2.8994	381.6517
$a_n = 0.8$	2.9739	411.8089
$a_n = 0.9$	3.0078	438.9479
$a_n = 1$	3.0212	463.9948

Table C.3: **VERY POOR SOIL CONDITIONS**. The nitrogen into the soil is fixed at $7\frac{\mu molN}{cm^3}$. The soil phosphorus is $0.01\frac{\mu molP}{cm^3}$. The model gives $\bar{\mathcal{E}} = 2.1$ and $\bar{\mathcal{C}} = 374.7987$

Constant value	Efficiency $\mathcal{E}$	Cost $\mathcal{C}$
$\gamma = 0$	1.3385	648.6218
$\gamma = 0.1$	2.2475	647.6246
$\gamma = 0.2$	2.4022	640.1798
$\gamma = 0.3$	2.3534	638.7953
$\gamma = 0.4$	2.2129	550.2735
$\gamma = 0.5$	2.0415	261.6195
$\gamma = 0.6$	1.8536	464.9322
$\gamma = 0.7$	1.5332	607.3268
$\gamma = 0.8$	1.0581	606.2186
$\gamma = 0.9$	0.9919	908.0760
$\gamma = 1$	0.8587	917.9052
$f_r = 0$	0.0646	745.4543
$f_r = 0.1$	0.4113	762.4076
$f_r = 0.2$	0.7559	741.3602
$f_r = 0.3$	0.9790	553.5495
$f_r = 0.4$	1.2178	310.5203
$f_r = 0.5$	1.7380	338.0195
$f_r = 0.6$	2.0698	373.8602
$f_r = 0.7$	2.2746	395.1469
$f_r = 0.8$	2.4097	411.9974
$f_r = 0.9$	2.5024	421.2970
$f_r = 1$	2.5666	425.0891
$a_n = 0$	0	41.1427
$a_n = 0.1$	0.1710	739.1516
$a_n = 0.2$	0.5598	681.9869
$a_n = 0.3$	0.9775	403.1284
$a_n = 0.4$	1.4038	277.4202
$a_n = 0.5$	1.7450	323.7759
$a_n = 0.6$	1.9658	365.6358
$a_n = 0.7$	2.1161	398.9251
$a_n = 0.8$	2.2201	428.6895
$a_n = 0.9$	2.2877	456.8706
$a_n = 1$	2.3359	478.8069

Table C.4: **RICH SOIL CONDITIONS**. The nitrogen into the soil is fixed at $12\frac{\mu molN}{cm^3}$. The soil phosphorus is $0.5\frac{\mu molP}{cm^3}$. The model gives $\bar{\mathcal{E}} = 2.659$ and $\bar{\mathcal{C}} = 980.5407$

Constant value	Efficiency $\mathcal{E}$	Cost $\mathcal{C}$
$\gamma = 0$	0.7386	599.2
$\gamma = 0.1$	1.3053	604.0
$\gamma = 0.2$	1.7507	602.2
$\gamma = 0.3$	2.1713	610.6
$\gamma = 0.4$	2.6194	985.7
$\gamma = 0.5$	2.9591	1072.9
$\gamma = 0.6$	2.9317	1069.1
$\gamma = 0.7$	2.4659	1012.8
$\gamma = 0.8$	1.6221	918.7
$\gamma = 0.9$	0.9248	873.1
$\gamma = 1$	0.6135	877.2
$f_r = 0$	0.0465	839.1
$f_r = 0.1$	0.8832	917.6
$f_r = 0.2$	2.3747	950.2
$f_r = 0.3$	2.5464	996.5
$f_r = 0.4$	2.0104	393
$f_r = 0.5$	1.7489	1048.6
$f_r = 0.6$	1.6013	1053.2
$f_r = 0.7$	1.5086	1054.1
$f_r = 0.8$	1.4474	1054.3
$f_r = 0.9$	1.4064	1057.2
$f_r = 1$	1.3795	1055.8
$a_n = 0$	0	281.1
$a_n = 0.1$	0.6859	885.9
$a_n = 0.2$	0.4168	889.7
$a_n = 0.3$	1.1220	901.1
$a_n = 0.4$	2.8409	903.3
$a_n = 0.5$	2.5604	902.7
$a_n = 0.6$	2.1450	992.5
$a_n = 0.7$	1.9136	1046.7
$a_n = 0.8$	1.7716	1058.2
$a_n = 0.9$	1.6763	1063.5
$a_n = 1$	1.6081	1064.8

Bibliography

[1] R. Karban, "Plant behaviour and communication," *Ecology letters*, vol. 11, no. 7, pp. 727–739, 2008.

[2] A. Arber, *The natural philosophy of plant form*. Cambridge University Press, 2012.

[3] J. Silvertown and D. M. Gordon, "A framework for plant behavior," *Annual Review of Ecology and Systematics*, vol. 20, no. 1, pp. 349–366, 1989.

[4] B. S. Younginger, D. Sirová, M. B. Cruzan, and D. J. Ballhorn, "Is biomass a reliable estimate of plant fitness?," *Applications in plant sciences*, vol. 5, no. 2, p. 1600094, 2017.

[5] R. J. Morris, *Mathematical Modelling in Plant Biology*. Springer, 2018.

[6] R. A. Feddes, H. Hoff, M. Bruen, T. Dawson, P. De Rosnay, P. Dirmeyer, R. B. Jackson, P. Kabat, A. Kleidon, A. Lilly, *et al.*, "Modeling root water uptake in hydrological and climate models," *Bulletin of the American meteorological society*, vol. 82, no. 12, pp. 2797–2810, 2001.

[7] T. Roose and A. Schnepf, "Mathematical models of plant–soil interaction," *Philosophical Transactions of the Royal Society A: Mathematical, Physical and Engineering Sciences*, vol. 366, no. 1885, pp. 4597–4611, 2008.

[8] M. J. Hawkesford, S. Kopriva, and L. J. De Kok, *Nutrient use efficiency in plants*. Springer, 2016.

[9] A. J. Bloom and K. M. Lancaster, "Manganese binding to rubisco could drive a photorespiratory pathway that increases the energy efficiency of photosynthesis," *Nature plants*, vol. 4, no. 7, p. 414, 2018.

[10] F. Migliaccio, P. Tassone, and A. Fortunati, "Circumnutation as an autonomous root movement in plants," *American journal of botany*, vol. 100, no. 1, pp. 4–13, 2013.

[11] E. Kolb, V. Legué, and M.-B. Bogeat-Triboulot, "Physical root–soil interactions," *Physical biology*, vol. 14, no. 6, p. 065004, 2017.

[12] E. Del Dottore, A. Mondini, A. Sadeghi, V. Mattoli, and B. Mazzolai, "An efficient soil penetration strategy for explorative robots inspired by plant root circumnutation movements," *Bioinspiration & biomimetics*, vol. 13, no. 1, p. 015003, 2017.

[13] A. Sadeghi, A. Mondini, E. Del Dottore, V. Mattoli, L. Beccai, S. Taccola, C. Lucarotti, M. Totaro, and B. Mazzolai, "A plant-inspired robot with soft differential bending capabilities," *Bioinspiration & biomimetics*, vol. 12, no. 1, p. 015001, 2016.

[14] E. Del Dottore, A. Sadeghi, A. Mondini, V. Mattoli, and B. Mazzolai, "Toward growing robots: a historical evolution from cellular to plant-inspired robotics," *Frontiers in Robotics and AI*, vol. 5, p. 16, 2018.

[15] E. Del Dottore, A. Mondini, A. Sadeghi, and B. Mazzolai, "Swarming behavior emerging from the uptake–kinetics feedback control in a plant-root-inspired robot," *Applied Sciences*, vol. 8, no. 1, p. 47, 2018.

[16] B. Mazzolai, "Plant-inspired growing robots," in *Soft Robotics: Trends, Applications and Challenges*, pp. 57–63, Springer, 2017.

[17] R. Vinter, *Optimal control*. Springer Science & Business Media, 2010.

[18] I. M. Ross, R. J. Proulx, M. Karpenko, and Q. Gong, "Riemann–stieltjes optimal control problems for uncertain dynamic systems," *Journal of Guidance, Control, and Dynamics*, vol. 38, no. 7, pp. 1251–1263, 2015.

[19] M. Palladino, "Necessary conditions for adverse control problems expressed by relaxed derivatives," *Set-Valued and Variational Analysis*, vol. 24, no. 4, pp. 659–683, 2016.

[20] P. Bettiol and N. Khalil, "Necessary optimality conditions for average cost minimization problems," *arXiv preprint arXiv:1901.04213*, 2019.

[21] H. H. Dixon and J. Joly, "On the ascent of sap.," *Proceedings of the Royal Society of London*, vol. 57, pp. 3–5, 1894.

[22] H. H. Dixon and J. Joly, "Xii. on the ascent of sap," *Philosophical Transactions of the Royal Society of London.(B.)*, no. 186, pp. 563–576, 1895.

[23] E. Münch, "Die stoffbewegungen in der pflanze.(gustav fischer: Jena)," 1930.

[24] K. H. Jensen, J. Liesche, T. Bohr, and A. Schulz, "Universality of phloem transport in seed plants," *Plant, cell & environment*, vol. 35, no. 6, pp. 1065–1076, 2012.

[25] S. Whitaker, "Flow in porous media i: A theoretical derivation of darcy's law," *Transport in porous media*, vol. 1, no. 1, pp. 3–25, 1986.

[26] Y.-L. Chuang, R. Oren, A. L. Bertozzi, N. Phillips, and G. G. Katul, "The porous media model for the hydraulic system of a conifer tree: linking sap flux data to transpiration rate," *Ecological Modelling*, vol. 191, no. 3-4, pp. 447–468, 2006.

[27] G. Manoli, S. Bonetti, J.-C. Domec, M. Putti, G. Katul, and M. Marani, "Tree root systems competing for soil moisture in a 3d soil–plant model," *Advances in water resources*, vol. 66, pp. 32–42, 2014.

[28] K. H. Jensen, K. Berg-Sørensen, H. Bruus, N. M. Holbrook, J. Liesche, A. Schulz, M. A. Zwieniecki, and T. Bohr, "Sap flow and sugar transport in plants," *Reviews of modern physics*, vol. 88, no. 3, p. 035007, 2016.

[29] T. Vogel, J. Votrubova, M. Dohnal, and J. Dusek, "A simple representation of plant water storage effects in coupled soil water flow and transpiration stream modeling," *Vadose Zone Journal*, vol. 16, no. 5, 2017.

[30] J. E. Flaherty, J. B. Keller, and S. Rubinow, "Post buckling behavior of elastic tubes and rings with opposite sides in contact," *SIAM Journal on Applied Mathematics*, vol. 23, no. 4, pp. 446–455, 1972.

[31] G. Batchelor, "1967, an introduction to fluid dynamics. cambridge: Cambridge university press," 1967.

[32] E.-D. Schulze, J. Čermák, M. Matyssek, M. Penka, R. Zimmermann, F. Vasicek, W. Gries, and J. Kučera, "Canopy transpiration and water fluxes in the xylem of the trunk of larix and picea trees—a comparison of xylem flow, porometer and cuvette measurements," *Oecologia*, vol. 66, no. 4, pp. 475–483, 1985.

[33] J. Čermák, J. Kučera, W. L. Bauerle, N. Phillips, and T. M. Hinckley, "Tree water storage and its diurnal dynamics related to sap flow and changes in stem volume in old-growth douglas-fir trees," *Tree physiology*, vol. 27, no. 2, pp. 181–198, 2007.

[34] T. Hölttä, H. Cochard, E. Nikinmaa, and M. Mencuccini, "Capacitive effect of cavitation in xylem conduits: results from a dynamic model," *Plant, Cell & Environment*, vol. 32, no. 1, pp. 10–21, 2009.

[35] G. K. Aldis, "The unstirred layer during osmotic flow into a tubule," *Bulletin of mathematical biology*, vol. 50, no. 5, pp. 531–545, 1988.

[36] L. Horwitz, "Some simplified mathematical treatments of translocation in plants.," *Plant Physiology*, vol. 33, no. 2, p. 81, 1958.

[37] A. L. Christy and J. M. Ferrier, "A mathematical treatment of munch's pressure-flow hypothesis of phloem translocation," *Plant Physiology*, vol. 52, no. 6, pp. 531–538, 1973.

[38] M. V. Thompson and N. M. Holbrook, "Application of a single-solute non-steady-state phloem model to the study of long-distance assimilate transport," *Journal of Theoretical Biology*, vol. 220, no. 4, pp. 419–455, 2003.

[39] T. Hölttä, T. Vesala, S. Sevanto, M. Perämäki, and E. Nikinmaa, "Modeling xylem and phloem water flows in trees according to cohesion theory and münch hypothesis," *Trees*, vol. 20, no. 1, pp. 67–78, 2006.

[40] P. S. Nobel *et al.*, *Physicochemical & environmental plant physiology*. Academic press, 1999.

[41] R. A. Millikan and E. S. Bishop, *Elements of electricity: a practical discussion of the fundamental laws and phenomena of electricity and their practical applications in the business and industrial world*. American Technical Society, 1917.

[42] K. T. S. Oldham, *The doctrine of description: Gustav Kirchhoff, classical physics, and the "purpose of all science" in 19 th-century Germany*. University of California, Berkeley, 2008.

[43] P. S. Nobel, "The boyle-van't hoff relation," *Journal of theoretical biology*, vol. 23, no. 3, pp. 375–379, 1969.

[44] I. Cowan, "Transport of water in the soil-plant-atmosphere system," *Journal of Applied Ecology*, pp. 221–239, 1965.

[45] P. Minchin, M. Thorpe, and J. Farrar, "A simple mechanistic model of phloem transport which explains sink priority," *Journal of experimental botany*, vol. 44, no. 5, pp. 947–955, 1993.

[46] F.-A. Daudet, A. Lacointe, J. Gaudillere, and P. Cruiziat, "Generalized münch coupling between sugar and water fluxes for modelling carbon allocation as affected by water status," *Journal of Theoretical Biology*, vol. 214, no. 3, pp. 481–498, 2002.

[47] A. Lacointe and P. E. Minchin, "Modelling phloem and xylem transport within a complex architecture," *Functional Plant Biology*, vol. 35, no. 10, pp. 772–780, 2008.

[48] P. E. Minchin and A. Lacointe, "Consequences of phloem pathway unloading/reloading on equilibrium flows between source and sink: a modelling approach," *Functional plant biology*, vol. 44, no. 5, pp. 507–514, 2017.

[49] J. Zhuang, G.-R. Yu, and K. Nakayama, "A series rcl circuit theory for analyzing non-steady-state water uptake of maize plants," *Scientific reports*, vol. 4, p. 6720, 2014.

[50] B. J. Choudhury and S. B. Idso, "Evaluating plant and canopy resistances of field-grown wheat from concurrent diurnal observations of leaf water potential, stomatal resistance, canopy temperature, and evapotranspiration flux," *Agricultural and forest meteorology*, vol. 34, no. 1, pp. 67–76, 1985.

[51] I. Ionenko, N. Dautova, and A. Anisimov, "Early changes of water diffusional transfer in maize roots under the influence of water stress," *Environmental and experimental botany*, vol. 76, pp. 16–23, 2012.

[52] J. Landsberg and N. Fowkes, "Water movement through plant roots," *Annals of Botany*, vol. 42, no. 3, pp. 493–508, 1978.

[53] C. Doussan, L. Pagès, and G. Vercambre, "Modelling of the hydraulic architecture of root systems: an integrated approach to water absorption—model description," *Annals of botany*, vol. 81, no. 2, pp. 213–223, 1998.

[54] C. DOUSSAN, G. VERCAMBRE, and L. PAGÈ, "Modelling of the hydraulic architecture of root systems: An integrated approach to water absorption—distribution of axial and radial conductances in maize," *Annals of Botany*, vol. 81, no. 2, pp. 225–232, 1998.

[55] C. Doussan, A. Pierret, E. Garrigues, and L. Pagès, "Water uptake by plant roots: Ii–modelling of water transfer in the soil root-system with explicit account of flow within the root system–comparison with experiments," *Plant and soil*, vol. 283, no. 1-2, pp. 99–117, 2006.

[56] M. Javaux, T. Schröder, J. Vanderborght, and H. Vereecken, "Use of a three-dimensional detailed modeling approach for predicting root water uptake," *Vadose Zone Journal*, vol. 7, no. 3, pp. 1079–1088, 2008.

[57] C. Schneider, S. Attinger, J.-O. Delfs, and A. Hildebrandt, "Implementing small scale processes at the soil-plant interface–the role of root architectures for calculating root water uptake profiles," *Hydrology and Earth System Sciences*, vol. 14, no. 2, pp. 279–289, 2010.

[58] R. A. Feddes, P. Kowalik, K. Kolinska-Malinka, and H. Zaradny, "Simulation of field water uptake by plants using a soil water dependent root extraction function," *Journal of Hydrology*, vol. 31, no. 1-2, pp. 13–26, 1976.

[59] N. Jarvis, "A simple empirical model of root water uptake," *Journal of Hydrology*, vol. 107, no. 1-4, pp. 57–72, 1989.

[60] V. Couvreur, J. Vanderborght, and M. Javaux, "A simple three-dimensional macroscopic root water uptake model based on the hydraulic architecture approach," *Hydrology and Earth System Sciences*, vol. 16, no. 8, pp. 2957–2971, 2012.

[61] B. Jakobsen and A. Dexter, "Effect of soil structure on wheat root growth, water uptake and grain yield. a computer simulation model," *Soil and Tillage Research*, vol. 10, no. 4, pp. 331–345, 1987.

[62] A. Diggle, "Rootmap—a model in three-dimensional coordinates of the growth and structure of fibrous root systems," *Plant and Soil*, vol. 105, no. 2, pp. 169–178, 1988.

[63] J. P. Lynch, K. L. Nielsen, R. D. Davis, and A. G. Jablokow, "Simroot: modelling and visualization of root systems," *Plant and Soil*, vol. 188, no. 1, pp. 139–151, 1997.

[64] L. Pages, M.-O. Jordan, and D. Picard, "A simulation model of the three-dimensional architecture of the maize root system," *Plant and Soil*, vol. 119, no. 1, pp. 147–154, 1989.

[65] C. Jourdan and H. Rey, "Modelling and simulation of the architecture and development of the oil-palm (t elaeis guineensis jacq.) root system," *Plant and soil*, vol. 190, no. 2, pp. 217–233, 1997.

[66] L. Wu, M. McGechan, N. McRoberts, J. Baddeley, and C. Watson, "Spacsys: integration of a 3d root architecture component to carbon, nitrogen and water cycling—model description," *Ecological Modelling*, vol. 200, no. 3-4, pp. 343–359, 2007.

[67] C. Godin and H. Sinoquet, "Functional–structural plant modelling," *New phytologist*, vol. 166, no. 3, pp. 705–708, 2005.

[68] D. Da Silva, L. Qin, C. DeBuse, and T. M. DeJong, "Measuring and modelling seasonal patterns of carbohydrate storage and mobilization in the trunks and root crowns of peach trees," *Annals of botany*, vol. 114, no. 4, pp. 643–652, 2014.

[69] T.-W. Chen, M. Henke, P. H. De Visser, G. Buck-Sorlin, D. Wiechers, K. Kahlen, and H. Stützel, "What is the most prominent factor limiting photosynthesis in different layers of a greenhouse cucumber canopy?," *Annals of botany*, vol. 114, no. 4, pp. 677–688, 2014.

[70] P. Stenberg, M. Mõttus, M. Rautiainen, and R. Sievänen, "Quantitative characterization of clumping in scots pine crowns," *Annals of botany*, vol. 114, no. 4, pp. 689–694, 2014.

[71] M. Yang, P. Défossez, F. Danjon, and T. Fourcaud, "Tree stability under wind: simulating uprooting with root breakage using a finite element method," *Annals of botany*, vol. 114, no. 4, pp. 695–709, 2014.

[72] F. Cartenì, F. Giannino, F. H. Schweingruber, and S. Mazzoleni, "Modelling the development and arrangement of the primary vascular structure in plants," *Annals of botany*, vol. 114, no. 4, pp. 619–627, 2014.

[73] H. Dale, A. Runions, D. Hobill, and P. Prusinkiewicz, "Modelling biomechanics of bark patterning in grasstrees," *Annals of botany*, vol. 114, no. 4, pp. 629–641, 2014.

[74] P. Prusinkiewicz, "Modeling plant growth and development," *Current opinion in plant biology*, vol. 7, no. 1, pp. 79–83, 2004.

[75] R. Heller, R. Esnault, and C. Lance, *Physiologie végétale: développement*. Dunod, 1998.

[76] J.-L. Julien, "P. mazliak—physiologie végétale ii. croissance et développement. herman, éditeirs des sciences et des arts, 15 x 22 cm. 575.," 2000.

[77] W. T. D'ARCY *et al.*, *ON GROWTH AND FORM*. STELLAR EDITIONS, 2016.

[78] R. Bastien and Y. Meroz, "The kinematics of plant nutation reveals a simple relation between curvature and the orientation of differential growth," *PLoS computational biology*, vol. 12, no. 12, p. e1005238, 2016.

[79] G. De Vries, T. Hillen, M. Lewis, J. Müller, and B. Schönfisch, *A course in mathematical biology: quantitative modeling with mathematical and computational methods*. SIAM, 2006.

[80] A. Gerwitz and E. Page, "An empirical mathematical model to describe plant root systems," *Journal of Applied Ecology*, pp. 773–781, 1974.

[81] R. Mulia and C. Dupraz, "Unusual fine root distributions of two deciduous tree species in southern france: What consequences for modelling of tree root dynamics?," *Plant and Soil*, vol. 281, no. 1-2, pp. 71–85, 2006.

[82] L. Dupuy, M. Vignes, B. McKenzie, and P. White, "The dynamics of root meristem distribution in the soil," *Plant, cell & environment*, vol. 33, no. 3, pp. 358–369, 2010.

[83] T. Roose, A. Fowler, and P. Darrah, "A mathematical model of plant nutrient uptake," *Journal of mathematical biology*, vol. 42, no. 4, pp. 347–360, 2001.

[84] P. Bastian, A. Chavarría-Krauser, C. Engwer, W. Jäger, S. Marnach, and M. Ptashnyk, "Modelling in vitro growth of dense root networks," *Journal of Theoretical Biology*, vol. 254, no. 1, pp. 99–109, 2008.

[85] N. Bessonov and V. Volpert, "Dynamical models of plant growth," *Mathematics Subject Classification*, 2014.

[86] H. R. Allen and M. Ptashnyk, "Mathematical modelling and analysis of the brassinosteroid and gibberellin signalling pathways and their interactions," *Journal of theoretical biology*, vol. 432, pp. 109–131, 2017.

[87] G.-Q. Sun, A. Chakraborty, Q.-X. Liu, Z. Jin, K. E. Anderson, and B.-L. Li, "Influence of time delay and nonlinear diffusion on herbivore outbreak," *Communications in Nonlinear Science and Numerical Simulation*, vol. 19, no. 5, pp. 1507–1518, 2014.

[88] L. P. Kadanoff, *Statistical physics: statics, dynamics and renormalization*. World Scientific Publishing Company, 2000.

[89] V. Méndez, D. Campos, and A. W. Sheppard, "A model for plant invasions: the role of distributed generation times," *Bulletin of mathematical biology*, vol. 71, no. 7, pp. 1727–1744, 2009.

[90] D. S. Chapman, C. Dytham, and G. S. Oxford, "Modelling population redistribution in a leaf beetle: an evaluation of alternative dispersal functions," *Journal of Animal Ecology*, vol. 76, no. 1, pp. 36–44, 2007.

[91] Y. Meroz, R. Bastien, and L. Mahadevan, "Spatio-temporal integration in plant tropisms," *Journal of the Royal Society Interface*, vol. 16, no. 154, p. 20190038, 2019.

[92] C. Darwin, "1872 the origin of species, 1st edn," 1859.

[93] R. C. Lewontin, "The units of selection," *Annual review of ecology and systematics*, vol. 1, no. 1, pp. 1–18, 1970.

[94] A. Makela, T. J. Givnish, F. Berninger, T. N. Buckley, G. D. Farquhar, and P. Hari, "Challenges and opportunities of the optimality approach in plant ecology," *Silva Fennica*, vol. 36, no. 3, pp. 605–614, 2002.

[95] H. Mooney and E. Dunn, "Photosynthetic systems of mediterranean-climate shrubs and trees of california and chile," *The American Naturalist*, vol. 104, no. 939, pp. 447–453, 1970.

[96] T. Givnish, "Ecological aspects of plant morphology: leaf form in relation to environment," *Acta Biotheoretica*, vol. 27, no. 6, pp. 83–142, 1978.

[97] H. Honda and J. B. Fisher, "Tree branch angle: maximizing effective leaf area," *Science*, vol. 199, no. 4331, pp. 888–890, 1978.

[98] J. Reynolds and J. Thornley, "A shoot: root partitioning model," *Annals of botany*, vol. 49, no. 5, pp. 585–597, 1982.

[99] A. Lacointe and P. E. Minchin, "Modelling phloem and xylem transport within a complex architecture," *Functional Plant Biology*, vol. 35, no. 10, pp. 772–780, 2008.

[100] I. Cowan and G. Farquhar, "Stomatal function in relation to leaf metabolism and environment.," in *Symposia of the Society for Experimental Biology*, vol. 31, p. 471, 1977.

[101] P. Hari, A. Mäkelä, E. Korpilahti, and M. Holmberg, "Optimal control of gas exchange," *Tree physiology*, vol. 2, no. 1-2-3, pp. 169–175, 1986.

[102] A. Mrad, S. Sevanto, J.-C. Domec, Y. Liu, M. Nakad, and G. Katul, "A dynamic optimality principle for water use strategies explains isohydric to anisohydric plant responses to drought," 2019.

[103] T. L. Vincent and H. R. Pulliam, "Evolution of life history strategies for an asexual annual plant model," *Theoretical Population Biology*, vol. 17, no. 2, pp. 215–231, 1980.

[104] M. Lindh, J. Johansson, K. Bolmgren, N. L. Lundstrom, A. Brannstrom, and N. Jonzén, "Constrained growth flips the direction of optimal phenological responses among annual plants," *New Phytologist*, vol. 209, no. 4, 2016.

[105] D. Cohen, "Maximizing final yield when growth is limited by time or by limiting resources," *Journal of Theoretical Biology*, vol. 33, no. 2, pp. 299–307, 1971.

[106] D. Cohen, "The optimal timing of reproduction," *The American Naturalist*, vol. 110, no. 975, pp. 801–807, 1976.

[107] J. Johansson, K. Bolmgren, and N. Jonzén, "Climate change and the optimal flowering time of annual plants in seasonal environments," *Global change biology*, vol. 19, no. 1, pp. 197–207, 2013.

[108] T. J. Givnish, "On the adaptive significance of leaf height in forest herbs," *The American Naturalist*, vol. 120, no. 3, pp. 353–381, 1982.

[109] E. Sheffer, S. A. Batterman, S. A. Levin, and L. O. Hedin, "Biome-scale nitrogen fixation strategies selected by climatic constraints on nitrogen cycle," *Nature Plants*, vol. 1, no. 12, p. 15182, 2015.

[110] A. Bressan, M. Palladino, and W. Shen, "Growth models for tree stems and vines," *Journal of Differential Equations*, vol. 263, no. 4, pp. 2280–2316, 2017.

[111] O. Franklin, C. A. Cambui, L. Gruffman, S. Palmroth, R. Oren, and T. Näsholm, "The carbon bonus of organic nitrogen enhances nitrogen use efficiency of plants," *Plant, cell & environment*, vol. 40, no. 1, pp. 25–35, 2017.

[112] C. Xu, R. Fisher, S. D. Wullschleger, C. J. Wilson, M. Cai, and N. G. McDowell, "Toward a mechanistic modeling of nitrogen limitation on vegetation dynamics," *PloS one*, vol. 7, no. 5, p. e37914, 2012.

[113] M. Lucas, Y. Guédon, C. Jay-Allemand, C. Godin, and L. Laplaze, "An auxin transport-based model of root branching in arabidopsis thaliana," *PLoS One*, vol. 3, no. 11, p. e3673, 2008.

[114] D. Muraro, H. Byrne, J. King, and M. Bennett, "The role of auxin and cytokinin signalling in specifying the root architecture of arabidopsis thaliana," *Journal of theoretical biology*, vol. 317, pp. 71–86, 2013.

[115] J. C. Locke, A. J. Millar, and M. S. Turner, "Modelling genetic networks with noisy and varied experimental data: the circadian clock in arabidopsis thaliana," *Journal of theoretical biology*, vol. 234, no. 3, pp. 383–393, 2005.

[116] F. G. Feugier and A. Satake, "Dynamical feedback between circadian clock and sucrose availability explains adaptive response of starch metabolism to various photoperiods," *Frontiers in plant science*, vol. 3, p. 305, 2013.

[117] E. Nikinmaa, R. Sievänen, and T. Hölttä, "Dynamics of leaf gas exchange, xylem and phloem transport, water potential and carbohydrate concentration in a realistic 3-d model tree crown," *Annals of botany*, vol. 114, no. 4, pp. 653–666, 2014.

[118] M. Seki, T. Ohara, T. J. Hearn, A. Frank, V. C. Da Silva, C. Caldana, A. A. Webb, and A. Satake, "Adjustment of the arabidopsis circadian oscillator by sugar signalling dictates the regulation of starch metabolism," *Scientific reports*, vol. 7, no. 1, p. 8305, 2017.

[119] J. H. Thornley, "Modelling shoot [ratio] root relations: the only way forward?," *Annals of Botany*, vol. 81, no. 2, pp. 165–171, 1998.

[120] J. Vos, L. Marcelis, and J. Evers, "Functional-structural plant modelling in crop production: adding a dimension," *Frontis*, pp. 1–12, 2007.

[121] C. Feller, P. Favre, A. Janka, S. C. Zeeman, J.-P. Gabriel, and D. Reinhardt, "Mathematical modeling of the dynamics of shoot-root interactions and resource partitioning in plant growth," *PloS one*, vol. 10, no. 7, p. e0127905, 2015.

[122] G. Manoli, C.-W. Huang, S. Bonetti, J.-C. Domec, M. Marani, and G. Katul, "Competition for light and water in a coupled soil-plant system," *Advances in Water Resources*, vol. 108, pp. 216–230, 2017.

[123] T. Vogel, M. Dohnal, J. Dusek, J. Votrubova, and M. Tesar, "Macroscopic modeling of plant water uptake in a forest stand involving root-mediated soil water redistribution," *Vadose Zone Journal*, vol. 12, no. 1, 2013.

[124] F. Hayat, M. A. Ahmed, M. Zarebanadkouki, G. Cai, and A. Carminati, "Measurements and simulation of leaf xylem water potential and root water uptake in heterogeneous soil water contents," *Advances in water resources*, vol. 124, pp. 96–105, 2019.

[125] R. E. Baker, J.-M. Pena, J. Jayamohan, and A. Jérusalem, "Mechanistic models versus machine learning, a fight worth fighting for the biological community?," *Biology letters*, vol. 14, no. 5, p. 20170660, 2018.

[126] L. Wolpert, C. Tickle, and A. M. Arias, *Principles of development*. Oxford University Press, USA, 2015.

[127] T. Watanabe, M. Yokozawa, S. Emori, K. Takata, A. Sumida, and T. Hara, "Developing a multilayered integrated numerical model of surface physics–growing plants interaction (minosgi)," *Global Change Biology*, vol. 10, no. 6, pp. 963–982, 2004.

[128] J. P. Lynch and K. M. Brown, "Topsoil foraging–an architectural adaptation of plants to low phosphorus availability," *Plant and Soil*, vol. 237, no. 2, pp. 225–237, 2001.

[129] G. Rubio, T. Walk, Z. Ge, X. Yan, H. Liao, and J. P. Lynch, "Root gravitropism and below-ground competition among neighbouring plants: a modelling approach," *Annals of Botany*, vol. 88, no. 5, pp. 929–940, 2001.

[130] V. Dunbabin, Z. Rengel, and A. Diggle, "Simulating form and function of root systems: efficiency of nitrate uptake is dependent on root system architecture and the spatial and temporal variability of nitrate supply," *Functional Ecology*, vol. 18, no. 2, pp. 204–211, 2004.

[131] L. Dupuy, P. J. Gregory, and A. G. Bengough, "Root growth models: towards a new generation of continuous approaches," *Journal of experimental botany*, vol. 61, no. 8, pp. 2131–2143, 2010.

[132] W. gang Hagemann, "Rv jean, phyllotaxis, a systematic study in plant morphogenesis, cambridge university press, cambridge, new york, melbourne (1994)," 1995.

[133] A. Hodge, "The plastic plant: root responses to heterogeneous supplies of nutrients," *New phytologist*, vol. 162, no. 1, pp. 9–24, 2004.

[134] Y. H. Chew, R. W. Smith, H. J. Jones, D. D. Seaton, R. Grima, and K. J. Halliday, "Mathematical models light up plant signaling," *The Plant Cell*, pp. tpc–113, 2014.

[135] A. Sadeghi, A. Tonazzini, L. Popova, and B. Mazzolai, "A novel growing device inspired by plant root soil penetration behaviors," *PloS one*, vol. 9, no. 2, p. e90139, 2014.

[136] A. Sadeghi, A. Mondini, and B. Mazzolai, "Toward self-growing soft robots inspired by plant roots and based on additive manufacturing technologies," *Soft robotics*, vol. 4, no. 3, pp. 211–223, 2017.

[137] T. Pons, H. Lambers, and F. Chapin III, "Plant physiological ecology," 1998.

[138] R. Sulpice, A. Flis, A. A. Ivakov, F. Apelt, N. Krohn, B. Encke, C. Abel, R. Feil, J. E. Lunn, and M. Stitt, "Arabidopsis coordinates the diurnal regulation of carbon allocation and growth across a wide range of photoperiods," *Molecular Plant*, vol. 7, no. 1, pp. 137–155, 2014.

[139] T. N. Buckley, "Modeling stomatal conductance," *Plant physiology*, vol. 174, no. 2, pp. 572–582, 2017.

[140] E. E. Goldschmidt and S. C. Huber, "Regulation of photosynthesis by end-product accumulation in leaves of plants storing starch, sucrose, and hexose sugars," *Plant physiology*, vol. 99, no. 4, pp. 1443–1448, 1992.

[141] M. Stitt, "Rising co2 levels and their potential significance for carbon flow in photosynthetic cells," *Plant, Cell & Environment*, vol. 14, no. 8, pp. 741–762, 1991.

[142] J. R. Evans, "Photosynthesis and nitrogen relationships in leaves of c 3 plants," *Oecologia*, vol. 78, no. 1, pp. 9–19, 1989.

[143] D. I. Arnon, "Phosphorus metabolism and photosynthesis," *Annual Review of Plant Physiology*, vol. 7, no. 1, pp. 325–356, 1956.

[144] C. A. Browne, "Liebig and the law of the minimum," *Liebig and after Liebig. Publication*, no. 16, pp. 71–82, 1942.

[145] A. M. Smith and M. Stitt, "Coordination of carbon supply and plant growth," *Plant, cell & environment*, vol. 30, no. 9, pp. 1126–1149, 2007.

[146] M. C. M. Martins, M. Hejazi, J. Fettke, M. Steup, R. Feil, U. Krause, S. Arrivault, D. Vosloh, C. M. Figueroa, A. Ivakov, *et al.*, "Feedback inhibition of starch degradation in arabidopsis leaves mediated by trehalose 6-phosphate," *Plant physiology*, pp. pp–113, 2013.

[147] E. Paparelli, S. Parlanti, S. Gonzali, G. Novi, L. Mariotti, N. Ceccarelli, J. T. van Dongen, K. Kölling, S. C. Zeeman, and P. Perata, "Nighttime sugar starvation orchestrates gibberellin biosynthesis and plant growth in arabidopsis," *The plant cell*, pp. tpc–113, 2013.

[148] T. Ohara and A. Satake, "Photosynthetic entrainment of the circadian clock facilitates plant growth under environmental fluctuations: perspectives from an integrated model of phase oscillator and phloem transportation," *Frontiers in plant science*, vol. 8, p. 1859, 2017.

[149] F. G. Feugier and A. Satake, "Hyperbolic features of the circadian clock oscillations can explain linearity in leaf starch dynamics and adaptation of plants to diverse light and dark cycles," *Ecological modelling*, vol. 290, pp. 110–120, 2014.

[150] M. J. Haydon, O. Mielczarek, F. C. Robertson, K. E. Hubbard, and A. A. Webb, "Photosynthetic entrainment of the arabidopsis thaliana circadian clock," *Nature*, vol. 502, no. 7473, p. 689, 2013.

[151] J. W. Hopmans and K. L. Bristow, "Current capabilities and future needs of root water and nutrient uptake modeling," in *Advances in agronomy*, vol. 77, pp. 103–183, Elsevier, 2002.

[152] S. J. Leghari, N. A. Wahocho, G. M. Laghari, A. HafeezLaghari, G. MustafaBhabhan, K. HussainTalpur, T. A. Bhutto, S. A. Wahocho, and A. A. Lashari, "Role of nitrogen for plant growth and development: A review," *Advances in Environmental Biology*, vol. 10, no. 9, pp. 209–219, 2016.

[153] R. Roy, A. Finck, G. Blair, and H. Tandon, "Plant nutrition for food security," *A guide for integrated nutrient management. FAO Fertilizer and Plant Nutrition Bulletin*, vol. 16, p. 368, 2006.

[154] E. Epstein, "Mineral nutrition of plants; principles and perspective," tech. rep., 1972.

[155] S.-D. Kung and S.-F. Yang, *Discoveries in plant biology*, vol. 3. World scientific, 2000.

[156] R. A. Narang, A. Bruene, and T. Altmann, "Analysis of phosphate acquisition efficiency in different arabidopsis accessions," *Plant Physiology*, vol. 124, no. 4, pp. 1786–1799, 2000.

[157] A. Jungk, C. Asher, D. Edwards, and D. Meyer, "Influence of phosphate status on phosphate uptake kinetics of maize (zea mays) and soybean (glycine max)," in *Plant Nutrition Physiology and Applications*, pp. 135–142, Springer, 1990.

[158] M. Y. Siddiqi, A. D. Glass, T. J. Ruth, and T. W. Rufty, "Studies of the uptake of nitrate in barley: I. kinetics of 13no3- influx," *Plant Physiology*, vol. 93, no. 4, pp. 1426–1432, 1990.

[159] E. Marin, M.-C. Thibaud, and F. Paul-lez Durance Cedex, "Measurement of 33p-po4 absorption kinetic constants in arabidopsis," *Plant Physiology*, 2015.

[160] Z. Kotur, Y. M. Siddiqi, and A. D. Glass, "Characterization of nitrite uptake in arabidopsis thaliana: evidence for a nitrite-specific transporter," *New Phytologist*, vol. 200, no. 1, pp. 201–210, 2013.

[161] Z. Yan, H. Guan, W. Han, T. Han, Y. Guo, and J. Fang, "Reproductive organ and young tissues show constrained elemental composition in arabidopsis thaliana," *Annals of botany*, vol. 117, no. 3, pp. 431–439, 2016.

[162] E. Truernit, "Plant physiology: the importance of sucrose transporters," *Current Biology*, vol. 11, no. 5, pp. R169–R171, 2001.

[163] C. Hermans, J. P. Hammond, P. J. White, and N. Verbruggen, "How do plants respond to nutrient shortage by biomass allocation?," *Trends in plant science*, vol. 11, no. 12, pp. 610–617, 2006.

[164] W. S. Harpole, J. T. Ngai, E. E. Cleland, E. W. Seabloom, E. T. Borer, M. E. Bracken, J. J. Elser, D. S. Gruner, H. Hillebrand, J. B. Shurin, *et al.*, "Nutrient co-limitation of primary producer communities," *Ecology letters*, vol. 14, no. 9, pp. 852–862, 2011.

[165] H. Poorter and O. Nagel, "The role of biomass allocation in the growth response of plants to different levels of light, co2, nutrients and water: a quantitative review," *Functional Plant Biology*, vol. 27, no. 12, pp. 1191–1191, 2000.

[166] H. Poorter, K. J. Niklas, P. B. Reich, J. Oleksyn, P. Poot, and L. Mommer, "Biomass allocation to leaves, stems and roots: meta-analyses of interspecific variation and environmental control," *New Phytologist*, vol. 193, no. 1, pp. 30–50, 2012.

[167] A. C. White, A. Rogers, M. Rees, and C. P. Osborne, "How can we make plants grow faster? a source–sink perspective on growth rate," *Journal of Experimental Botany*, vol. 67, no. 1, pp. 31–45, 2015.

[168] D. A. Herms and W. J. Mattson, "The dilemma of plants: to grow or defend," *The quarterly review of biology*, vol. 67, no. 3, pp. 283–335, 1992.

[169] C. C. de Groot, L. F. Marcelis, R. van den Boogaard, W. M. Kaiser, and H. Lambers, "Interaction of nitrogen and phosphorus nutrition in determining growth," *Plant and Soil*, vol. 248, no. 1-2, pp. 257–268, 2003.

[170] V. Fageria, "Nutrient interactions in crop plants," *Journal of plant nutrition*, vol. 24, no. 8, pp. 1269–1290, 2001.

[171] J. L. Moseley, T. Allinger, S. Herzog, P. Hoerth, E. Wehinger, S. Merchant, and M. Hippler, "Adaptation to fe-deficiency requires remodeling of the photosynthetic apparatus," *The EMBO Journal*, vol. 21, no. 24, pp. 6709–6720, 2002.

[172] C. Granier, C. Massonnet, O. Turc, B. Muller, K. Chenu, and F. Tardieu, "Individual leaf development in arabidopsis thaliana: a stable thermal-time-based programme," *Annals of botany*, vol. 89, no. 5, pp. 595–604, 2002.

[173] W. A. Hoffmann and H. Poorter, "Avoiding bias in calculations of relative growth rate," *Annals of botany*, vol. 90, no. 1, pp. 37–42, 2002.

[174] A. M. Smith, S. C. Zeeman, and S. M. Smith, "Starch degradation," *Annu. Rev. Plant Biol.*, vol. 56, pp. 73–98, 2005.

[175] V. Mengin, E.-T. Pyl, T. Alexandre Moraes, R. Sulpice, N. Krohn, B. Encke, and M. Stitt, "Photosynthate partitioning to starch in arabidopsis thaliana is insensitive to light intensity but sensitive to photoperiod due to a restriction on growth in the light in short photoperiods," *Plant, cell & environment*, vol. 40, no. 11, pp. 2608–2627, 2017.

[176] S. Güsewell, "N: P ratios in terrestrial plants: variation and functional significance," *New phytologist*, vol. 164, no. 2, pp. 243–266, 2004.

[177] M. Trull, M. Guiltinan, J. Lynch, and J. Deikman, "The responses of wild-type and aba mutant arabidopsis thaliana plants to phosphorus starvation," *Plant, Cell & Environment*, vol. 20, no. 1, pp. 85–92, 1997.

[178] H. Peng, Y. Chen, Z. Yan, and W. Han, "Stage-dependent stoichiometric homeostasis and responses of nutrient resorption in amaranthus mangostanus to nitrogen and phosphorus addition," *Scientific reports*, vol. 6, p. 37219, 2016.

[179] A. G. Good, A. K. Shrawat, and D. G. Muench, "Can less yield more? is reducing nutrient input into the environment compatible with maintaining crop production?," *Trends in plant science*, vol. 9, no. 12, pp. 597–605, 2004.

[180] F. Chardon, J. Barthélémy, F. Daniel-Vedele, and C. Masclaux-Daubresse, "Natural variation of nitrate uptake and nitrogen use efficiency in arabidopsis thaliana cultivated with limiting and ample nitrogen supply," *Journal of Experimental Botany*, vol. 61, no. 9, pp. 2293–2302, 2010.

[181] T. R. Bates and J. P. Lynch, "The efficiency of arabidopsis thaliana (brassicaceae) root hairs in phosphorus acquisition," *American Journal of Botany*, vol. 87, no. 7, pp. 964–970, 2000.

[182] M. Bacon, *Water use efficiency in plant biology*. John Wiley & Sons, 2009.

[183] F. Zhang, J. Shen, J. Zhang, Y. Zuo, L. Li, and X. Chen, "Rhizosphere processes and management for improving nutrient use efficiency and crop productivity: implications for china," in *Advances in agronomy*, vol. 107, pp. 1–32, Elsevier, 2010.

[184] I. Ciereszko, "Regulatory roles of sugars in plant growth and development," *Acta Societatis Botanicorum Poloniae*, vol. 87, no. 2, 2018.

[185] G. G. Maina, J. S. Brown, and M. Gersani, "Intra-plant versus inter-plant root competition in beans: avoidance, resource matching or tragedy of the commons," *Plant Ecology*, vol. 160, no. 2, pp. 235–247, 2002.

[186] J. K. Hale, "Ordinary differential equations, robert e," *Krieer, New York*, 1980.

[187] E. A. Coddington and N. Levinson, *Theory of ordinary differential equations*. Tata McGraw-Hill Education, 1955.

[188] G. Floquet, "Sur les équations différentielles linéaires à coefficients périodiques," in *Annales scientifiques de l'École normale supérieure*, vol. 12, pp. 47–88, 1883.

[189] J. A. Richards, *Analysis of periodically time-varying systems*. Springer Science & Business Media, 2012.

[190] A. L. de Araujo, A. Lemos, A. M. Alves, and K. M. Pedroso, "Some results on riccati equations, floquet theory and applications," *Journal of Fixed Point Theory and Applications*, vol. 20, no. 1, p. 43, 2018.

[191] R. C. Leegood and G. E. Edwards, "Carbon metabolism and photorespiration: temperature dependence in relation to other environmental factors," in *Photosynthesis and the Environment*, pp. 191–221, Springer, 1996.

[192] E. A. Ainsworth and S. P. Long, "What have we learned from 15 years of free-air co2 enrichment (face)? a meta-analytic review of the responses of photosynthesis, canopy properties and plant production to rising co2," *New phytologist*, vol. 165, no. 2, pp. 351–372, 2005.

[193] S. Gilroy and P. Masson, *Plant Tropisms*. John Wiley & Sons, 2008.

[194] K. Ritz, *The architecture and biology of soils: Life in inner space*. Cabi, 2011.

[195] E. Oleghe, M. Naveed, E. M. Baggs, and P. D. Hallett, "Plant exudates improve the mechanical conditions for root penetration through compacted soils," *Plant and soil*, vol. 421, no. 1-2, pp. 19–30, 2017.

[196] A. G. Bengough and C. E. Mullins, "Mechanical impedance to root growth: a review of experimental techniques and root growth responses," *Journal of soil science*, vol. 41, no. 3, pp. 341–358, 1990.

[197] J. E. Fisher, "Evidence of circumnutational growth movements of rhizomes of poa pratensis l. that aid in soil penetration," *Canadian Journal of Botany*, vol. 42, no. 3, pp. 293–299, 1964.

[198] C. Darwin and F. Darwin, *The power of movement in plants*. D. Appleton, 1881.

[199] M. Stolarz, "Circumnutation as a visible plant action and reaction: physiological, cellular and molecular basis for circumnutations," *Plant signaling & behavior*, vol. 4, no. 5, pp. 380–387, 2009.

[200] S. N. Shabala and I. A. Newman, "Root nutation modelled by two ion flux-linked growth waves around the root," *Physiologia Plantarum*, vol. 101, no. 4, pp. 770–776, 1997.

[201] A. H. Brown, "Circumnutations: from darwin to space flights.," *Plant Physiology*, vol. 101, no. 2, p. 345, 1993.

[202] A. Johnsson, "Circumnutations: results from recent experiments on earth and in space," *Planta*, vol. 203, no. 1, pp. S147–S158, 1997.

[203] A. Dexter, "Advances in characterization of soil structure," *Soil and tillage research*, vol. 11, no. 3-4, pp. 199–238, 1988.

[204] C. S. Bester and R. P. Behringer, "Collisional model of the drag force of granular impact," in *EPJ Web of Conferences*, vol. 140, p. 03017, EDP Sciences, 2017.

[205] M. J. Hutchings and E. A. John, "The effects of environmental heterogeneity on root growth and root/shoot partitioning," *Annals of Botany*, vol. 94, no. 1, pp. 1–8, 2004.

[206] M. Kondo, P. Pablico, D. Aragones, R. Agbisit, J. Abe, S. Morita, and B. Courtois, "Genotypic and environmental variations in root morphology in rice genotypes under upland field conditions," in *Roots: The Dynamic Interface between Plants and the Earth*, pp. 189–200, Springer, 2003.

[207] E. Del Dottore, A. Mondini, A. Sadeghi, V. Mattoli, and B. Mazzolai, "Circumnutations as a penetration strategy in a plant-root-inspired robot," in *2016 IEEE International Conference on Robotics and Automation (ICRA)*, pp. 4722–4728, IEEE, 2016.

[208] J. Yan, B. Wang, and Y. Zhou, "A root penetration model of arabidopsis thaliana in phytagel medium with different strength," *Journal of plant research*, vol. 130, no. 5, pp. 941–950, 2017.

[209] F. Migliaccio, A. Fortunati, and P. Tassone, "Arabidopsis root growth movements and their symmetry: Progress and problems arising from recent work," *Plant signaling & behavior*, vol. 4, no. 3, pp. 183–190, 2009.

[210] J.-P. Verbelen, T. D. Cnodder, J. Le, K. Vissenberg, and F. Baluška, "The root apex of arabidopsis thaliana consists of four distinct zones of growth activities: meristematic zone, transition zone, fast elongation zone and growth terminating zone," *Plant signaling & behavior*, vol. 1, no. 6, pp. 296–304, 2006.

[211] A. Tonazzini, L. Popova, F. Mattioli, and B. Mazzolai, "Analysis and characterization of a robotic probe inspired by the plant root apex," in *2012 4th IEEE RAS & EMBS International Conference on Biomedical Robotics and Biomechatronics (BioRob)*, pp. 1134–1139, IEEE, 2012.

[212] A. K. Mishra, F. Tramacere, R. Guarino, N. M. Pugno, and B. Mazzolai, "A study on plant root apex morphology as a model for soft robots moving in soil," *PloS one*, vol. 13, no. 6, p. e0197411, 2018.

[213] A. French and M. G. Ebison, *Introduction to classical mechanics*. Springer Science & Business Media, 2012.

[214] R. Albert, M. Pfeifer, A.-L. Barabási, and P. Schiffer, "Slow drag in a granular medium," *Physical review letters*, vol. 82, no. 1, p. 205, 1999.

[215] S. Takada and H. Hayakawa, "Drag law of two-dimensional granular fluids," *Journal of Engineering Mechanics*, vol. 143, no. 1, p. C4016004, 2016.

[216] R. Jewel, A. Panaitescu, and A. Kudrolli, "Micromechanics of intruder motion in wet granular medium," *Physical Review Fluids*, vol. 3, no. 8, p. 084303, 2018.

[217] C. Collinson and T. Roper, *Particle Mechanics*. Butterworth-Heinemann, 1995.

[218] A. V. Rao, "A survey of numerical methods for optimal control," *Advances in the Astronautical Sciences*, vol. 135, no. 1, pp. 497–528, 2009.

[219] T. J. Böhme and B. Frank, "Hybrid systems, optimal control and hybrid vehicles," *Cham, CH: Springer International*, 2017.

[220] F. Biral, E. Bertolazzi, and P. Bosetti, "Notes on numerical methods for solving optimal control problems," *IEEJ Journal of Industry Applications*, vol. 5, no. 2, pp. 154–166, 2016.

[221] A. Dexter and J. Hewitt, "The deflection of plant roots," *Journal of Agricultural Engineering Research*, vol. 23, no. 1, pp. 17–22, 1978.

[222] G. Whiteley, W. Utomo, and A. Dexter, "A comparison of penetrometer pressures and the pressures exerted by roots," *Plant and Soil*, vol. 61, no. 3, pp. 351–364, 1981.

[223] F. Tedone and M. Palladino, "Hamilton-Jacobi-Bellman Equation for Control Systems with Friction," *arXiv e-prints*, p. arXiv:1909.08380, Sep 2019.

[224] J. L. Mullen, E. Turk, K. Johnson, C. Wolverton, H. Ishikawa, C. Simmons, D. Söll, and M. L. Evans, "Root-growth behavior of the arabidopsis mutantrgr1: roles of gravitropism and circumnutation in the waving/coiling phenomenon," *Plant Physiology*, vol. 118, no. 4, pp. 1139–1145, 1998.

[225] J. J. Moreau, "Evolution problem associated with a moving convex set in a hilbert space," 1977.

[226] J. J. Moreau, "Numerical aspects of the sweeping process," *Computer methods in applied mechanics and engineering*, vol. 177, no. 3-4, pp. 329–349, 1999.

[227] V. Acary, O. Bonnefon, and B. Brogliato, *Nonsmooth Modeling and Simulation for Switched Circuits*, vol. 69. Springer, 2010.

[228] P. Drábek, P. Krejcí, and P. Takác, *Nonlinear differential equations*, vol. 404. CRC Press, 1999.

[229] A. Tanwani, B. Brogliato, and C. Prieur, "Observer design for unilaterally constrained lagrangian systems: A passivity-based approach," *IEEE Transactions on Automatic Control*, vol. 61, no. 9, pp. 2386–2401, 2015.

[230] A. Bressan and P. Michele, "Well-posedness of a model for the growth of tree stems and vines," *Discrete & Continuous Dynamical Systems - A*, vol. 38, 2017.

[231] J. J. Ye and J. Zhu, "Hamilton-jacobi theory for a generalized optimal stopping time problem," *Nonlinear Analysis*, vol. 34, no. 3, pp. 1029–1053, 1998.

[232] J. Ye, "Discontinuous solutions of the hamilton–jacobi equation for exit time problems," *SIAM Journal on Control and Optimization*, vol. 38, no. 4, pp. 1067–1085, 2000.

[233] M. Malisoff, "Viscosity solutions of the bellman equation for exit time optimal control problems with vanishing lagrangians," *SIAM Journal on Control and Optimization*, vol. 40, no. 5, pp. 1358–1383, 2002.

[234] G. Colombo and M. Palladino, "The minimum time function for the controlled moreau's sweeping process," *SIAM Journal on Control and Optimization*, vol. 54, no. 4, pp. 2036–2062, 2016.

[235] T. Donchev, V. Rios, and P. Wolenski, "Strong invariance and one-sided lipschitz multifunctions," *Nonlinear Analysis: Theory, Methods & Applications*, vol. 60, no. 5, pp. 849–862, 2005.

[236] R. J. Aumann, "Integrals of set-valued functions," *Journal of Mathematical Analysis and Applications*, vol. 12, no. 1, pp. 1–12, 1965.

[237] Z. Artstein, "Parametrized integration of multifunctions with applications to control and optimization," *SIAM Journal on Control and Optimization*, vol. 27, no. 6, pp. 1369–1380, 1989.

[238] J. Saint-Pierre and S. Sajid, "Parametrized integral of multifunctions in banach spaces," *Journal of mathematical analysis and applications*, vol. 239, no. 1, pp. 49–71, 1999.

[239] C. Castaing and M. Valadier, *Convex analysis and measurable multifunctions*, vol. 580. Springer, 2006.

[240] J.-P. Aubin and H. Frankowska, *Set-valued analysis*. Springer Science & Business Media, 2009.

[241] V. Veliov, "Lipschitz continuity of the value function in optimal control," *Journal of Optimization Theory and Applications*, vol. 94, no. 2, pp. 335–363, 1997.

[242] P. R. Wolenski and Y. Zhuang, "Proximal analysis and the minimal time function," *SIAM journal on control and optimization*, vol. 36, no. 3, pp. 1048–1072, 1998.

[243] R. Buckdahn, H. Frankowska, and M. Quincampoix, "Viability of an open set for stochastic control systems," *Stochastic Processes and their Applications*, vol. 129, no. 10, pp. 4108 – 4118, 2019.

[244] H. Frankowska, H. Zhang, and X. Zhang, "Necessary optimality conditions for local minimizers of stochastic optimal control problems with state constraints," *Transactions of the American Mathematical Society*, vol. 372, p. 1, 02 2019.

[245] R. Hermann and A. Krener, "Nonlinear controllability and observability," *IEEE Transactions on automatic control*, vol. 22, no. 5, pp. 728–740, 1977.

[246] A. Isidori, *Nonlinear control systems: an introduction*. Springer Science & Business Media, 2013.